

**CHARACTERIZATION OF SYNAPTIC TRANSMISSION  
ABNORMALITIES IN NEUROLOGICAL DISORDERS  
OF THE PRESYNAPTIC TERMINAL**

**DISSERTATION**

for the award of the degree  
“Doctor rerum naturalium” (Dr. rer. nat.)  
of the Georg-August-Universität Göttingen

within the doctoral program  
Cellular and Molecular Physiology of the Brain  
of the Göttingen Graduate Center for Neurosciences, Biophysics  
and Molecular Biosciences (GGNB)

submitted by  
AISHA MUNAWAR AHMAD (née GHUMAN)  
born in Eberbach, Germany

November 2021, Göttingen



## **Members of the Examination Board**

### **Thesis Committee**

PROF. DR. NILS BROSE

Department of Molecular Neurobiology  
Max Planck Institute of Experimental Medicine Göttingen

PROF. DR. THOMAS DRESBACH

Department of Anatomy and Embryology  
University Medical Center Göttingen

PROF. DR. TIAGO FLEMING OUTEIRO

Experimental Neurodegeneration  
University Medical Center Göttingen

## **Members of the Examination Board**

Reviewer: PROF. DR. NILS BROSE

Department of Molecular Neurobiology  
Max Planck Institute of Experimental Medicine Göttingen

2<sup>nd</sup> Reviewer: PROF. DR. THOMAS DRESBACH

Department of Anatomy and Embryology  
University Medical Center Göttingen

## **Further Members of the Examination Board**

PROF. DR. CHRISTINE STADELMANN-NESSLER

Institute for Neuropathology  
University Medical Center Göttingen

PROF. DR. SWEN HÜLSMANN

Clinics for Anesthesiology  
University Medical Center Göttingen

PROF. DR. DR. OLIVER SCHLÜTER

Psychiatry and Psychotherapy  
University Medical Center Göttingen

Date of oral examination: 17.01.2022

# CONTENTS

<b>LIST OF FIGURES</b> .....	<b>IV</b>
<b>LIST OF TABLES</b> .....	<b>V</b>
<b>ABBREVIATIONS</b> .....	<b>VI</b>
<b>ABSTRACT</b> .....	<b>1</b>
<b>1 INTRODUCTION</b> .....	<b>3</b>
1.1 <i>UNC13</i> – Historical Perspective and Overview .....	3
1.2 Molecular Interplay with Presynaptic Proteins .....	7
1.2.1 Syntaxin .....	7
1.2.2 Rab3-Interacting Molecule (RIM).....	8
1.2.3 Calmodulin.....	9
1.2.4 Doc2 .....	10
1.2.5 Msec7-1 .....	11
1.2.6 $\beta$ -Spectrin.....	12
1.3 Munc13s Facilitate SV Priming.....	12
1.3.1 Electron Microscopy Unveiling Munc13-Dependent SV Docking.....	13
1.3.2 Munc13 Priming Function .....	14
1.4 Munc13 at the SV Release Site/AZ.....	15
1.4.1 Munc13 Localization.....	15
1.4.2 Recruitment of Munc13s to the AZ .....	15
1.5 Munc13s and Short-Term Synaptic Plasticity .....	17
1.6 Synaptic Disorders and Genetic Inheritance .....	20
1.6.1 Synaptopathies and SNAREopathies .....	22
1.6.2 Munc13 in Brain Pathology/Munc13-Related Brain Disorders .....	22
1.7 Autaptic Culture System .....	24
1.8 Project Background and Aims.....	25
<b>2 MATERIALS</b> .....	<b>26</b>
<b>3 METHODS</b> .....	<b>31</b>
3.1 Molecular Biology .....	31
3.1.1 Site-Directed Mutagenesis .....	31
3.1.2 Bacterial Transformation .....	32
3.1.3 Bacterial Inoculation, DNA Amplification and Sequencing .....	32

3.1.4	Restriction Digest and DNA Gel Extraction .....	32
3.1.5	Ligation.....	33
3.2	Cell Biology .....	33
3.2.1	HEK293FT Cell Culture .....	33
3.2.2	Lentivirus Production with HEK293FT Cells .....	34
3.2.3	Astrocyte Microisland Culture .....	34
3.2.4	Autaptic Mouse Hippocampal Neuron Culture.....	35
3.2.5	Electrophysiological Measurements .....	35
3.2.6	Immunocytochemistry .....	36
3.3	Confocal Fluorescence Microscopy .....	37
3.3.1	Image Acquisition.....	37
3.3.2	Image Analysis .....	38
3.3.3	Image Processing.....	39
<b>4</b>	<b>RESULTS .....</b>	<b>40</b>
4.1	Functional Assessment of Human Patient-Specific Variants.....	40
4.1.1	Munc13-1 <sup>G808D</sup> Patient Variant .....	41
4.1.1.1	Genetics and Clinical Data.....	41
4.1.1.2	Munc13-1 <sup>G808D</sup> Boosts Spontaneous Release.....	43
4.1.1.3	Munc13-1 <sup>G808D</sup> Increases the Vesicular Release Probability.....	44
4.1.1.4	Munc13-1 <sup>G808D</sup> Enhances Short-Term Synaptic Depression .....	46
4.1.2	Munc13-1 <sup>Arg202</sup> Patient Variant.....	48
4.1.2.1	Genetics and Clinical Data.....	48
4.1.2.2	Spontaneous Release Characteristics in Low and High External Ca <sup>2+</sup> .....	50
4.1.2.3	Munc13-1 <sup>R202H</sup> Abates Synaptic Strength.....	52
4.1.2.4	Munc13-1 <sup>R202H</sup> Facilitates at 10 Hz Frequency.....	54
4.1.3	Munc13-1 <sup>E52K</sup> Patient Variant.....	57
4.1.3.1	Genetics and Clinical Data.....	57
4.1.3.2	Spontaneous and Evoked Release Characteristics of Variant Munc13-1 <sup>E52K</sup> .....	59
4.1.4	Munc13-1 <sup>R799Q</sup> and Munc13-1 <sup>N1013S</sup> Patient Variants.....	61
4.1.4.1	Genetics and Clinical Data for the Patient Variant Munc13-1 <sup>R799Q</sup> .....	61
4.1.4.2	Synaptic Transmission Largely Normal in Munc13-1 <sup>R799Q</sup> -Expressing Neurons...63	
4.1.4.3	Genetics and Clinical Data of the Patient Variant Munc13-1 <sup>N1013S</sup> .....	66
4.1.4.4	Synaptic Transmission Largely Normal in Munc13-1 <sup>N1013S</sup> -Expressing Neurons ..68	
4.1.5	Expression Levels of Munc13-1 Patient-Specific Variants .....	71
4.1.5.1	The Number of Synapses is Similar under all Recorded Conditions.....	74
4.1.5.2	N-terminal Variations Impair Munc13-1 Localization in Synapses .....	75
4.1.5.3	Neurons Expressing N1013S Variation Show Stronger Presynaptic Signal .....	77

<b>5</b>	<b>DISCUSSION .....</b>	<b>78</b>
5.1	Munc13-1 Associated Neurodevelopmental Disorder.....	78
5.2	Functional Assessment of Human Patient-Specific Variants using Autaptic Culture .....	80
5.2.1	Gain of Function in the Munc13-1 <sup>G808D</sup> .....	82
5.2.2	Loss of Function in the Munc13-1 <sup>R202H</sup> .....	84
5.2.3	The Munc13-1 <sup>E52K</sup> Variation Leads to a Loss of Function Phenotype.....	86
5.2.4	Wildtype-Like Rescue in Munc13-1 <sup>R799Q</sup> and Munc13-1 <sup>N1013S</sup> Variations.....	88
5.3	Munc13-1 Subcellular Localization and Quantification in Autaptic Neurons.....	90
5.4	Conclusion.....	91
<b>6</b>	<b>BIBLIOGRAPHY .....</b>	<b>93</b>
	<b>ACKNOWLEDGEMENTS .....</b>	<b>102</b>
	<b>CURRICULUM VITAE .....</b>	<b>104</b>

# List of Figures

<b>FIGURE 1:</b> ISOFORM-SPECIFIC EXPRESSION OF MUNC13 mRNA IN RAT BRAIN. ....	4
<b>FIGURE 2:</b> IN THE ABSENCE OF MUNC13-1 AND MUNC13-2 SV DOCKING IS FULLY ABOLISHED . ....	13
<b>FIGURE 3:</b> MODEL OF MUNC13-1 RELEASE SITE RECRUITMENT ..... ..	16
<b>FIGURE 4:</b> FIJI SCRIPT FOR IMAGE PROCESSING. .... ..	39
<b>FIGURE 5:</b> THE GENETIC AND CLINICAL SPECTRUM OF HUMAN UNC13A PATIENT CARRYING G808D ..... ..	42
<b>FIGURE 6:</b> MUNC13-1 <sup>G808D</sup> SUBSTANTIALLY INCREASES SPONTANEOUS RELEASE PROBABILITY. .... ..	44
<b>FIGURE 7:</b> MUNC13-1 <sup>G808D</sup> INCREASES SYNAPTIC STRENGTH AND VESICULAR RELEASE PROBABILITY ..... ..	45
<b>FIGURE 8:</b> ENHANCED DEPRESSION IN MUNC13-1 <sup>G808D</sup> EXPRESSING NEURONS..... ..	47
<b>FIGURE 9:</b> GENETIC AND CLINICAL PHENOTYPE OF THREE HUMAN PATIENTS CARRYING MUNC13-1 <sup>R202H</sup> ..... ..	49
<b>FIGURE 10:</b> SPONTANEOUS RELEASE CHARACTERISTICS IN MUNC13-1 <sup>R202H</sup> EXPRESSING NEURONS..... ..	51
<b>FIGURE 11:</b> MUNC13-1 <sup>R202H</sup> SIGNIFICANTLY REDUCES EVOKED RELEASE CHARACTERISTICS IN LOW $Ca^{2+}$ . .... ..	53
<b>FIGURE 12:</b> MUNC13-1 <sup>R202H</sup> SIGNIFICANTLY REDUCES SYNAPTIC STRENGTH IN HIGH $Ca^{2+}$ ..... ..	53
<b>FIGURE 13:</b> SHORT-TERM SYNAPTIC FACILITATION IN MUNC13-1 <sup>R202H</sup> EXPRESSING NEURONS..... ..	55
<b>FIGURE 14:</b> SHORT-TERM SYNAPTIC PLASTICITY IN MUNC13-1 <sup>R202H</sup> EXPRESSING NEURONS..... ..	56
<b>FIGURE 15:</b> GENETIC AND CLINICAL PHENOTYPE OF A HUMAN PATIENT CARRYING MUNC13-1 <sup>E52K</sup> ..... ..	58
<b>FIGURE 16:</b> MUNC13-1 <sup>E52K</sup> ABOLISHES EVOKED RELEASE, PARTIALLY SUPPORTS SPONTANEOUS RELEASE..... ..	60
<b>FIGURE 17:</b> GENETIC AND CLINICAL PHENOTYPE OF A MUNC13-1 <sup>R799Q</sup> VARIANT ..... ..	62
<b>FIGURE 18:</b> SPONTANEOUS RELEASE CHARACTERISTICS IN MUNC13-1 <sup>R799Q</sup> EXPRESSING NEURONS..... ..	64
<b>FIGURE 19:</b> EVOKED RELEASE CHARACTERISTICS IN MUNC13-1 <sup>R799Q</sup> -EXPRESSING NEURONS. .... ..	64
<b>FIGURE 20:</b> SHORT-TERM SYNAPTIC PLASTICITY IN MUNC13-1 <sup>R799Q</sup> -EXPRESSING NEURONS..... ..	65
<b>FIGURE 21:</b> GENETIC AND CLINICAL PHENOTYPE OF A HUMAN PATIENT CARRYING MUNC13-1 <sup>N1013S</sup> ..... ..	67
<b>FIGURE 22:</b> SPONTANEOUS RELEASE CHARACTERISTICS IN MUNC13-1 <sup>N1013S</sup> EXPRESSING NEURONS. .... ..	69
<b>FIGURE 23:</b> EVOKED RELEASE CHARACTERISTICS IN MUNC13-1 <sup>N1013S</sup> EXPRESSING NEURONS..... ..	69
<b>FIGURE 24:</b> NO CHANGE IN SHORT-TERM SYNAPTIC PLASTICITY CHARACTERISTICS IN MUNC13-1 <sup>N1013S</sup> ..... ..	70
<b>FIGURE 25:</b> CONFOCAL MICROSCOPY OF MUNC13-1 <sup>WT</sup> , MUNC13-1 <sup>E52K</sup> , MUNC13-1 <sup>R202H</sup> AND NON-INFECTED..... ..	72
<b>FIGURE 26:</b> CONFOCAL MICROSCOPY OF MUNC13-1 <sup>R799Q</sup> , MUNC13-1 <sup>G808D</sup> , MUNC13-1 <sup>N1013S</sup> ..... ..	73
<b>FIGURE 27:</b> SYNAPSE NUMBER OF MUNC13-1 DISEASE-RELATED VARIANTS EXPRESSING NEURONS..... ..	74
<b>FIGURE 28:</b> NUMBER OF MUNC13-1 COLOCALIZING SYNAPSES ..... ..	76
<b>FIGURE 29:</b> QUANTIFICATION OF THE MUNC13-1 SIGNAL INTENSITY..... ..	76
<b>FIGURE 30:</b> QUANTIFICATION OF THE VGLUT1 SIGNAL INTENSITY ..... ..	77

# List of Tables

<b>TABLE 1:</b> SURFACE CREATION PARAMETERS DEFINED IN IMARIS.....	38
<b>TABLE 2:</b> AMINO ACID IDENTITY AMONGST MUNC13-1 ISOFORMS FROM RAT, HUMAN AND MOUSE.....	80



# Abbreviations

AA	Amino acid
ACh	Acetylcholine
ADHD	Attention-deficit hyperactivity disorder
ALS	Amyotrophic lateral sclerosis
AP	Action potential
ARF	ADP ribosylation factor
AZ	Active zone
C	Cysteine
Ca <sup>2+</sup>	Calcium, Ionized
CaCl <sub>2</sub>	Calcium chloride
<i>Caenorhabditis elegans</i>	<i>C. elegans</i>
CaM	Calmodulin
cDNA	Complementary Desoxyribonucleic acid
CE	Cryptic exon
CML	C2B-MUN Linker
CO <sub>2</sub>	Carbon dioxide
<i>CPLX1/2</i>	Complexin 1/2
D	Aspartic acid
DAG	Diacylglycerol
ddH <sub>2</sub> O	Double-distilled water
DIV	Day <i>in vitro</i>
DKO	Double knockout
DMEM	Dulbecco's Modified Eagle Medium
DMSO	Dimethyl sulfoxide
dNTPs	Desoxynucleotide triphosphates
Doc2	Double C2-like domain-containing protein
DPSS	Diode-pumped solid-state laser
E	Glutamic acid
EDTA	Ethylenediaminetetraacetic acid
EEG	Electroencephalogram
EGFP	Enhanced Green Fluorescent Protein
EGTA	Egtazic acid

EPSCs	Evoked postsynaptic currents
EYFP	Enhanced yellow fluorescent protein
FBS	Fetal bovine serum
FRAP	Fluorescence recovery after photobleaching
FTD	Frontotemporal dementia
G	Glycine
GABA	$\gamma$ -aminobutyric acid
GFP	Green fluorescent protein
GH	Growth hormone
GMOs	Genetically modified organisms
gnomAD	The Genome Aggregation Database
GTP	Guanosine-5'-triphosphate
GWAS	Genome-wide association studies
HBSS	Hanks' Balanced Salt Solution
HEK	Human embryonic kidney
HeNe	Helium-neon
HEPES	N-2-Hydroxyethylpiperazine-N'-2-ethane sulphonic acid
<i>H.S.</i>	<i>Homo sapiens</i>
IDR	Intrinsically disordered region
K	Lysine
K <sup>+</sup>	Potassium ion
KCl	Potassium chloride
kDa	Kilo Dalton
kHz	Kilo Hertz
LB	Lysogeny broth
LoF	Loss-of-function
LUT	Lookup table
MAP2	Microtubule-associated protein 2
MEM	Minimum essential medium
mEPSC	Miniature excitatory postsynaptic currents
Met	Methionine
Mg <sup>2+</sup>	Magnesium
MgCl <sub>2</sub>	Magnesium chloride
MHD1	Munc13-homology domain 1

MHD2	Munc13-homology domain 2
mRNA	Messenger ribonucleic acid
NA	Numerical aperture
Na <sub>2</sub> ATP	Adenosine 5'-triphosphate disodium salt hydrate
NaATP	Sodium adenosine triphosphate
NaCl	Sodium chloride
NaGTP	Guanosine 5'-triphosphate sodium salt hydrate
NBA-A	Neurobasal-A Medium
NEAA	Non-Essential Amino Acids
NGS	Normal goat serum
NMR spectroscopy	Nuclear magnetic resonance spectroscopy
ns	Non-significant
NTP	Nucleoside triphosphate
PAL	Photoaffinity labelling
PBS	Phosphate-buffered saline
PCR	Polymerase chain reaction
PDBu	Phorbol-12,13-dibutyrate
PE	Phorbol ester
PFA	Paraformaldehyde
PIP	Phosphatidylinositol phosphat
PKC	Protein kinase C
PLL	Poly-L-Lysine
pVR	Probability of vesicular release
Q	Glutamine
R	Arginine
RIM	Rab3-Interacting Molecule
R.N.	<i>Rattus norvegicus</i>
rpm	Round per minute
RRP	Readily releasable pool
RT	Room temperature
SCGNs	Superior cervical ganglion neurons
Shank 2	SH3 and multiple ankyrin repeat domains 2
SNAP25	Synaptosomal-associated protein, 25kDa

SNARE	Soluble N-ethylmaleimide-sensitive-factor attachment receptor
SNP	Single nucleotide polymorphism
STD	Short-term depression
STE	Short-term enhancement
STORM	Stochastic optical reconstruction microscopy
STP	Short-term plasticity
STXBP1	Syntaxin-binding protein 1
SV	Synaptic vesicle
SYNGAP1	Synaptic Ras GTPase-activating protein 1
SYT1	Synaptotagmin 1
SYX1	Syntaxin 1
TDP-43	Transactive response (TAR) DNA binding protein 43 kDa
TPA	Tetradecanoylphorbol acetate
Trp	Tryptophan
TTX	Tetrodotoxin
U/ml	Units/mililiter
ubMunc13	Ubiquitous Munc13
V	Valine
VAMP2	Vesicle-associated membrane protein 2/ synaptobrevin
VGCCs	Voltage-gated calcium channels
VGLUT1	Vesicular glutamate transporter 1
WES	Whole-exome sequencing
WT	Wildtype
Y2H	Yeast two-hybrid

# Abstract

Seminal methodological advancements in the field of human genetics now allow for low-cost sequencing of complete coding genomes, and rich sources of corresponding data now exist for healthy and patient cohorts, allowing for the identification of possibly pathogenic variations. However, lagging behind is the identification of mechanisms by which such variations lead to disease, both at the molecular and cellular levels. Multiple genetic studies of neurodevelopmental and neuropsychiatric disorders now point to a central role of synaptic transmission in the etiology of such disorders. This project aims to shed light on molecular mechanisms and synaptic transmission abnormalities underlying a novel disorder of the presynaptic terminal – associated with variations in the *UNC13A* gene that translates into the Munc13-1 protein.

Munc13-1 is a large, multi-domain protein absolutely essential for priming synaptic vesicles (SV) to the active zone plasma membrane. The absence of Munc13-1 in mice leads to severely compromised synaptic transmission that is lethal. Evidence also exists pointing to the fact that Munc13-1 is pivotal for nervous system function in humans. Recently, the first patient with a *de novo* variant in the Munc13-1 protein, was described. The patient phenotype was characterized by a dyskinetic movement disorder, developmental delay and autism. The patient variant, P814L, leads to a gain of function of both excitatory and inhibitory synaptic transmission – neurons expressing this variant exhibited an increase in the basal SV release probability and aberrant patterns of short-term synaptic plasticity during trains of action potentials. Following this publication, a collaboration with the group of Prof. Dr. med. Anita Rauch from the Institute of Medical Genetics at the University of Zurich was initiated. This research group excels in the collection of patient data and in in-depth genetic analysis of human material. By now, around 40 patients were identified, who carry *de novo* or biallelic variants in the *UNC13A* gene, presenting with variable neurological and neuropsychiatric conditions. The patient variants are distributed over the entire Munc13-1 protein sequence and in every functional domain.

In this thesis, I am presenting electrophysiological and immunocytochemistry data analysing the functional consequences of five patient variants, characterized using the mouse hippocampal autaptic neuron culture system. One variant mirroring the phenotype of the previously reported P814L mutation confirms the reproducibility of our experimental system and its ability to accurately capture a phenotypic-functional relationship. Beyond that, I distinguish two distinct mechanisms in disease. One group of patients accumulating in the highly conserved C2B-MUN-Linker domain elicits a gain of function in synaptic transmission properties. In contrast, a

second group of patients accumulates on the less conserved N-terminus and displays a loss of function phenotype in our electrophysiological measurements. My findings uncover two distinct mechanisms governing disease manifestation in *UNC13A* patients, and emphasize the significance of genetic variants in synaptic proteins as causal for brain disorders.

# 1 Introduction

## 1.1 *UNC13* – Historical Perspective and Overview

Historically, the term ‘unc’ was first introduced by Sydney Brenner in his large body of work on *Caenorhabditis elegans* (*C. elegans*), where he defined a plethora of genes by mapping mutants exhibiting modified morphology and behaviour. Mutant animals deviating from the standard movement pattern were classified as ‘uncoordinated’, culminating in a catalogue of genes termed ‘unc’. In this context the *unc-13* gene was described as one of the most severely affected mutants, with irregular pharyngeal movement and paralysis (Brenner, 1974). Antibody staining revealed strikingly abnormal axonal growth of sensory neurons, misplaced processes in two types of inhibitory motor neurons and a defective cell body arrangement (Siddiqui, 1990). In additional assays mutant *unc-13* worms demonstrated resistance to toxic acetylcholinesterase inhibitors and elevated accumulation of acetylcholine (ACh) without affecting choline acetyltransferase or choline levels, pointing to a presynaptic neurotransmitter release deficiency (Nguyen et al., 1995). The *unc-13* was subsequently cloned. It encodes for a large protein consisting of 1734 amino acids wherein homology was detected for a 300 amino acid long region characterized by a cysteine-rich sequence with the regulatory C1 domain of protein kinase C (PKC), known to bind diacylglycerol (DAG) and phorbol ester (PE). Accordingly, Ca<sup>2+</sup>-dependent PE binding to a recombinant *unc-13* gene product was demonstrated (Kazanietz et al., 1995). A second region with a sequence similarity to the C2 domain of PKC was also detected (Maruyama and Brenner, 1991). Next, the UNC-13 protein with a molecular mass of approximately 190 kDa was isolated from *C. elegans* cell extracts, enabling to test the PE binding properties of UNC-13. PE binding occurred with high affinity and in a stereospecific manner. In particular, the phospholipids phosphatidylserine and phosphatidylinositol, but the latter to a lesser extent stimulated PE binding. Zinc also proved to be indispensable for PE binding. Sequence alignment with PKC and other C1 domain containing proteins identified six cysteines, two histidines and six additional amino acids as consensus residues necessary for PE binding (Ahmed et al., 1992).

Cloning efforts to identify the mammalian homolog of *unc-13* revealed three highly conserved *UNC13* genes termed Munc13-1 (‘Mammalian Unc’; 1735 amino acid residues, 196 kDa), Munc13-2 (1985 amino acid residues, 222 kDa) and Munc13-3 (2204 amino acid residues, 249 kDa) (Augustin et al., 1999a). All three isoforms are expressed in the brain, and Munc13-1 was additionally shown to be enriched at presynaptic compartments. Subcellular fractionation

experiments revealed an enrichment in the synaptic plasma membrane fraction, characteristic of a peripheral membrane protein. Sequence analysis unveiled a second C2 domain in the C-terminus of the mammalian Munc13s and a third C2 domain unique to the Munc13-1 protein located in the non-conserved N-terminal region. Only the middle C2 domain (C2B) exhibits  $\text{Ca}^{2+}$ -dependent phospholipid binding properties (Brose et al., 1995).

The mRNA expression pattern of the three Munc13 isoforms, analyzed by *in situ* hybridization, revealed a uniform distribution of Munc13-1 mRNA in the whole brain, whereas Munc13-2 mRNA was restricted to rostral and Munc13-3 expression occurred in rather caudal regions of the brain. Isoform-specific antibodies confirmed this pattern and revealed synaptic enrichment of all three isoforms. Immunocytochemistry in the rat cerebellum displayed the accumulation of Munc13-1 and Munc13-3 in presynapses, where particularly Munc13-3 localizes to granule cell axon terminals (Augustin et al., 1999a).

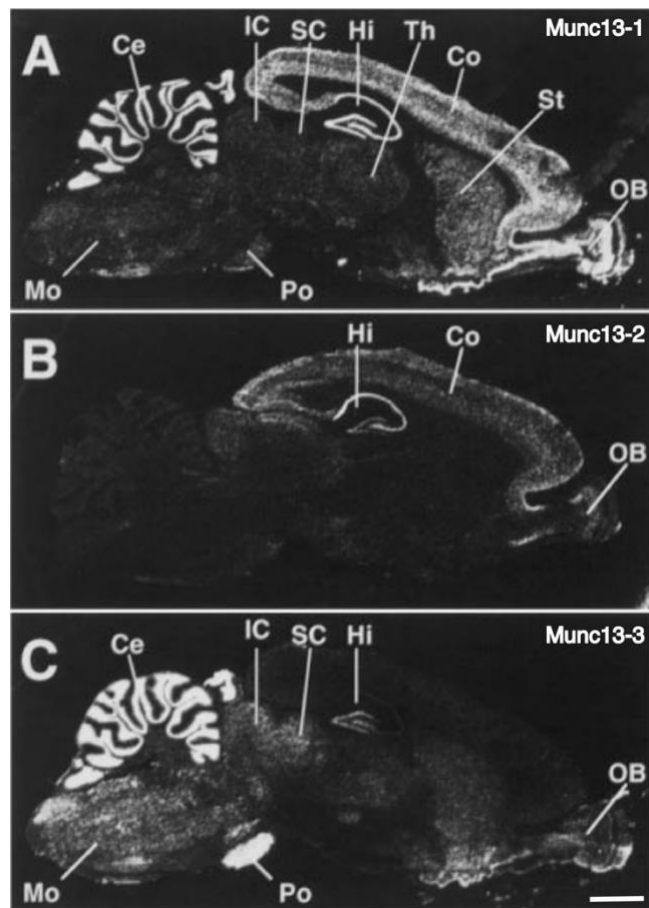


**Figure 1: Isoform-specific expression of Munc13 mRNA in rat brain.** Autoradiographs from *in situ* hybridization in rat brain showing Munc13 isoform-specific mRNA (**A** Munc13-1, **B** Munc13-2, **C** Munc13-3) expression pattern. Abbreviations: Ce, cerebellum; Co, cerebral cortex; Hi, hippocampus; IC, inferior colliculus; Mo, medulla oblongata; OB, olfactory bulb; Po, pons; SC, superior colliculus; St, striatum; Th, thalamus. Scale bar: 3.5 mm. Figure was adapted from (Augustin et al., 1999a).



In a Munc13-1 knock out (KO) mouse, glutamatergic excitatory transmission is severely hampered, although the neurons develop wild-type looking synapses, evident in ultrastructural analysis. No spontaneous release was measured, and evoked release was detected only in a minor subset of synapses. However, inhibitory  $\gamma$ -aminobutyric acid (GABA) containing neurons were able to release neurotransmitter in similar levels to those recorded in wildtype synapses, suggesting that inhibitory neurons rely on a different release mechanism than in excitatory neurons (Augustin et al., 1999b). A landmark study contributed to the completion of this picture, in which both splice isoforms of Munc13-2 were knocked out in parallel to the Munc13-1 isoform. In Munc13-1/2 double KO neurons, complete cessation of evoked and spontaneous neurotransmission was witnessed in both excitatory and inhibitory neurons, although synapse development remained unaffected. This led to the conclusion that Munc13-2 is capable of compensating for the loss of Munc13-1 in inhibitory, but not in excitatory neurons (Varoqueaux et al., 2002). The function of Munc13s was termed 'Priming', to reflect a molecular action on SVs that in ultrastructural analysis appeared docked to the plasma membrane but could not be released in Munc13-deficient synapses.

Similar to the *C. elegans* UNC-13, the mammalian homologue Munc13-1 binds PE and DAG with high affinity. Upon PE binding, all Munc13 isoforms translocate to the plasma membrane in fibroblasts. Munc13-1 was shown to enhance evoked and spontaneous neurotransmission as opposed to a PE-insensitive mutant Munc13-1<sup>H567K</sup> when overexpressed in presynapses of *Xenopus* neuromuscular junction, proving Munc13-1 to be a target of the DAG second messenger pathway, thereby influencing presynaptic neurotransmitter release (Betz et al., 1998). The functional role of PE and DAG regulation of Munc13 activity was subsequently studied using a knock-in (KI) mouse line where Munc13-1 carries a mutation in the C1 domain. The importance of the DAG second messenger signalling pathway through Munc13-1 was evident by the fact that mice carrying the  $\beta$ -PE/DAG-binding deficient variant Munc13-1<sup>H567K</sup> die shortly after birth (Rhee et al., 2002). In hippocampal excitatory Munc13-1<sup>H567K</sup>/Munc13-2<sup>KO</sup> neurons, a higher vesicular release probability was measured, alongside a strong, 50% reduction in the number of readily-releasable SVs. This, in turn, led to an aberrant pattern of synaptic depression during periods of high frequency stimulation. A crystal structure of the Munc13-1 C1 domain showed that the domain comprises of two  $\beta$ -sheets, a short C-terminal  $\alpha$ -helix and two Zn<sup>2+</sup>-binding sites, corresponding largely to the structure of the PKC C1 domain. NMR spectroscopy revealed that a conserved tryptophan side chain occludes the Munc13-1 DAG binding site, thereby impeding ligand binding as a unique feature of the Munc13-1 C1 domain in contrast to PKC C1 domain structure (Shen et al., 2005).

A search for the functional, priming domains of Munc13-1 revealed that the C-terminal residues 1100-1735 containing both Munc13-homology domains (MHD1 and MHD2) and the C2C domain downstream thereof are indispensable for its function (Stevens et al., 2005). Munc13s are not only critical in CNS neurons, but also function in cholinergic neuromuscular junctions, and their absence has been implicated in abnormal synaptogenesis and loss of neurotransmission. Morphological aberrations with respect to size, number, distribution and shape of neuromuscular synapses as well as motor neuron count and muscle cell development manifest in reduced neurotransmission. In stark contrast to CNS synapses, neuromuscular junction synapses are capable of residual transmitter release in the absence of Munc13 proteins, expressed in the form of markedly enhanced spontaneous quantal acetylcholine release (Varoqueaux et al., 2005).

To investigate the steady-state expression levels and turnover dynamics of Munc13-1 at the presynaptic site, a knockin mouse in which Munc13-1 was tagged with the yellow fluorescent protein (EYFP) was generated. In fluorescence recovery after photobleaching (FRAP) experiments, a continuous disappearance and retrieval of Munc13-1<sup>EYFP</sup> into the presynapse provided two different exchange kinetics, with 3 min for 40 % of the protein pool and an exchange time constant of 80 min for 60 % of the protein amount (Kalla et al., 2006). A protein turnover study measured a lifetime of approximately 10 days for murine Munc13-1 before degradation (Fornasiero et al., 2018).

## 1.2 Molecular Interplay with Presynaptic Proteins

### 1.2.1 Syntaxin

The severe phenotype in the *C. elegans unc-13* mutant advocated a crucial role for the protein. Considering its insensitivity to the acetylcholinesterase inhibitor assay and the similarity to the *unc-18* mutant animals phenotype, whose *Drosophila* homologue was established as a regulator for neurotransmitter release and its binding to the exocytotic core complex component syntaxin was known, a similar role for *unc-13* was postulated (Wu et al., 1998). To test this hypothesis, interaction partners of Munc13-1, the rat homologue of *unc-13*, were assessed in a yeast two-hybrid (Y2H) assay and by means of immunoprecipitation and cosedimentation analyses. A direct interaction of the Munc13-1 C-terminal residues 1181-1736 to the second of two predicted coiled coil domains in the N-terminus of the soluble N-ethylmaleimide sensitive factor (NSF) attachment protein receptor (SNARE) protein syntaxin was demonstrated. Immunoprecipitation and cosedimentation experiments revealed that Munc13-1 can form a complex with other SNARE proteins like synaptobrevin and SNAP25, and to a lesser extent with synaptotagmin isoforms. Since these candidates were only detected in immunoprecipitation and cosedimentation experiments, but were not found in the Y2H screen, they were suggested to associate with Munc13-1 via syntaxin and as part of an intermediate exocytotic core complex (Betz et al., 1997).

Evidence for Munc13-1 interaction to the syntaxin N-terminus corroborated studies in *Drosophila*, mouse and *C. elegans* that proposed a role for *unc-13* function in the SV priming step of exocytosis, a molecular step that is essential for the preparation of SVs for release (Sudhof, 1995). On the other hand, NMR spectroscopy revealed a closed conformation of syntaxin, where the N-terminus of syntaxin occupies its SNARE motifs and prevents SNARE protein assembly (Dulubova et al., 1999). To understand the two binding modes of the syntaxin N-terminus, the role of the closed conformation of syntaxin through its N-terminus was tested by introducing two point mutations (L166A, E167A) disrupting the closed conformation and promoting a constitutively open form of syntaxin (*unc-64*) in *C. elegans*. The open configuration of syntaxin rescued the aberrant behavioural phenotypes in syntaxin null mutants (*unc-64*) showcasing its efficacy as a substitute of wildtype syntaxin. The fully functional open configuration of syntaxin questioned the contribution of the *unc-13*-syntaxin binding. Therefore, it was investigated whether the *unc-13*-syntaxin interaction is critical for SV priming. A role for *unc-13* in opening syntaxin was confirmed in an *unc-13*-, *unc-64*-deficient animal, wherein rescue with wildtype syntaxin failed, but the open form of syntaxin partially rescued the behavioural phenotype and restored evoked and

spontaneous synaptic neurotransmission, thereby highlighting the need for *unc-13* to interact with the N terminus of syntaxin to facilitate opening (Richmond et al., 2001). The molecular mechanism of SNARE complex assembly mediated by Munc13-1 was finally resolved using NMR and fluorescence spectroscopy, that monitored the transition from the firmly bound closed syntaxin-1-Munc18-1 complex, in which the syntaxin N-terminal H<sub>abc</sub> domain is attached to its SNARE motif, to a mature SNARE complex, showing that the process is accelerated by weak and transient Munc13-1 MUN domain interaction with the syntaxin-1 SNARE motif. Integrating previously presented physiological data, the molecular role of Munc13-1 in SV priming encompasses the transitioning of the tightly-bound closed syntaxin-1-Munc18-1 interaction to the SNARE complex (Ma et al., 2011).

Ternary *trans* SNARE complex assembly is catalyzed by Munc13-1 in a two-step process while inducing optimal Ca<sup>2+</sup> sensitivity. Firstly, Munc-18-1-mediated alignment of plasma membrane associated syntaxin-1A and SNAP-25 takes place. Secondly, plasma membrane associated syntaxin-1A and vesicular synaptobrevin-2 alignment is autonomously promoted by Munc13-1 in a parallel orientation, independent of Munc18. Consistent with this role of Munc13-1 as a priming factor promoting proper subconfigurations of the SNARE complex components, neuronal overexpression of the constitutively open syntaxin-1A<sup>LE</sup> mutant in Munc13-1/2 DKO mice in comparison to a Munc13-1 overexpression was only able to slightly restore neurotransmitter release indicating the importance of proper ternary *trans* SNARE complex arrangement (Lai et al., 2017).

## 1.2.2 Rab3-Interacting Molecule (RIM)

Munc13-1 and the Rab3-Interacting Molecule RIM1 were independently identified as active zone proteins, tightly bound to the presynaptic cytomatrix in neurons, and, in case of RIM1, also at retinal ribbon presynapses. RIM1 is a 180 kDa protein containing a PDZ and two C2 domains. Its N-terminally located zinc finger is known to bind Rab3A and other GTP-bound Rab3 proteins (Wang et al., 1997). A structural interaction between the N-terminal C2A domain of Munc13-1 and ubMunc13-2 with the N-terminal zinc finger region in RIM1 in juxtaposition to the  $\alpha$ -helix that serves as Rab3 binding site has been demonstrated in Y2H screens as well as in cosedimentation and immunoprecipitation assays. NMR spectroscopy revealed that the three molecules could bind in parallel and therefore were likely to form a ternary complex essential for priming (Dulubova et al., 2005).

Physiological evidence points to a critical functional role for the Munc13/RIM interaction in the SV cycle upstream of SV fusion. Overexpression of a RIM-binding-deficient Munc13-1 construct in Munc13-1 knockout neurons resulted in a dramatic reduction of the readily releasable pool (RRP) of vesicles and greatly reduced evoked excitatory responses (Betz et al., 2001). In RIM knockout mice, Munc13-1 levels are reduced by 60% and concomitantly priming is compromised, indicating that RIM is important to stabilize Munc13 (Calakos et al., 2004; Schoch et al., 2002). Electrophysiological analysis of a Munc13-binding deficient RIM zinc finger domain in the calyx of Held synapse revealed a severely decreased pool size demonstrating that the RIM/Munc13-1 interaction determines the amount of primed and readily releasable SVs. (Dulubova et al., 2005).

Alongside forming central protein interactions, the active zone recruitment of Munc13s was proven to be accomplished through RIM1 $\alpha$  interaction (Andrews-Zwilling et al., 2006). A further step to understanding the molecular role of Munc13-1/RIM interaction was achieved, when NMR spectroscopy combined with X-ray diffraction detected the existence of a Munc13-1 homodimer connected through the C2A domain competing with the Munc13-1/RIM1 $\alpha$  heterodimer (Lu et al., 2006). Structure-function analyses demonstrated that RIMs mediate vesicle docking and priming by disrupting Munc13 homodimerization and establishing a heterodimer with the Munc13-1 C2A domain (Camacho et al., 2017; Deng et al., 2011).

An additional role for Rim in *C. elegans* is that its interaction to the vesicle-associated GTPase Rab3A targets vesicles to the presynaptic density adjacent to calcium channels (Gracheva et al., 2008). This was reproduced in mouse, where the RIM PDZ domain directly interacts with the C-termini of the N- and P/Q-type Ca<sup>2+</sup> channels localizing them to the presynapse. In this context, RIM deletion abolished neurotransmission drastically, while its N-terminus rescued vesicle priming (Kaesler et al., 2011). Removal of RIM isoforms at the calyx of Held synapse resulted in decreased presynaptic Ca<sup>2+</sup> channel density as well as reduced docked SVs (Han et al., 2011).

### 1.2.3 Calmodulin

Calmodulin (CaM) is a highly abundant protein in the brain that can bind an array of proteins in a Ca<sup>2+</sup>-dependent and Ca<sup>2+</sup>-independent fashion. All four Munc13 isoforms interact with CaM in a Ca<sup>2+</sup>-dependent manner, transducing residual Ca<sup>2+</sup> signaling to the SV release machinery. Munc13-1 and ubMunc13-2 contain a conserved CaM binding domain, whereas bMunc13-2 and Munc13-3 possess non-conserved binding motifs. Ca<sup>2+</sup> titration combined with photoaffinity labelling (PAL) revealed that Ca<sup>2+</sup>/CaM binding is already favoured upon small elevations in intracellular

Ca<sup>2+</sup> concentrations, with basal presynaptic Ca<sup>2+</sup> levels ranging between 50-250 nM (Dimova et al., 2006; Lipstein et al., 2012; Zikich et al., 2008).

Employing PAL and NMR spectroscopy identified the three-dimensional structure of Ca<sup>2+</sup>/CaM in complex with Munc13-1 and ubMunc13-2 indicating an antiparallel arrangement, with the binding mediated through a 1-5-8-26 CaM recognition motif in the N-termini of Munc13-1 and ubMunc13-2. CaM harbours two homologous domains, each encompassing two Ca<sup>2+</sup> binding helix-loop-helix motifs, named EF hand motifs that are joined by a flexible linker. The EF hands are two flexibly attached structural modules, termed as N-module and C-module, able to efficiently sense Ca<sup>2+</sup> at  $\mu$ M concentrations by adopting a half-loaded and fully loaded state respectively. A conformational change in the EF hand motifs mediated upon Ca<sup>2+</sup> binding uncovers a hydrophobic groove that binds amphiphilic  $\alpha$ -helices. The C-module establishes a high affinity complex of Munc13 with the C-terminal CaM domain by anchoring the amphiphilic  $\alpha$ -helix of Munc13-1 by its hydrophobic 1-5-8 residues to the C-terminal CaM domain whereby a conserved hydrophobic anchor residue in position 1 (Trp-464 in Munc13-1 and Trp-387 in ubMunc13-2) interacts with CaM residues Met-124 and Met-144 while Ca<sup>2+</sup>/CaM is bound. The N-module binds the Munc13-1 tryptophan residue at position 26 to the N-terminal CaM domain, but with lower affinity (Dimova et al., 2009; Rodriguez-Castaneda et al., 2010).

Abolishing the binding of Ca<sup>2+</sup>-CaM to Munc13-1 and ubMunc13-2 by mutagenesis of this anchoring residue was shown to block Ca<sup>2+</sup>-CaM binding and led to a reduced activity during high-frequency stimulation of neurons expressing these mutants in culture, suggesting that Ca<sup>2+</sup>-CaM binding to Munc13s boosts SV priming in neurons (Junge et al., 2004). These findings were later confirmed in vitro using a knock-in mutant carrying a point mutation in the Ca<sup>2+</sup>-CaM anchoring site. Electrophysiological recordings in the calyx of Held synapse pinpointed this effect to a reduction in the rate of SV replenishment, identifying a signalling pathway between activity induced elevations in Ca<sup>2+</sup> and Munc13-dependent SV priming (Lipstein et al., 2013).

## 1.2.4 Doc2

Like Munc13s, the Doc2 protein contains two Ca<sup>2+</sup> and phospholipid binding C2 domains. Contrary to Munc13, Doc2 concentrates on SVs. Among two identified isoforms, Doc2 $\alpha$  is prevalent in neurons and Doc2 $\beta$  is expressed ubiquitously. A Y2H screen of the rat brain cDNA and co-immunoprecipitation in PC12 cells identified Munc13 as an interactor of Doc2. Functional interaction of Doc2 $\alpha$  and Munc13-1 was shown, in a co-expression system measuring growth

hormone (GH) release, to occur downstream of DAG/PE binding during  $\text{Ca}^{2+}$ -dependent exocytosis. The interaction site of Doc2 $\alpha$  is located N-terminally at amino acid residues 13-37 and in case of Munc13-1 in the C-terminal region covering amino acids 851-1461 (Orita et al., 1997). Monitoring subcellular distribution of Doc2 $\beta$  and Munc13-1 GFP fusion protein constructs in HEK293 cells suggested a mechanistic involvement of Doc2 $\beta$  in PE-dependent Munc13-1 plasma membrane translocation, because upon PE stimulation, Doc2 $\beta$  translocation occurred only in the presence of Munc13-1 and was prevented by the same blocking agents as for blocking Munc13-1 translocation, but not for PKC (Duncan et al., 1999). In line with this, coexpression of fluorescently labelled Doc2 $\beta$  and Munc13-1 revealed a  $\text{Ca}^{2+}$ -dependent Munc13-1 translocation to the plasma membrane. Further, the expression of a DAG-binding deficient Munc13-1<sup>H567K</sup> was shown to reduce co-translocation with Doc2 $\beta$  at the plasma membrane, pointing to a  $\text{Ca}^{2+}$ - and Doc2 $\beta$ -dependent Munc13-1 plasma membrane translocation mechanism (Friedrich et al., 2013). Examining the physiological role of Doc2 $\alpha$ -Munc13-1 interaction in superior cervical ganglion neurons (SCGNs) revealed that upon inhibition of the Doc2 $\alpha$ -Munc13-1 interaction, synaptic transmission was inhibited. During high frequency stimulation the inhibitory effect on synaptic transmission increased, suggesting the involvement of the Doc2 $\alpha$ -Munc13-1 interaction in neurotransmitter release (Mochida et al., 1998).

### 1.2.5 Msec7-1

Msec7-1 is a guanine nucleotide exchange factor for the ARF family G-proteins that regulate membrane trafficking in different subcellular compartments. Pertaining to its role in the presynapse, enhanced neurotransmission was evidenced for msec7-1 overexpression in *Xenopus* neuromuscular junctions (Ashery et al., 1999).

The msec7 family consists of two more members, namely msec7-2 and msec7-3. All three isoforms share highly conserved structures characterized by an N-terminal coiled-coil domain, a sec7 homology domain, and a C-terminal pleckstrin homology domain (Telemenakis et al., 1997). A Y2H screen identified the first 59 amino acid residues of msec7-1 as binding to the C-terminus of Munc13-1 (AA 1181-1736). Cosedimentation and affinity chromatography experiments using rat brain extracts confirmed this finding. Since the Munc13-1 interaction domain for msec7-1 is precisely the region of syntaxin binding, immunoprecipitation assays were conducted to test whether a triple-protein complex can be formed, demonstrating that a simultaneous binding of msec7-1 to Munc13-1 and to syntaxin is possible (Neeb et al., 1999).

## 1.2.6 $\beta$ -Spectrin

A novel brain-specific isoform of  $\beta$ -Spectrin, termed as  $\beta$  SpIII $\Sigma$ 1, was identified as Munc13-1 interactor through a Y2H screen of the rat brain cDNA library and was visibly enriched in the SVs and plasma membrane. Binding was observed for 932-1347 AA residues of Munc13-1 and for 1779-2076 AA residues of  $\beta$  SpIII $\Sigma$ 1. Since the spectrin protein family majorly constitutes the plasma membrane-associated cytoskeleton, the reorganization of which plays a regulatory role in  $\text{Ca}^{2+}$ -dependent exocytosis, it is assumed that the observed Munc13-1 and  $\beta$  SpIII $\Sigma$ 1 interaction must be somewhat critical for neurotransmission (Sakaguchi et al., 1998). Whether this interaction occurs *in situ*, and its physiological impact on synaptic transmission are not clear to date.

## 1.3 Munc13s Facilitate SV Priming

Originally, the SV priming process was defined as a molecular, fusion-competent state of SVs, evolving after the docking of SVs at the plasma membrane. This notion resulted from combined electron microscopy and electrophysiology experiments using Munc13 mutants, showing that the loss of the RRP in Munc13 KO mice is not accompanied by an ultrastructural change in synapses of such neurons (Varoqueaux et al., 2002). By then, a role for Munc13 as a key SV priming protein had been determined in mice, *Drosophila* and *C. elegans*. Knocking out Munc13-1, in mice or in the respective orthologs *Drosophila* and *C. elegans*, either completely blocked SV priming as evidenced in the latter two invertebrate species or in mice was compromised up to 90%, without affecting GABAergic synapses (Aravamudan et al., 1999; Augustin et al., 1999b; Richmond et al., 1999).

Over the last two decades, methodological advancements in electron microscopy gradually established the priming state of SVs as the functional equivalent of the docking state of SVs. In high-pressure frozen samples of *C. elegans unc-13* null mutants and Munc13-1/2 DKO mice, SVs were found in proximity to, but not in contact with the plasma membrane alluding to the fact that the complete loss of neurotransmission in the context of electrophysiological experiments was due to the absence of SV docking (Imig et al., 2014; Siksou et al., 2009; Weimer et al., 2006).



### 1.3.1 Electron Microscopy Unveiling Munc13-Dependent SV Docking

In the process of investigating the site of vesicle priming and its SV distribution, the *unc-13* protein was labelled with immunogold particles in synapses of *C. elegans* neuromuscular junctions. These experiments revealed *unc-13* localization predominantly near presynaptic dense projections, namely AZs. The use of high-pressure freezing for sample processing enabled, for the first time, the accurate quantification of the ultrastructural distribution of plasma membrane-docked SVs relative to dense projections in *unc-13* deficient and wild-type animals. In the absence of *unc-13*, a striking reduction in plasma membrane-contacting vesicles in close vicinity of dense projections was observed, rendering the membrane-attached vesicles to be the morphological counterparts of primed vesicles (Weimer et al., 2006).

Another ultrastructural study of the Munc13-1/2 double knockout synapse in high pressure frozen cultured murine hippocampal slices validated this finding. In Munc13-deficient slices, the number of SVs remained similar to the wildtype count. Beyond that, a drastic loss of docked SVs became evident in Munc13-1/2 DKO synapses, and SVs accumulated within the first 40 nm from the AZ (Siksou et al., 2009). Confirming these findings, Imig *et al.* employed mice lacking SNARE proteins, proteins implicated in SNARE stabilization such as synaptotagmin and complexins as well as priming proteins of the CAPS and Munc13 family. By means of high-pressure freezing and subsequent freeze substitution, they generated electron tomography micrographs from organotypic hippocampal slices of these mice. The electron micrographs were subjected to comparative analysis facilitating molecular and morphological evaluation on a nanometer scale. In synapses lacking Munc13-1 and Munc13-2, SVs agglomerated 8-10 nm from the AZ in an undocked state, complemented by a major loss of docked SVs within 5 nm from the active zone (Imig et al., 2014).

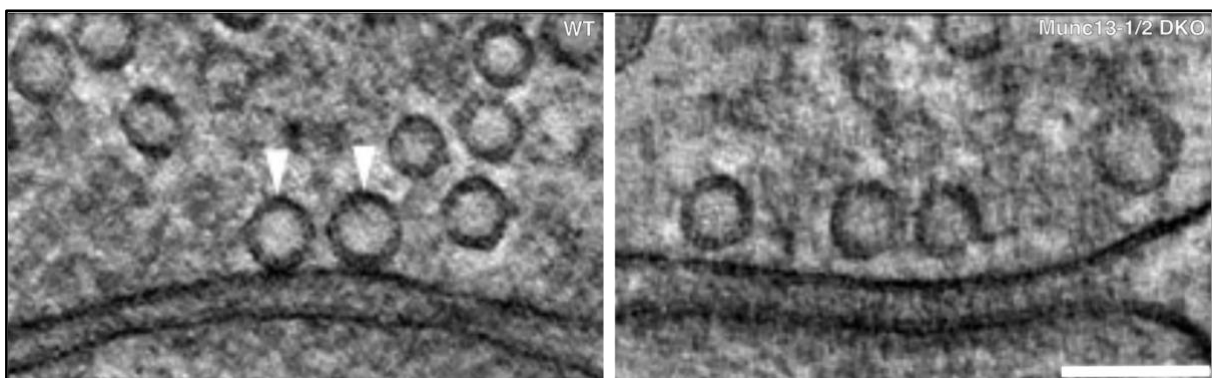


**Figure 2: In the absence of Munc13-1 and Munc13-2 SV docking is fully abolished** (Imig et al., 2014).

Based on these studies, SV docking was substantiated as the morphological manifestation of the functional SV priming process, in which evoked and spontaneous synaptic currents in Munc13-1/2 double knockout mouse neurons had completely vanished.

### 1.3.2 Munc13 Priming Function

A major constituent of the priming reaction is the formation of the SNARE complex involving the membrane-anchored syntaxin and SNAP-25 and the vesicle-associated synaptobrevin. An interaction of the syntaxin N-terminus with Munc13-1 maintains an open conformation of syntaxin and thereby promotes SNARE complex formation (Hammarlund et al., 2007; Richmond et al., 2001). In Munc13-1 a C-terminal region containing both Munc13-homology domains and the C2C domain was shown to be responsible for interacting with syntaxin, without which priming is perturbed (Stevens et al., 2005). Later it was shown that precisely the MUN domain, the largest part of the region between C2B and C2C domain, catalyzes Munc18-1-syntaxin-1 transition to the SNARE complex performing a central role in SV priming (Yang et al., 2015).

The indispensable role of Munc13-1 alongside Munc18-1 in neurotransmitter release was demonstrated by means of *in vitro* reconstitution assays of membrane fusion in that both proteins are required to facilitate *trans*-SNARE complex assembly that is resistant to NSF- $\alpha$ -SNAP-mediated disassembly and precedes synaptotagmin-1-Ca<sup>2+</sup> mediated fusion (Ma et al., 2013). The transition from the syntaxin-1/Munc18-1 complex to the SNARE complex catalyzed by the Munc13-1 MUN domain is predicated on the interaction of the Munc13-1 MUN domain with two conserved residues (R151, I155) in the syntaxin-1 linker region causing a conformational change that can accommodate synaptobrevin-2 and SNAP-25 attachment (Wang et al., 2017). Additionally, Munc13-1 independently provides a template for the promotion of a syntaxin-synaptobrevin subconfiguration and together with Munc18-1 promotes a syntaxin-SNAP-25 configuration that result in proper SNARE complex assembly (Lai et al., 2017).

This evidence argues for a complex network of manifold protein interactions rendering possible a concurrent spatially and temporally controlled neurotransmission, especially by the intervention of Munc13-1 multifunctionality.

## 1.4 Munc13 at the SV Release Site/AZ

### 1.4.1 Munc13 Localization

Munc13s are active zone proteins. The distribution of Munc13 isoforms at the calyx of Held synapse, a gigantic glutamatergic synapse of the brain stem, was examined utilizing Munc13-1 fluorescent protein knockin mice. Immunocytochemical synapses revealed that the Munc13 isoforms Munc13-1, ubMunc13-2 and Munc13-3 were expressed, whereas Munc13-1 was most abundantly present and greatly colocalizing with the active zone protein Bassoon, in contrast to ubMunc13-2 and Munc13-3, that showed a more diffused pattern (Chen et al., 2013). In the adult mouse retina, particularly at photoreceptor and bipolar cell ribbon synapses, ubMunc13-2 is the only Munc13 isoform detected, and immunogold labelling identified it at the presynaptic membrane and close to the canonical AZ, but not at the ribbon itself. Interestingly, electroretinographic recordings revealed no major defect in transmitter release upon ubMunc13-2 deletion, with normal ribbon-associated vesicle docking visible at electron-microscopic level. Unlike the tightly regulated transmitter release by Munc13s at central nervous system (CNS) synapses, these findings point to a minor role of ubMunc13-2 for synaptic release at ribbon synapses (Cooper et al., 2012).

Super-resolution imaging of the AZ of *Drosophila* neuromuscular junction revealed an isoform-specific interaction of Unc13A and Unc13B with different scaffolding protein complexes and a distinct temporal and spatial localization to a maturing AZ. Placement of Unc13B at a 120 nm distance around Ca<sup>2+</sup> channels is taken on by Syd-1 and Liprin- $\alpha$ , whereas Unc13A is recruited by Bruchpilot and Rim-binding protein and positioned at 70 nm proximity to Ca<sup>2+</sup> channels, which mark the center of the AZ (Bohme et al., 2016).

### 1.4.2 Recruitment of Munc13s to the AZ

Munc13-1/RIM1 functional interaction was found to generate fusion-competent SVs and regulate neurotransmission (Betz et al., 2001; Schoch et al., 2002). These findings were corroborated with extensive work utilizing RIM and Munc13 mutants, combined with electrophysiological analysis, protein-protein interaction assays, electron microscopy, and NMR and X-ray crystallography, resulting in a model that depicts RIM as an activator of Munc13 that serves to position Munc13 at the AZ. Munc13 molecules homodimerize at the C2A domain. This homodimerization prevents Munc13 function and is alleviated by the action of the RIM zinc finger domain, that binds to the

C2A domain, breaking inactive homodimers and replacing them by active, AZ-localized heterodimers. Munc13-1 is likely active at its heterodimeric form, or in a monomeric form, and an equilibrium between these two states likely exists, with the signalling cues controlling it still unclear (Camacho et al., 2017; Deng et al., 2011; Lu et al., 2006).

Munc13 recruitment to the AZ of *Drosophila melanogaster* glutamatergic neuromuscular synapses is dependent on the N-terminal domain that is relevant for AZ targeting in a specific and stable manner as shown by super-resolution microscopy. Overexpression of the Munc13-1 N-terminal fragment on a wildtype background misplaced the native Munc13-1 protein going hand in hand with fewer functional release sites. In contrast, expression of a Munc13-1 C-terminal fragment generated ectopic release sites with transient localization likely distant from  $\text{Ca}^{2+}$  channels and exhibited decreased AP-evoked activity with increased spontaneous activity leading to increased release sites and a low probability of release measured by intravital live imaging. While AZ scaffolding proteins partake in spontaneous and AP-evoked release, the amount of Munc13-1 defines the spontaneous or AP-evoked release at single AZs. These findings infer a role for Munc13-1 as active participator in release site formation and localization. Munc13-1 comprised of its N-terminal and C-terminal domain is relevant for exact and stable release site placement and thus controls synaptic function (Reddy-Alla et al., 2017).

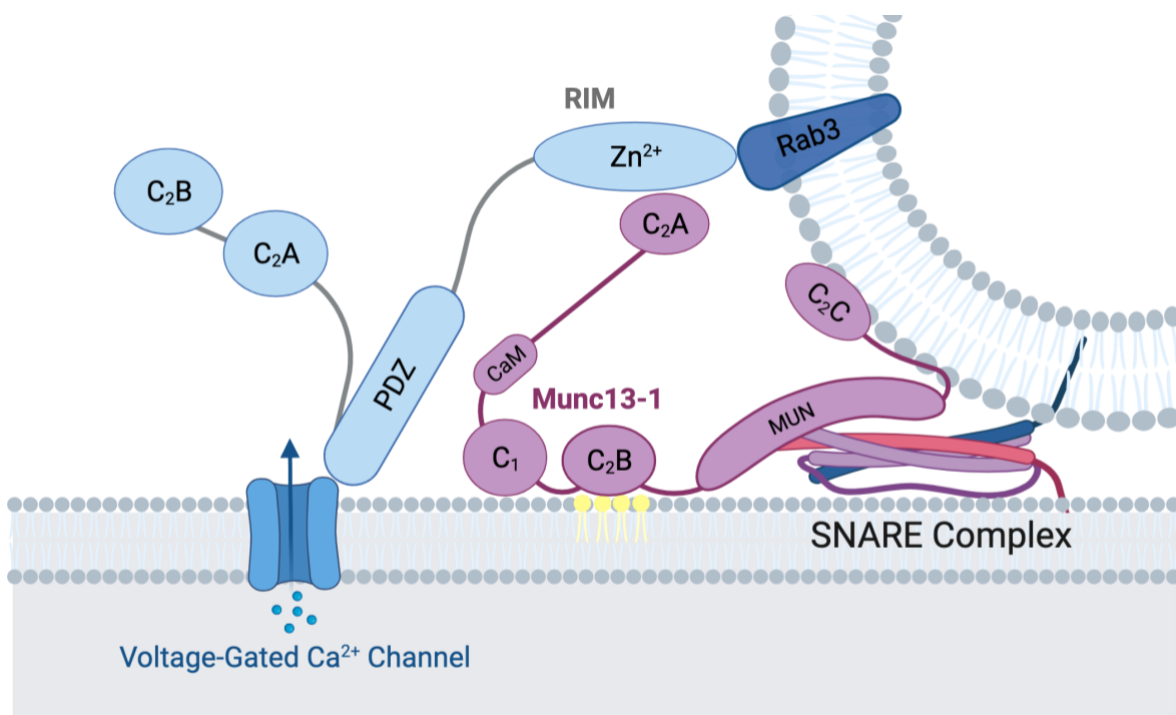


**Figure 3: Model of Munc13-1 release site recruitment via interaction of its C2A domain with the RIM zinc finger.** Created with BioRender.com, inspired by (Das et al., 2013) and [https://egrove.olemiss.edu/hon\\_thesis/984](https://egrove.olemiss.edu/hon_thesis/984).

The supramolecular nanoscale composition of Munc13-1 at the AZ of individual synapses was examined based on an approach that applied an optical glutamate sensor in combination with stochastic optical reconstruction microscopy (STORM) enabling the evaluation of quantal release parameters in single synapses from rat hippocampal neurons. It was established that the amount of Munc13-1 corresponds to the number of quantal release sites in synapses. Moreover, multiple self-assembled clusters of Munc13-1, termed as nanoassemblies, were shown to recruit syntaxin-1, therefore proposed to constitute the entity of quantal release sites at AZs in synapses. While previously conducted electron microscopy studies in Munc13-deficient animals crystallized the importance of Munc13s for SV docking proclaiming it as a morphological correlate to SV priming, this contribution is proposing Munc13-1 as the molecular correlate of the latter processes (Sakamoto et al., 2018).

## 1.5 Munc13s and Short-Term Synaptic Plasticity

Synapses dynamically alter their transmitter release efficacy when challenged with high-frequency stimulation in the form of action potential trains. This phenomenon is termed synaptic short-term plasticity (STP), as it is typically reversed within short time scales of milliseconds to minutes, depending on the stimulation paradigm (Zucker and Regehr, 2002). STP properties are markedly different in synapse subtypes. But how are these differences brought about and what does it signify physiologically?

Many parameters are crucial to set the level of STP in synapses. The initial efficiency of release, as often reflected by the basal vesicular release probability, will affect STP such that high release probability synapses will often exhibit short-term synaptic depression (STD), where the efficacy of the evoked release declines during the train, reaching low steady-state levels. Low release probability synapses will exhibit short-term synaptic enhancement (STE). The release probability of the synapse is increased during periods of stimulation in response to elevation of presynaptic  $\text{Ca}^{2+}$  concentration fluctuations during neuronal activity. Synaptic activation will cause the depletion of the RRP of SVs, contributing to the decrease of EPSC efficacy. However, in parallel, the accumulation of  $\text{Ca}^{2+}$  will also lead to enhancement of the SV replenishment rate. All these, and additional processes at both the pre- and postsynaptic compartment, ultimately determine the time-course and magnitude of presynaptic STP.

Knocking out Munc13-1 in mice reduces evoked excitatory neurotransmitter release by 90%. Munc13-2, that is shown to co-express in a subpopulation of hippocampal excitatory neurons, accounts for the 10% of the remaining release. To study the relationship between Munc13

isoform expression and activity, reduced synaptic efficacy and STP, Munc13-1/2 double knock-out neurons were rescued with cDNA encoding either Munc13-1 and ubMunc13-2 and studied for their neurotransmitter release properties using electrophysiology. When stimulated with high frequency action potential trains, glutamatergic synapses expressing Munc13-1 exhibit short-term synaptic depression, similar to the pattern of plasticity exhibited by WT hippocampal glutamatergic neuron in culture. In strong contrast, synapses expressing ubMunc13-2- showed a gradual increase in the efficacy of release and augmentation of EPSC amplitude, a hallmark of STE. That the expression pattern of Munc13s modulated STP into two different directions, was interpreted to propose that SV priming is critical for the refilling of the readily-releasable pool during activity, and that the rate in which the pool can be filled may be faster for the ubMunc13-2 isoform. However, the concomitant changes in the initial efficacy of release make it difficult to prove this hypothesis, and the changes were also attributed to changes in RRP size and vesicular release probability emerging from the activity of the two isoforms under excess  $\text{Ca}^{2+}$  during activity (Rosenmund et al., 2002).

How is synaptic activity signalling to change the function of Munc13-1? Munc13s can directly bind  $\text{Ca}^{2+}$  through a  $\text{Ca}^{2+}$ -dependent phospholipid binding C2B domain. To address the role of this domain in transducing elevations in presynaptic  $\text{Ca}^{2+}$  into ubMunc13-2 activation, two distinct mutations were utilized. Normally, the Munc13 C<sub>2</sub>B domain would require high levels of PIP and PIP<sub>2</sub> for  $\text{Ca}^{2+}$ -dependent phospholipid binding to occur. A mutation of the lysine 630 residue to tryptophan, which is hydrophobic in nature, enabled  $\text{Ca}^{2+}$ -dependent binding to the phospholipid membrane containing lower PIP<sub>2</sub> concentrations than usually required. Mutating aspartate 629 and 635 to asparagine resulted in the elimination of  $\text{Ca}^{2+}$  binding, thus impairing synaptic facilitation (Shin et al., 2010). Neurons expressing these variants show drastically altered STP characteristics during neuronal activity, allowing to conclude that  $\text{Ca}^{2+}$  and phospholipid signalling through the Munc13 C<sub>2</sub>B domain affect STP.

Munc13 is additionally equipped with an amphipathic helix that acts as evolutionary conserved CaM binding site (see section 1.2.3 on Calmodulin). A  $\text{Ca}^{2+}$ -CaM-Munc13 complex forms with the rise of  $\text{Ca}^{2+}$  levels in the range of 50-250 nM. Abolishing  $\text{Ca}^{2+}$ -CaM binding to Munc13 through mutagenesis impairs activity-dependent vesicle priming activity, pointing to an increase in priming activity as the main role of  $\text{Ca}^{2+}$ -CaM signalling (Junge et al., 2004). In support of this, a CaM inhibitor application in the calyx of Held synapse inhibited fast RRP refilling (Sakaba and Neher, 2001). This phenomenon of  $\text{Ca}^{2+}$ -CaM mediated modulation of priming activity was also demonstrated for the bMunc13-2 and Munc13-3 isoforms, that are only expressed in certain neuronal subtypes and possess diverse CaM-binding sequences. Electrophysiological experiments

have proven a positive effect of  $\text{Ca}^{2+}$ -CaM interaction on priming activity, leading to increased RRP size after activity, resulting in robust STD of neurotransmitter release. Taken together, it has been proposed that the properties of STP vary according to the prevalence of Munc13 isoforms in a neuronal cell (Lipstein et al., 2012). An in-depth study of the calyx of Held synapse using knockin mice that express the Munc13-1  $\text{Ca}^{2+}$ -CaM insensitive variant Munc13-1<sup>W464R</sup> further corroborated the involvement of the  $\text{Ca}^{2+}$ -CaM-Munc13-1 complex in determining STP characteristics in intact tissue. Munc13-1<sup>W464R</sup> synapses express stronger STD in conjunction with high-frequency stimulation leading to the presumption that the generation of the  $\text{Ca}^{2+}$ -CaM-Munc13-1 complex in the normal state induces increased RRP refilling rate (Lipstein et al., 2013). Another STP modulating mechanism is harboured in the DAG/PE-dependent regulation of neurotransmitter release by the potentiation of presynaptic efficacy through the C1 domain of Munc13-1. Following high-frequency stimulation, elevated  $\text{Ca}^{2+}$  causes DAG generation by phospholipase C (PLC), which acts as a second messenger that enhances Munc13-1 priming activity. The role of Munc13-1 in this regard was tested in mouse hippocampal neurons expressing a DAG/PE binding-deficient variant Munc13-1<sup>H567K</sup>. In comparison to wildtype, mutant neurons displayed much stronger STD and retarded refilling of RRP during high-frequency stimulation pointing to the need of proper C1 domain function for maintaining high levels of transmitter release during repetitive stimuli at high frequency (Rhee et al., 2002). As a follow up, Basu *et al.* defined a higher basal vesicular release probability (pVR) in the mutant Munc13-1<sup>H567K</sup> as the root cause for stronger STD during enhanced activity, reflecting the pVR of PDBu-potentiated wildtype neurons. Basically, the H567K mutation represents a PDBu-potentiated Munc13-1 (Basu et al., 2007).

In summary, Munc13-1 is a critical  $\text{Ca}^{2+}$  effector governing the replenishment rates of the RRP in an array of synapses *in vitro* and *in vivo*, acting as a determinant of STP by influencing synaptic recovery following high-frequency stimulations. Because the characteristics of STP are different in each synapse type, a prevalent hypothesis is that a malfunction in Munc13 activity will manifest in neuronal-subtype specific effects, thus, potentially, interfering with the delicate balance of synaptic transmission in neuronal networks.

## 1.6 Synaptic Disorders and Genetic Inheritance

In recent years, clinical genetics have attracted immense attention by the advancement of low-cost genetic testing, making it widely accessible. Whole genomes of healthy and patient individuals are being surveyed for single-nucleotide polymorphisms in population-based studies and more importantly for rare mutations in single patients. An array of genetic analysis, such as linkage analysis and segregation-based analysis on whole genome sequences, is associating patterns of genetic variations in different genetic loci to their inheritance by diseased individuals in distinct populations (Rajabli et al., 2021). Such disease-centered approaches fall under the umbrella of genome-wide association studies (GWAS), which classify patients according to disease and screen their genomes for putative, frequent risk variants (Cross-Disorder Group of the Psychiatric Genomics, 2013). By now, GWAS studies have linked variants in synaptic proteins to many psychiatric, neurological and childhood developmental disorders, such as schizophrenia (Fromer et al., 2014; Purcell et al., 2014), bipolar disorder (Cross-Disorder Group of the Psychiatric Genomics, 2013), amyotrophic lateral sclerosis (ALS) (Diekstra et al., 2012), autism (De Rubeis et al., 2014; Gai et al., 2012) and several other disorders that are presumably caused by synaptic dysfunction. Combined with *in silico* predictions, this approach can serve as pertinent but not sufficient means to draw a solid link between genotype and phenotype in patients.

Supporting the notion that synapses play a role in the etiology of disease, there is a large body of evidence linking autism spectrum disorders (ASD) to mutations in three critical and abundant constituents of the pre- and postsynapse, namely neurexin (Nrxn1) (Szatmari et al., 2007), Shank3 (Durand et al., 2007; Gauthier et al., 2009) and neuroligins (Nlgn3, Nlgn4) (Jamain et al., 2003; Nguyen et al., 2020). Experimental data suggests that neuroligins contribute to the activity-dependent remodelling of neural circuits (Scheiffele et al., 2000). Both, the presynaptic cell adhesion protein neurexin, and the postsynaptic cell adhesion protein neuroligin are crucial for synapse function and mouse survival (Missler et al., 2003; Varoqueaux et al., 2006). The postsynaptic scaffolding protein Shank3 is vital for cortico-striatal circuit function in Shank3 mutant mice that are marked by autistic-like behaviour (Peca et al., 2011).

Traditionally, mice serve as a main model to study human synaptic brain disease. The mammalian genome corresponds well to the human genome and introducing disease-related variations manifests in behavioural and physiological deficits in genetically modified mice that can be measured to document the impact of the variation (Grant et al., 1992; Silva et al., 1992). Accordingly, many synaptic proteins are being studied for their role in synaptic disease at the



cellular and functional level utilizing multiple patient-specific variants causing neurodevelopmental symptoms in dozens of patients, amongst them synaptotagmin1 (Baker et al., 2018) and syngap1 (Berryer et al., 2013; Mignot et al., 2016).

Different modes of genetic disease inheritance can be inferred from large-scale patient genomic data:

1. **Haploinsufficiency:** a state of heterozygosity in which the healthy allele is insufficient to compensate for the pathogenic allele. Three different types of haploinsufficiency can be distinguished. The first type occurs in the form of loss-of-function (LoF) or missense mutations affecting mRNA or protein stability but not necessarily perturbing protein function. A second type is described as functional haploinsufficiency that leads to impaired protein function by the appearance of a mutation. Thirdly, neomorph haploinsufficiency defines missense mutations that arise in larger multidomain proteins interfering with specific interaction partners.
2. A **dominant negative mode of inheritance** occurs when an adverse gain of function (GoF) effect of a mutated protein interferes with the function of the wild-type protein.
3. A **recessive mode of inheritance** occurs when homozygous or compound heterozygous ('biallelic') mutations caused by LoF or missense while heterozygous carriers remain asymptomatic (Sørensen, 2021) Alternatively, this type of inheritance may manifest when an individual inherits one loss of function allele and one allele with a mutation, a state referred to as 'biallelic null'.

Importantly, a considerable number of mutations occurring all over the gene is known in healthy individuals, even in regions adjacent to pathogenic mutations, that appear to be tolerated. These tolerated mutations are collected in databases such as genome aggregation database (gnomAD), comprising the genome or exome sequences of thousands of healthy individuals, thereby providing means to differentiate between tolerated and pathogenic mutations.

### 1.6.1 Synaptopathies and SNAREopathies

Neuronal SNARE proteins act in concert with their key regulators to constitute SV priming and fusion. A mutation in one of the eight human genes (*SYX1A/B*, *SNAP25*, *VAMP2*, *SYT1*, *CPLX1/2*, *STXBP1*, *UNC13A*, *RIMS1/2*) encoding the neuronal SNARE machinery proteins is defined as SNAREopathy, a subclass of synaptopathies, which encompass all relevant synaptic proteins and the disorders associated with their dysfunction. Null mutant mice for the SNAREopathy genes exhibit lethal phenotypes, indicating the lack of redundancy for these genes and more importantly, their contribution to highly specialized tasks. Several paralogs of the SNAREopathy genes exist that partly compensate protein function, but the indispensable fast and synchronized neurotransmitter release appears irreplaceable. Given the importance of neurotransmission at synapses and the ensuing STP phenomenon for higher brain function, it is not surprising that mutations in the genes encoding the SNARE machinery proteins will prove detrimental to the brain. In recent years, hundreds of SNAREopathy patients have been identified with mutations in one of the eight relevant, abovementioned genes exhibiting a vast variety of symptoms. Correlating the manifold symptoms to the identity of the mutated gene is challenging. Bearing in mind that SNARE machinery proteins exert diverse biological functions in different neuronal subtypes, as well as in several cellular environments, alongside their function in the completion of the SV cycle, the diverse clinical manifestations and distinct pathogenesis for each pathogenic are somewhat to be expected (Sørensen, 2021).

### 1.6.2 Munc13 in Brain Pathology/Munc13-Related Brain Disorders

The first *de novo* mutation in the *UNC13A* gene was discovered by whole-exome sequencing (WES) on a patient, who clinically manifested delayed neurological development, dyskinetic movement and autism spectrum disorder, together with attention-deficit hyperactivity disorder (ADHD). Electrophysiological experiments for functional assessment of the variant, proline 814 to leucine (in mice, Munc13-1<sup>P827L</sup>) expressed in autaptic neuronal cultures (see section 1.7 on autaptic culture system) from Munc13-1/2 DKO neurons revealed a gain of function effect on both excitatory and inhibitory synaptic transmission. Neurons expressing the variant demonstrated increased evoked postsynaptic current (EPSC) amplitudes, more frequent spontaneous release events, and a higher basal SV release probability due to increased SV fusogenicity. These were accompanied by atypical STP characteristics during repetitive action potential firing. In line with these findings, a behavioural assay in *C. elegans* expressing the corresponding proline to leucine mutation in the

UNC-13L protein, that employs a cholinesterase inhibitor called aldicarb, resulted in faster paralysis pointing towards enhanced presynaptic release. One proposal for a possible disease mechanism was the interference of the Proline-Leucine mutation with  $\text{Ca}^{2+}$ -affinity of the C2B domain by potentially inducing a conformational change due to their proximity in the primary protein structure (Lipstein et al., 2017). In this context a conserved C2B-MUN linker (CML) region maintains the autoinhibitory function of the C1-C2B tandem domain. Disruption of this linker motif by a short sequence insertion enhanced acetylcholine secretion as was seen upon C2B domain deletion when assessing aldicarb sensitivity in *C. elegans*. Further, the Proline-Leucine mutation described previously in the patient was able to revoke the inhibitory state of the  $\text{Ca}^{2+}$ -unbound C2B domain into a state of hypersecretion suggesting an inhibitory role of the CML region on the C2B domain (Michelassi et al., 2017).

In parallel, another Munc13-1 patient with a homozygous stop-codon mutation in the N-terminal C2A domain at amino acid position 102 was characterized with cortical hyperexcitability, microcephaly and myasthenia. In vitro analysis of neuromuscular transmission had revealed depletion of the RRP by 90% with a normal probability of quantal release. The patient demised at 50 months of age suffering from respiratory failure (Engel et al., 2016).

Growing evidence is linking common *UNC13A* variants in amyotrophic lateral sclerosis (ALS) patients to poor prognosis in pathogenesis. In the search for potential therapeutic targets in patients with ALS, a genome-wide association screen combined with disease susceptibility and survival analyses was conducted in a large cohort of sporadic ALS patients and detected was a common genetic variant rs12608932 in the *UNC13A* gene that was linked to disease susceptibility and precisely to shorter survival (Diekstra et al., 2012). Additional studies in different patient cohorts have repeatedly identified shared polymorphisms in *UNC13A* as risk factors for ALS and frontotemporal dementia (FTD) (Diekstra et al., 2014; van Eijk et al., 2017; van Es et al., 2009). Due to clinicopathological similarities FTD and ALS are mentioned collectively, while they also share common risk variants in the *UNC13A* gene. On a molecular level, both neurodegenerative disorders are characterized by the misplacement of the RNA-binding protein TDP-43. Upon TDP-43 decrease in the nucleus, a so-called cryptic exon (CE) is included in *UNC13A* leading to a nonsense translation entailing protein decay and deficiency. This CE inclusion was demonstrated in cultured cells and patient brains in the context of two typical single-nucleotide polymorphisms (SNPs) found in the non-coding region of the *UNC13A* (Anna-Leigh Brown, 2021).

Given that Munc13-1 in mouse is mandatory in facilitating SV priming, which is paramount to neurotransmitter release, its emerging visibility in the context of human patients only reinforces the need for an in-depth investigation on its functional properties.

## 1.7 Autaptic Culture System

The phrase ‘autapse’ dates back to 1972, stemming from an effort by Van Der Loos and Glaser to describe neurons forming synapses on themselves. Back then, autapses were found in pyramidal cells from rabbit occipital cortex preparations whilst tracking their processes by microscopy, to map their connections to surrounding neurons (Van Der Loos, 1972). In search of a previous description of this phenomenon, the authors of the manuscript came across an article by Held on the structure of neurons and their processes from 1897, who evidenced Golgi-impregnated autapse-bearing Purkinje cells in adult human cerebellar cortex and several autapse-bearing lower motor neurons. Moreover, in three additional reports from 1971, dendrites projecting on their own cellular axon found a mention but were not taken much into consideration. Based on these documentations, the presence of autapse-bearing neurons in the brain was postulated.

In 1991, Bekkers and Stevens developed a protocol culturing single hippocampal rat neurons on small islands of a collagen-lysin containing substrate. In the absence of neighbouring neurons, these neurons form autaptic synapses onto themselves. By characterizing their electrical properties, they further substantiated the existence of excitatory and inhibitory responses from autapses as had been similarly measured in non-autaptic cells (Bekkers and Stevens, 1991). Further refinement of this protocol was committed by Pyott and Rosenmund, with additional analyses of the readily-releasable vesicle pool properties, spontaneous and evoked responses as well as high frequency stimulation protocols, which majorly shaped our current protocol. A novel feature of their experimental paradigm was the addition of astrocyte feeder cells onto the substrate coated microislands and the attachment of a fast-flow system capable of administering different reagents to the respective neurons subjected to analysis and an exchange of the extracellular bath solution within 20-30 ms (Pyott and Rosenmund, 2002). In its final form, this system is optimal for studying the function of synaptic proteins, as it enables studies on knockout and knockin animals, the documentation of phenotypes from otherwise lethal animals, cell autonomous phenotypes, and drug stimulations. All in all, it facilitates a simple analysis because assumptions on the number of connecting neurons do not have to be made.

For these reasons, the autaptic culture system remains to date the best system for conducting structure-function studies of presynaptic protein in the field. The work presented here relies on protocols adapted from Burgalossi *et al.* (Burgalossi et al., 2012).

## 1.8 Project Background and Aims

Previous work conducted in the Department of Molecular Neurobiology at the Max Planck Institute of Experimental Medicine described a novel brain disorder associated with a variation in the coding sequence of the *UNC13A* gene. The patient variant manifesting in disease was a key determinant in igniting this large-scale project. Once the findings were published, a series of clinicians and geneticists lined up to share atypical hits in the *UNC13A* gene from their patients genome and exome sequencing. An endeavour was taken to keep track of the reported patient variants and their respective phenotypes, which culminated in a coordinated effort to form an interdisciplinary collaboration between geneticists responsible for data collection and genetic screening, clinicians who took up the responsibility of reporting a large collection of the patients respective clinical symptoms and our effort to functionally characterize handpicked phenotypically severe variants. The accumulation of dozens of patients since the inception of this project provides solid reason to conclude that variants in the Munc13-1 protein lead to disease. But are all discovered variants causal for disease?

I hypothesize that pathogenic patient variants lead to deficits in neurotransmitter efficacy and plasticity. Hence, I characterize neurotransmitter deficits in neurons expressing *UNC13A* patient mutations in autaptic neuronal cultures. Herewith, I seek to identify variant-specific mechanisms that converge into neurological dysfunction. In a broader context, this shall help understand the cellular pathomechanisms of this novel neuropsychiatric disorder pertaining to the Munc13 protein.

In the framework of this project, I use the autaptic neuronal culture system to investigate the pathogenicity of patient specific variations in *UNC13A* to synaptic transmission. First, patient-specific variations are introduced in the rat Munc13-1 cDNA and the wildtype protein, or the protein variant is reintroduced via lentiviral particles into cultured mouse hippocampal excitatory neurons, obtained from a Munc13-1 and Munc13-2 double knockout mouse line. Infected neurons are then studied using whole-cell voltage clamp recordings. By analyzing several variants in different domains of the protein, I investigate how Munc13-1 protein function is manifested in human disease.

## 2 Materials

Antibody	Source	Dilution	Identifier
Mouse monoclonal GFP	Merck Millipore	1:250	MAB3580
Rabbit polyclonal VGLUT1	Synaptic Systems	1:1000	135 302
Guinea pig polyclonal Shank 2	Synaptic Systems	1:250	162 204
Chicken polyclonal MAP2	Novus Biologicals	1:1000	NB300-213
Goat anti-Mouse Alexa 488	Thermo Fisher Sc.	1:2000	A11029
Goat anti-Rabbit Alexa 633	Thermo Fisher Sc.	1:2000	A21071
Goat anti-Guinea Pig Alexa 568	Abcam	1:2000	Ab175714
Goat anti-Chicken Alexa 405	Abcam	1:1000	Ab175674

Bacterial Strain, Cell line & Mouse Lines	Source
Escherichia coli ElectroTen-Blue	Agilent Technologies
HEK 293FT	Thermo Fisher Scientific
Munc13-1 KO	Augustin et al., 1999b
Munc13-2 KO	Varoqueaux et al., 2002

Commercial Kits	Source
EndoFree Plasmid Maxi Kit	Qiagen
ISOLATE II PCR and Gel Kit	Bioline
Zyppy Plasmid Miniprep Kit	Zymo Research

Consumables	Source
Amicon Ultra-15 Centrifugal Filter Unit	Merck
Borosilicate glass with fire polished ends without filament, GB150-8P	Science Products
Cellstar Culture Dish, PS, 145/20 MM	Greiner Bio-One
Gene Pulser/Micro Pulser Electroporation Cuvettes, 0.1 cm gap	Bio-Rad
Luer-Lok syringe, 30 ml	Becton, Dickinson and Company

<b>Consumables</b>	<b>Source</b>
MF-Millipore Membrane Filter, 0.45 µm pore size	Merck
Superfrost Plus adhesion slides	Menzel Gläser

<b>Enzymes</b>	<b>Source</b>
BstEII-HF	New England Biolabs, Inc.
DpnI	New England Biolabs, Inc.
NheI-HF	New England Biolabs, Inc.
PspXI	New England Biolabs, Inc.
Pfu Turbo Polymerase Cx	Agilent Technologies
T4 DNA Ligase	New England Biolabs, Inc.

<b>Hardware</b>	<b>Source</b>
Digidata 1440A Data Acquisition System	Axon Instruments/Molecular Devices
DS-11 FX µVolume Spectrophotometer	Biozym
Electrophoresis Power Supply - EPS 301	Amersham
Horizon 11-14 Gel Electrophoresis System	Gibco Life Technologies
MicroPulser Electroporator	Bio-Rad
MultiClamp 700B Amplifier	Axon Instruments/Molecular Devices
PTC-225 Tetrad Thermocycler System	MJ Research/Bio-Rad
P-97 Flaming/Brown type micropipette puller	Sutter Instrument
Safe Imager 2.0 Blue Light Transilluminator	Thermo Fisher Scientific
Thermomixer Compact 5350	Eppendorf

<b>Oligonucleotide</b>	<b>Sequence</b>
37356	Forward
Munc13-1_R201H_F	5'-CAGTGATTATCATAGTGAGACGA-3'
37357	Reverse
Munc13-1_R201H_R	5'-TCGTCTCACTATGATAATCACTG-3'
37760	Forward
Munc13-1_G821D_F	5'-CAGTGTGGAGATCAAAGACGAGGAGAAGGTGGCACC-3'

Oligonucleotide	Sequence
37761	Reverse
Munc13-1_G821D_R	5'-GGTGCCACCTTCTCCTCGTCTTTGATCTCCACACTG-3'
37866	Forward
Munc13-1_N1026S_F	5'-CCTACGAGTACATCTTCAGCAACTGTCATGAGCTCTA-3'
37867	Reverse
Munc13-1_N1026S_R	5'-TAGAGCTCATGACAGTTGCTGAAGATGTACTCGTAGG-3'
38215	Forward
Munc13-1_E52K_F	5'-GCTGGGAGCAGGACTTCATGTTTAAGATCAACCGCC-3'
38216	Reverse
Munc13-1_E52K_R	5'-GGCGGTGATCTTAAACATGAAGTCCTGCTCCCAGC-3'
38656	Forward
Munc13-1_R812Q_F	5'-GTCGGGCGCCATTCAGCTTCACATCAGTG-3'
38657	Reverse
Munc13-1_R812Q_R	5'-CACTGATGTGAAGCTGAATGGCGCCCGAC-3'

Reagent	Source
Agarose	Thermo Fisher Scientific
Ampicillin Sodium Salt	Sigma-Aldrich
Aqua-Poly/Mount	Polysciences
Adenosine 5'-triphosphate disodium salt hydrate (Na <sub>2</sub> ATP)	Sigma-Aldrich
Bovine Serum Albumin, lyophilized powder	Sigma-Aldrich
B-27 Supplement (50x), serum free	Thermo Fisher Scientific
Calcium chloride	Sigma-Aldrich
Creatine phosphate	Sigma-Aldrich
Creatine phosphokinase	Sigma-Aldrich
Dimethyl sulfoxide (DMSO)	Sigma-Aldrich
dNTPs (2.5 mM)	Bioline
Dulbecco's Balanced Salt Solution (DPBS), no calcium, no magnesium	Thermo Fisher Scientific
Dulbecco's Modified Eagle Medium (DMEM)	Thermo Fisher Scientific



Reagent	Source
Ethylenediaminetetraacetic acid (EDTA)	Sigma-Aldrich
Egtazic acid (EGTA)	Calbiochem/ Sigma-Aldrich
Fetal Bovine Serum, heat inactivated	Thermo Fisher Scientific
GelGreen Nucleic Acid Gel Stain	Biotium
Gel Loading Dye (6x)	Thermo Fisher Scientific
Geneticin Selective Antibiotic (G418 Sulfate)	Thermo Fisher Scientific
GeneRuler 1 kb DNA Ladder	Thermo Fisher Scientific
Gibco Normal Goat Serum	Thermo Fisher Scientific
Glucose monohydrate	Sigma-Aldrich
Glycine	Sigma-Aldrich
GlutaMAX Supplement	Thermo Fisher Scientific
Guanosine 5'-triphosphate sodium salt hydrate (NaGTP)	Sigma-Aldrich
Hanks' Balanced Salt Solution (HBSS), no calcium, no magnesium	Thermo Fisher Scientific
(HEPES) N-2-Hydroxyethylpiperazine-N'-2-ethane sulphonic acid	Carl Roth
Image-iT FX signal enhancer	Thermo Fisher Scientific
Kanamycin Sulfate Salt	Sigma-Aldrich
L-Cysteine, crystalline powder	Sigma-Aldrich
L-Glutamine (200mM, 100x)	Thermo Fisher Scientific
Lipofectamine 2000 Transfection Reagent	Thermo Fisher Scientific
Magnesium chloride	Sigma-Aldrich
MEM Non-Essential Amino Acids Solution (100x)	Thermo Fisher Scientific
Neurobasal-A Medium (NBA-A)	Thermo Fisher Scientific
Opti-MEM Reduced-Serum Medium	Thermo Fisher Scientific
Papain, Suspension (100 mg)	Worthington
Paraformaldehyde	Serva Electrophoresis
Penicillin-Streptomycin (10.000 U/ml)	Thermo Fisher Scientific
Phorbol-12,13-dibutyrate (PDBu)	Calbiochem
Poly-L-Lysine (PLL)	Thermo Fisher Scientific
Potassium chloride (KCl)	Merck
Sodium butyrate	Sigma-Aldrich

<b>Reagent</b>	<b>Source</b>
Sodium chloride (NaCl)	Merck
Sucrose	Sigma-Aldrich
Tetrodotoxin citrate	Tocris Bioscience
Triton X-100	Roche
Trizma hydrochloride	Sigma-Aldrich
Trypsin-EDTA (0.05 %), phenol red	Thermo Fisher Scientific
Trypsin inhibitor from chicken egg white	Sigma-Aldrich
UltraPure Agarose	Thermo Fisher Scientific
10x CutSmart Buffer	New England Biolabs, Inc.
10x Pfu Buffer Turbo	Agilent Technologies
10x T4 DNA Ligase Reaction Buffer	New England Biolabs, Inc.

<b>Recombinant DNA</b>	<b>Source</b>
pCRII-TOPO_Munc13-1_BstEII-PspXI	Dr. Noa Lipstein
pCRII-TOPO_Munc13-1_NheI-BstEII	Dr. Noa Lipstein
pF(syn)Wgrbn_Munc13-1_EGFP	Dr. Noa Lipstein

<b>Software</b>	<b>Source</b>
Adobe Illustrator 25.1	Adobe
Axograph 1.4.3	AxoGraph Scientific
Clampex 10.1	Molecular Devices
EndNote X9.3.3	Michael O. McCracken
FIJI-ImageJ 2.1.0	Open Source
GraphPad Prism 9.0.0	GraphPad Software, LLC
Igor Pro	Wavemetrics
Imaris 9.8.0	Oxford Instruments
Microsoft Excel & Word 16.54	Microsoft 365 Subscription
MultiClamp 700B	Molecular Devices
SeqBuilder Pro 17.0.2	DNASTAR, Inc.
Zen (Black Edition)	Carl Zeiss Microscopy

## 3 Methods

### 3.1 Molecular Biology

#### 3.1.1 Site-Directed Mutagenesis

Human patient specific variations were subcloned into a pCRII-TOPO vector containing either a 2 kb long sequence of the Munc13-1 WT rat cDNA flanked by the restriction enzymes NheI and BstEII or into a pCRII-TOPO vector encompassing a 1.5 kb long c-terminal segment of the Munc13-1 WT cDNA enclosed by the restriction enzymes BstEII and PspXI. The aforementioned pCRII-TOPO vectors served as template for the polymerase chain reaction and were chosen according to the respective position of the desired point mutation in the Munc13-1 WT DNA. Primers for inducing point mutations corresponding to the human patient mutations (listed under Materials → Oligonucleotides) were designed using the QuickChange Primer Design tool from Agilent<sup>1</sup> and orders were placed with the DNA Core Facility (AGCT Lab) that is based in our department. The PCR was run with the following components at the following conditions.

<u>PCR reaction mixture</u>		<u>PCR cycling program</u>
Template DNA (100ng)	– 1 µl	① 95 °C for 1 min
Forward Primer (5pmol)	– 2.5 µl	② 95 °C for 50 sec
Reverse Primer (5pmol)	– 2.5 µl	③ 56 °C for 50 sec
dNTPs (2.5 mM)	– 2 µl	④ 68 °C for 5 min
10x Pfu Buffer Turbo	– 5 µl	⑤ 18 cycles of step 2-4
Pfu Turbo Polymerase Cx	– 1 µl	⑥ 68 °C for 7 min
Double-distilled water (ddH <sub>2</sub> O)	– 36 µl	⑦ cooling at 12 °C
Total Volume	– 50 µl	

The PCR product was digested with 1 µl DpnI for 1.5 hours at 37 °C, whereby the non-mutated template was cleaved at its methylated sites, which are absent in the PCR amplified DNA.

---

<sup>1</sup> <https://www.agilent.com/store/primerDesignProgram.jsp>

### 3.1.2 Bacterial Transformation

1  $\mu$ l PCR product was transformed into 50  $\mu$ l ElectroTen-Blue bacteria that are particularly competent for electroporation. Bacteria were thawed on ice and incubated with DNA for about a minute. The transformation was performed with an electric pulse of 1.8 kV in a dry, precooled electroporation cuvette. Subsequently, bacteria were immediately resuspended in 1 ml LB-medium and kept at 37 °C while shaking at 900 rpm for 1 hour. Before spreading on an LB-agar plate with the suitable antibiotic for selection of positive clones, bacteria were spun down at maximum speed for 1 min to settle in the bottom of the tube. Two-thirds of the supernatant LB-medium was discarded, and the remaining LB-medium was resuspended with the sedimented bacteria and plated. Bacterial plates were kept at 37 °C overnight.

### 3.1.3 Bacterial Inoculation, DNA Amplification and Sequencing

Colonies emerging on an LB-agar plate that contains selection antibiotics are a sign of successful bacterial transformation. Nevertheless, it needs to be confirmed that the designed point mutations were successfully introduced by PCR. Therefore, single colonies were picked with sterile pipette tips and several tubes containing 3 ml LB-medium with antibiotic were inoculated with one colony each. Tubes were kept shaking at 37 °C and 210 rpm overnight (~16 hours). On the following day DNA was isolated using the Zyppy Plasmid Miniprep Kit as per manufacturer's instructions. DNA concentration was measured by pipetting 1  $\mu$ l elution onto a spectrophotometer, and 1.6  $\mu$ g DNA were handed over to the in-house DNA Core Facility for sequencing. Once the resulting sequences turned out as intended, DNA was amplified in larger amounts with the help of the Qiagen EndoFree Plasmid Maxi Kit.

### 3.1.4 Restriction Digest and DNA Gel Extraction

Unc13a rat DNA is a 5 kb long construct that is suboptimal for PCR based cloning. Hence, a part of its sequence was inserted into a pCRII-TOPO vector. After successful mutation, following abovementioned procedure, the mutant sequence was subcloned into a lentiviral vector denominated as pF(syn)Wgrbn\_Munc13-1\_EGFP. Subcloning was achieved by double-digesting 3  $\mu$ g DNA of both, the TOPO-vector containing the mutant Unc13a and the lentiviral vector containing the native Unc13a construct with the same restriction enzymes (NheI-HF 1 $\mu$ l/ $\mu$ g, BstEII-HF 1 $\mu$ l/ $\mu$ g, PspXI 2 $\mu$ l/ $\mu$ g) using the recommended quantity. 10x Cut Smart Buffer and

10x Bovine Serum Albumin were added and the reaction was topped up with ddH<sub>2</sub>O to a total volume of 200 µl. After keeping at 37 °C for 2 hours the digestion reaction was arrested through heat inactivation at 85 °C for 20 min. The digested DNA was loaded together with 6x Gel Loading Dye and 10 µl of 1 kb GeneRuler DNA Ladder was added to one column on a large 1 % agarose gel. DNA fragments were separated for 3 hours at 100 Volt. Since the gel was prepared with 5 µl GelGreen Nucleic Acid Gel Stain in 150 ml dissolved agarose, the DNA was illuminated with blue light preventing it from UV damage. The desired bands were cut out with a clean scalpel and cleaned up using the Bioline ISOLATE II PCR and Gel Kit.

### 3.1.5 Ligation

Two fragments were attained from the double digest, the lentiviral vector backbone and the insert that was restricted from the pCRII-TOPO vector. Before setting up a ligation reaction the gel extracted DNA concentration was measured. In a 20 µl reaction volume a 1:3 vector to insert molar ratio was used, which can be distinguished using the NEBioCalculator<sup>2</sup> tool. Additionally, 10x T4 DNA Ligase Buffer and 1 µl T4 DNA Ligase were added and the volume was filled to 20 µl with ddH<sub>2</sub>O. The tube containing the ligation mixture was placed on a cold water bath (~16 °C) overnight. To verify positive vector-insert ligation 1 µl of the ligation reaction was transformed into ElectroTen-Blue bacteria and colonies were picked for DNA amplification and sequencing.

## 3.2 Cell Biology

### 3.2.1 HEK293FT Cell Culture

HEK293FT are fast growing, easy-to-transfect cells optimized for lentivirus production. Cells were maintained in 15 cm culture dishes at 37°C with 5% CO<sub>2</sub> level and 95% humidity until reaching approximately 80-90% confluency. At this stage cells demand to be subcultured to remain viable. Therefore, after washing with PBS once, cells were treated with 0.05% Trypsin for a maximum of 5 min to detach from the culture dish and resuspended in at least double the amount of fresh culture media to neutralize the trypsin. Culture media composed of Dulbecco's Modified Eagle's Medium (DMEM), 10% FBS, 100 U/ml Penicillin/Streptomycin (P/S), 1% MEM Non-Essential Amino Acids (NEAA) and 1% L-Glutamine (2 mM) was supplemented with Geneticin (G418)

---

<sup>2</sup> <https://nebiocalculator.neb.com/#!/ligation>

for its antibacterial properties. The cell suspension was diluted according to the desired density and dispensed into new culture dishes.

### 3.2.2 Lentivirus Production with HEK293FT Cells

High viral titers were achieved with lower passage numbers of HEK293FT cells. Hence cells grown on 15 cm dishes with passage numbers up to P25 were trypsinized, then resuspended in 15 ml OptiMEM containing 10% FBS and seeded on a Poly-L-Lysin (PLL) coated dish to provide for solid attachment of the cells before proceeding with transfection on the following day. The PLL coating was performed for an hour at 37°C and dishes were washed twice with PBS prior to seeding cells. On the day of transfection 40 µg of recombinant DNA was aliquoted together with 16 µg of each Packaging and Envelope DNA in 6 ml OptiMEM. In parallel 60 µl Lipofectamine 2000 and 6 ml OptiMEM were premixed in a separate tube and both tubes were incubated for 5 min at room temperature after inverting the tubes several times. This preparation serves one 15 cm dish. The following steps were conducted in a laboratory with declared biosafety level 2 (S2), a prerequisite when producing genetically modified organisms (GMOs). Both aliquots were mixed up under the fume hood in the S2 lab. An hour later the DNA-Lipofectamine mixture was poured on top of the HEK293FT cells, and the cells were placed at 37°C for a further 6 hours until medium change. Therefore, old medium was replaced by 20 ml of DMEM with 2% FBS, 1% P/S and 10mM Sodium butyrate and virus was harvested 48 hours later. Medium was collected in a 50 ml tube and centrifuged for 5 min at 2000 rpm and 4°C. Using a Luer-Lok syringe the supernatant was filtered through a 0.45 µm filter and spun in a 100 K Amicon® centrifugal filter unit for 10 min at 3500 rpm and 4°C. The flow-through was discarded and the virus collected in the Amicon tube was washed with 10-15 ml Neurobasal medium twice at 4000 rpm and 4°C for about 15-20 min. Then followed two washing steps with TBS keeping the same settings for as long as the virus was concentrated enough. Per 15 cm dish an amount of 250 µl was aimed and flash-frozen in liquid nitrogen after being aliquoted as per requirement. The virus was kept at -80°C for longer-term storage.

### 3.2.3 Astrocyte Microisland Culture

6-well culture plates seeded with astrocytes forming shapes of small circular islands were produced for the purpose of growing primary single hippocampal neurons on top that form synapses onto themselves and thus were called autaptic neurons. The maintenance and continuous improvement

of this method was kindly performed by Prof. Dr. Jeong Seop Rhee, Dr. ChungKu Lee, Dr. Hong Jun Rhee as well as Anja Günther and Jieun Oh. The corresponding steps for producing such astrocytic microisland cultures were performed as described in Burgalossi *et al.* (Burgalossi et al., 2012).

### 3.2.4 Autaptic Mouse Hippocampal Neuron Culture

Munc13-1/2 double-knockout mice were taken out of the womb of the mother at embryonic day 18 by caesarean section immediately after sacrificing the mother through cervical dislocation. The obtained litter was examined for double-knockout mice, which were identified by their physical appearance characterized by spinal curvature and completely absent reflexes. For confirmation of the genotype, a tail biopsy was provided to the in-house 'AGCT lab' for genotyping.

Autaptic hippocampal neuron cultures were prepared precisely as stated in Burgalossi *et al.* (Burgalossi et al., 2012). The seeding density of hippocampal neurons was increased to 3500-4000 neurons per well. On the second day *in vitro* (DIV) three 6-well plates were infected with Munc13-1 wild type and Munc13-1 mutant virus resulting in 9 wells per treatment condition respectively. Between DIV 12 to 15 cultures were subjected to electrophysiological measurements. Additionally, cultures were fixed for immunocytochemistry at DIV 13.

### 3.2.5 Electrophysiological Measurements

Whole cell voltage clamp recordings were performed to measure current changes across the autaptic neuronal cell membranes. The electrophysiological setup enabling such measurements comprised an inverted microscope (Zeiss) for visualization of the cells. Attached were the electronic devices Axon 700B amplifier for recording and amplifying the signal controlled by the MultiClamp 700B software and the Axon Instrument digitizer Digidata 1440A device responsible for analogue to digital conversion that displayed and recorded the signal in the Clampex 10.1 software. Borosilicate glass pipettes with an outer diameter of 1.5 mm were pulled at the micropipette puller P-97 and employed with a pipette resistance ranging between 2.3-3.3 M $\Omega$ , which by experience served best to minimize series resistance and obtain a gigaseal in the context of our autaptic neuronal cell culture experiments. The patch-pipette solution consisted of 136 mM KCl, 17.8 mM HEPES, 1 mM EGTA, 4.6 mM MgCl<sub>2</sub>, 4 mM NaATP, 0.3 mM Na<sub>2</sub>GTP, 15 mM creatine phosphate, and 5 U/ml phosphocreatine kinase (315-320 mOsmol/liter), pH 7.4. Neurons between 12-16 days *in vitro* (DIV) were depolarized from -70 mV holding potential to 0

mV for 1 ms and evoked EPSCs were recorded employing a sampling rate of 10 kHz and a 3 kHz Bessel filter. EPSCs were only recorded with a series resistance ( $R_s$ ) below 12 M $\Omega$  with a 50% correction of the  $R_s$  compensation. During electrophysiological recording sessions, cells were permanently perfused with extracellular solution (140 mM NaCl, 2.4 mM KCl, 10 mM HEPES, 10 mM Glucose, 4 mM CaCl<sub>2</sub>, 4 mM MgCl<sub>2</sub> (320 mOsmol/liter, pH 7.3)) using a custom-built fast flow system that additionally allowed for rapid application and exchange of different pharmacological solutions. Estimates of the RRP were achieved by a 7-second-long application of 500 mM hypertonic sucrose diluted in extracellular solution. To evaluate short-term plasticity, each cell underwent a series of depolarizations at 1, 10 and 40 Hz frequency for 10 s, 3 s and 1 s respectively. Miniature EPSC recordings were obtained by application of 300 nM tetrodotoxin (TTX) for a period of 100 s. As final treatment cells were subjected to 1  $\mu$ M PDBU application for 1 min.

### 3.2.6 Immunocytochemistry

Protein quantification analysis was performed through immunostaining of autaptic hippocampal cultures with the protein of interest and corresponding markers for relative expression analysis. Therefore, lentivirus treated autaptic hippocampal neuron samples were fixed at DIV13. One wash with PBS was carried out in the S2 lab and the following steps were conducted in the S1 area. Samples were washed with PBS again and incubated in 4% paraformaldehyde (PFA) for 18 min with gentle agitation. After another wash with PBS samples were treated with 50mM Glycine for 10 min to quench any possible background noise from unreacted PFA residues. Finally, samples were washed thrice with PBS and stored in a large quantity of PBS (3-4 ml/6-well), tightly wrapped in parafilm, at 4°C for several weeks until further use. Alternatively, the immunostaining protocol was continued. Prior to permeabilization samples were treated with 4 drops of Image-iT FX signal enhancer in 1.5-2 ml PBS per 6-well and kept shaking for 20 min. Permeabilization was carried out with 0.1% Triton X-100 and 2.5% normal goat serum (NGS) diluted in PBS for 30 min at gentle shaking. Next, blocking was performed involving two washes with 2.5% NGS in PBS for a total 15 min. The primary antibodies were diluted in blocking solution and coverslips were mounted upside down on 150  $\mu$ l antibody solution placed on parafilm and kept for 2.5 hours at room temperature (RT) or overnight at 4°C, both in a wet chamber to prevent drying up the samples. Coverslips were washed thrice with 0.1% Triton X-100 and 2.5% NGS in PBS and subsequently mounted upside down in 150  $\mu$ l secondary antibody solution in a dark, wet chamber for 45 min at RT. Then followed five washing steps with 0.1% Triton X-100 and 2.5% NGS in



PBS and two washing steps in PBS each lasting 2-5 min and protected from light. At last, the coverslips were cut in half with the help of a diamond pen. Before mounting on a glass slide, coverslip pieces were dipped in double distilled water and the excess water was allowed to drip off on paper tissue. Two coverslip halves were carefully mounted on one glass slide by lowering each on a drop of Aqua-Poly/Mount in an angular fashion avoiding air bubble formation.

## 3.3 Confocal Fluorescence Microscopy

### 3.3.1 Image Acquisition

Images were acquired with the confocal laser scanning microscope Zeiss LSM 880 for high resolution in optical sections in all three dimensions (x, y and z). Visualization of images happened in the Zen black software. Overview images were generated using the 10x objective and single neuron images were then obtained using the 40x oil objective with a numerical aperture (NA) of 1.4 in combination with the Argon laser (405 nm, 488 nm), Diode-pumped solid-state laser (DPSS) (561 nm) and Helium-neon laser (HeNe) (633 nm) for excitation of four different wavelengths to detect the four different fluorophores tagged to the structures that were labelled in the samples. First, the light path configuration was set up by choosing the detectors and their corresponding spectral range for excitation and emission. Photomultiplier tube detectors were chosen for the far-red spectrum of light excitation at 633 nm and the blue spectrum of light excitation at 405 nm. For excitation at 488 nm and 561 nm, a sensitive gas detector allowing for a wide detection range was split into two parts, but both parts were bound to the same voltage for the gain setting. All four excitation wavelengths were categorized in channels and optimized individually with respect to the parameters laser power and gain, which were additionally adjusted in all focal planes to avoid over saturation of the signal. The following settings were specified for image acquisition. A frame size of 900x900 was chosen according to the Rayleigh criterion to optimize pixel size to 240 nm with the NA of 1.4 in use. Each line was scanned twice bidirectionally at speed 9 and produced an 8-bit image. Z-stacks with a step size of 0.41 microns covering the neuron from top to bottom were acquired. Neurons exceeding the field of view with their processes were imaged with the help of the tile scan function by creating 10% overlap and stitched afterwards.

### 3.3.2 Image Analysis

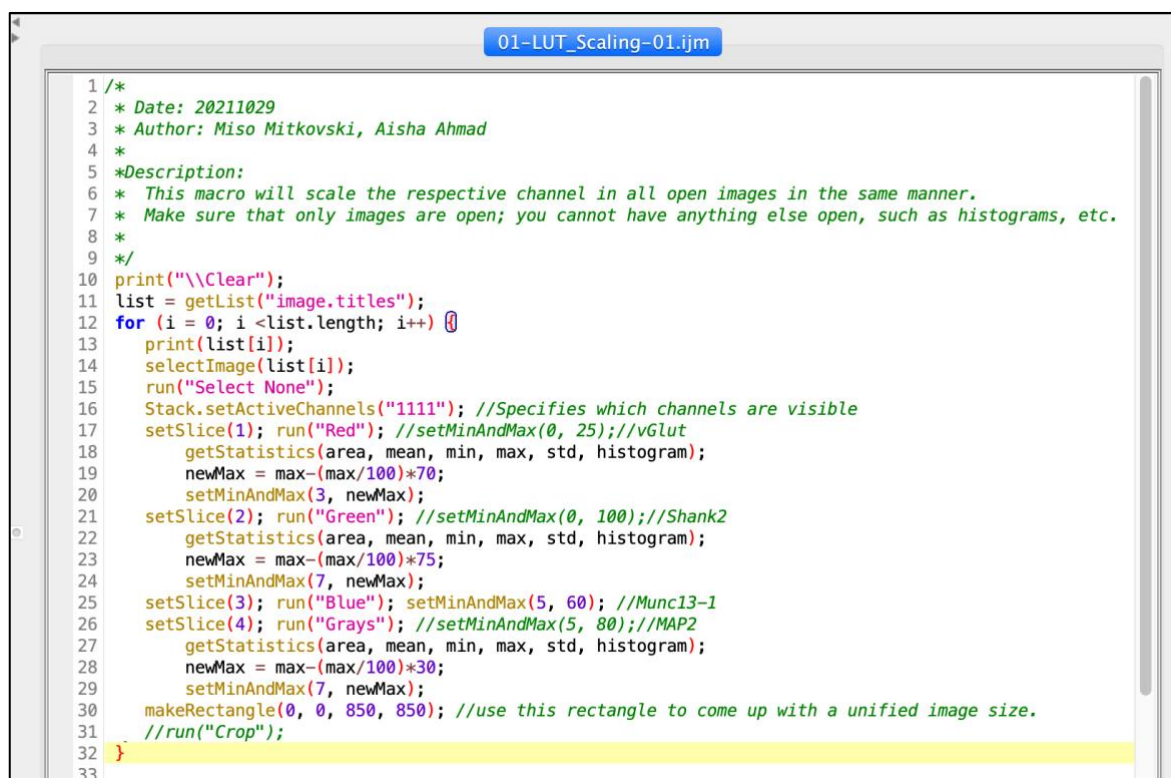
Multicolour images of samples from six different treatment conditions labelled with four different antibodies were analyzed in the Imaris 9.8.0 software. Surfaces were created for each antibody staining after thresholding and applying a set of surface creation parameters (see Table 1). Colocalization of VGLUT1 and Shank2 punctate surfaces, occurring within the MAP2 surface area that visualizes the neuronal soma and dendrites, accounted for the number of synapses. In a second step, the VGLUT1 and Shank2 overlap was defined as one surface that was overlapped with the EGFP surface to quantify the colocalizing puncta that enumerate the amount of Munc13-1 expressing synapses. The final readout was provided as the number of objects on a per cell basis. Graphs and statistical analysis were accomplished using GraphPad Prism9.0.0.

**Table 1:** Surface Creation Parameters defined in Imaris.

Surface Creation Parameters	MAP2	VGlut1	Shank2	EGFP/ M13-1	VGlut1_Shank2	Munc13-1 VGlut1_Shank2
	Enable Region Growing					
	Enable Shortest Distance					
Source Channel	4	1	2	3	1	3
	Enable Smooth					
Surface Grain Size [ $\mu\text{m}$ ]	0,2	0,25	0,2	0,2	0,25	0,2
	Enable Eliminate Background					
Diameter of Largest Sphere [ $\mu\text{m}$ ]	1	0,25	0,25	0,25	0,25	0,25
Manual Threshold Value	2	0.35	2.5	3	0.35	3
Region Growing Estimated Diameter [ $\mu\text{m}$ ]	2,36	0,3	0,3	0,3	0,3	0,3
'Quality' above automatic threshold (AT) or above	AT	1	1	1	1	1
'Volume' above [ $\mu\text{m}^3$ ]	0,02	0,03	0,03	0,03	0,03	0,03
Shortest Distance to MAP2 below	-	0,5	0,5	0,5	0,5	0,5
Shortest Distance to Shank2/VGlut1+Shank2 below	-	-	-	-	$1\text{e}^{-10}$	$1\text{e}^{-10}$

### 3.3.3 Image Processing

The representative immunostained images in the results (see section 3.1.5) have been processed in FIJI and assembled in Adobe Illustrator. For each image, the maximum projection of the acquired z-stacks was adjusted for the lower and upper limits of the display range in the brightness and contrast tool in each channel and equally across images to subtract background fluorescence arising from nonspecific astrocytic staining. Therefore, the following macro was employed to uniformly process all images and apply the same lookup table (LUT) to each channel. Additionally, the images were cropped to  $850 \mu\text{m}^2$ , converted to RGB format and a  $20 \mu\text{m}$  scale bar was added. On the whole neuron image, a smaller inset of uniform size ( $170 \mu\text{m}^2$ ) was positioned in an area with prominent dendritic processes and was cropped and scaled up five times to match the size of the whole neuron image. The inset is either shown as a triple channel image lacking the Munc13-1 signal or as a single channel image displaying only the Munc13-1/EGFP signal, which was modified to the LUT called Cyan Hot with added calibration bar to exemplify the signal intensity differences in the different mutants. The scale bar for the inset images was set to  $5 \mu\text{m}$ .



```

1 /*
2  * Date: 20211029
3  * Author: Miso Mitkovski, Aisha Ahmad
4  *
5  *Description:
6  * This macro will scale the respective channel in all open images in the same manner.
7  * Make sure that only images are open; you cannot have anything else open, such as histograms, etc.
8  *
9  */
10 print("\Clear");
11 list = getList("image.titles");
12 for (i = 0; i <list.length; i++) {
13     print(list[i]);
14     selectImage(list[i]);
15     run("Select None");
16     Stack.setActiveChannels("1111"); //Specifies which channels are visible
17     setSlice(1); run("Red"); //setMinAndMax(0, 25); //vGlut
18     getStatistics(area, mean, min, max, std, histogram);
19     newMax = max-(max/100)*70;
20     setMinAndMax(3, newMax);
21     setSlice(2); run("Green"); //setMinAndMax(0, 100); //Shank2
22     getStatistics(area, mean, min, max, std, histogram);
23     newMax = max-(max/100)*75;
24     setMinAndMax(7, newMax);
25     setSlice(3); run("Blue"); setMinAndMax(5, 60); //Munc13-1
26     setSlice(4); run("Grays"); //setMinAndMax(5, 80); //MAP2
27     getStatistics(area, mean, min, max, std, histogram);
28     newMax = max-(max/100)*30;
29     setMinAndMax(7, newMax);
30     makeRectangle(0, 0, 850, 850); //use this rectangle to come up with a unified image size.
31     //run("Crop");
32 }
33

```

Figure 4: FIJI script for image processing.

## 4 Results

### 4.1 Functional Assessment of Human Patient-Specific Variants

The major aim of my PhD was to unravel the cell biological mechanisms underlying a brain disorder caused by variations in the UNC13A gene. For that, I characterized the functional differences in synaptic transmission in neurons expressing the Munc13-1 WT protein or a mutated version of the Munc13 protein carrying a disease-associated variant.

At the beginning of this project, two case studies of patients carrying mutations in the human UNC13A gene and associated clinical illnesses have been reported. (Engel et al., 2016; Lipstein et al., 2017) The first case was a homozygous mutation truncating Munc13-1 at amino acid 102 and leading to a full loss of the protein reported by Engel *et al.*, which was diagnosed as a fatal syndrome originating from diverse clinical manifestations, including cortical hyperexcitability, microcephaly and myasthenia. Direct interaction with the patient enabled a clinical microelectrode assay to evaluate deficits in the patients neuromuscular transmission, indicating severely reduced spontaneous release frequency and a substantial depletion of the readily releasable pool by 90 %. The second study, led by Nils Brose and Noa Lipstein from the Molecular Neurobiology Department at the Max Planck Institute for Experimental Medicine (Lipstein et al., 2017), identified a *de novo* human UNC13A patient variant (Proline 814 to leucine; P814L), and utilized the *in vitro* autaptic neuronal culture system to functionally assay the implications of the variation on synaptic transmission. Hippocampal glutamatergic Munc13-1/2 DKO neurons were rescued using lentiviral particles carrying the cDNA encoding the Munc13-1 WT protein or the disease-related Munc13-1 protein variant. Assessment of the functional properties of neurons expressing Munc13-1 variant in comparison to the Munc13-1 WT protein was achieved by whole-cell voltage clamp electrophysiology. This methodology also served as experimental paradigm for this project. It was adopted as it represents a standardized analysis of a large array of neurotransmitter release properties, has been successfully used in multiple structure-function studies for characterizing presynaptic protein function, and as an approach that would produce a functional readout comparable to that documented in Lipstein *et al.* Harnessing the autaptic neuronal culture system, I characterized several UNC13A variations that were identified by our collaboration partners Reza Asadollahi and Dr. Anita Rauch (Institute of Medical Genetics, Zurich) in human patients, linking variant protein structure with potential perturbances in the variant protein function. My ultimate

aim was classifying these variants either as putative risk factors for pathogenicity, or merely as rare polymorphisms, and, amongst the pathogenic variants, identify convergent mechanisms at the cellular level.

### 4.1.1 Munc13-1<sup>G808D</sup> Patient Variant

#### 4.1.1.1 Genetics and Clinical Data

The following group of six patients were identified to carry a *de novo* single-nucleotide exchange in their UNC13A sequence, resulting in a variation of amino acid 808 of the Munc13-1 protein. In four patients the nucleotide exchange 2423G>A results in the exchange of a glycine (G) residue by an aspartic acid (D) residue. Patients five and six carry an exchange from G to valine (V) (2423G>T) or to a cysteine (C) (2422G>T), respectively (Figure 5 B). the classification of these exchanges as *de novo* variants, relies on the finding, that these variations were not found at their parents' genome based on whole-exome sequencing.

Figure 5 A illustrates the Munc13-1 protein domain structure. A dashed box roughly outlines the region that is shown as three-dimensional protein structure in Figure 5 C, showcasing amino acid G808 in a loop (in orange) connecting the C2B domain (green) and the MUN domain (responsible for syntaxin-1 binding in blue). Clinical diagnosis of the patients revealed a diverse spectrum of neurological and neurodevelopmental symptoms, of which the major symptoms are listed in Figure 5 D. The patients exhibit intellectual disability and developmental delay accompanied by abnormal behaviour. Additionally, motor function is compromised, which manifests in decreased muscle tone (hypotonia), tremor and occasionally observed musculoskeletal abnormalities. The incidence of seizures and abnormal electroencephalogram (EEG) recordings is witnessed concomitant to abnormal cerebral imaging. It is noteworthy that the clinical picture of all six abovementioned patients is strikingly similar and resembles the symptoms known from the P814 patients and similarly found overlapping in an additional patient that carries an AA exchange from lysine (K) to glutamic acid (E) at position 811, which is sandwiched between the G808 and P814. Movies of the patients with the P814L<sup>3</sup> and K811E<sup>4</sup> mutation can be found online.

---

<sup>3</sup> <https://www.jci.org/articles/view/90259/sd/2>

<sup>4</sup> <https://sites.google.com/view/rozakrecioch>

Sequence alignment shown in Figure 5 E reveals the evolutionary conservation of the affected glycine in human, rat, fruit fly and in the nematode *C. elegans*, as well as among all mammalian Munc13 isoforms. With the genetic and clinical data at hand, I set to determine whether the G808 patient variant plays a role in the etiology of neurological disorder in the patients. Of note, since we first became acquainted with a patient carrying the glycine to aspartic acid mutation G808D, cloning was designed to mimic this particular mutation resulting in the exchange of glycine to aspartic acid in the Munc13-1 WT protein instead of valine or cysteine.

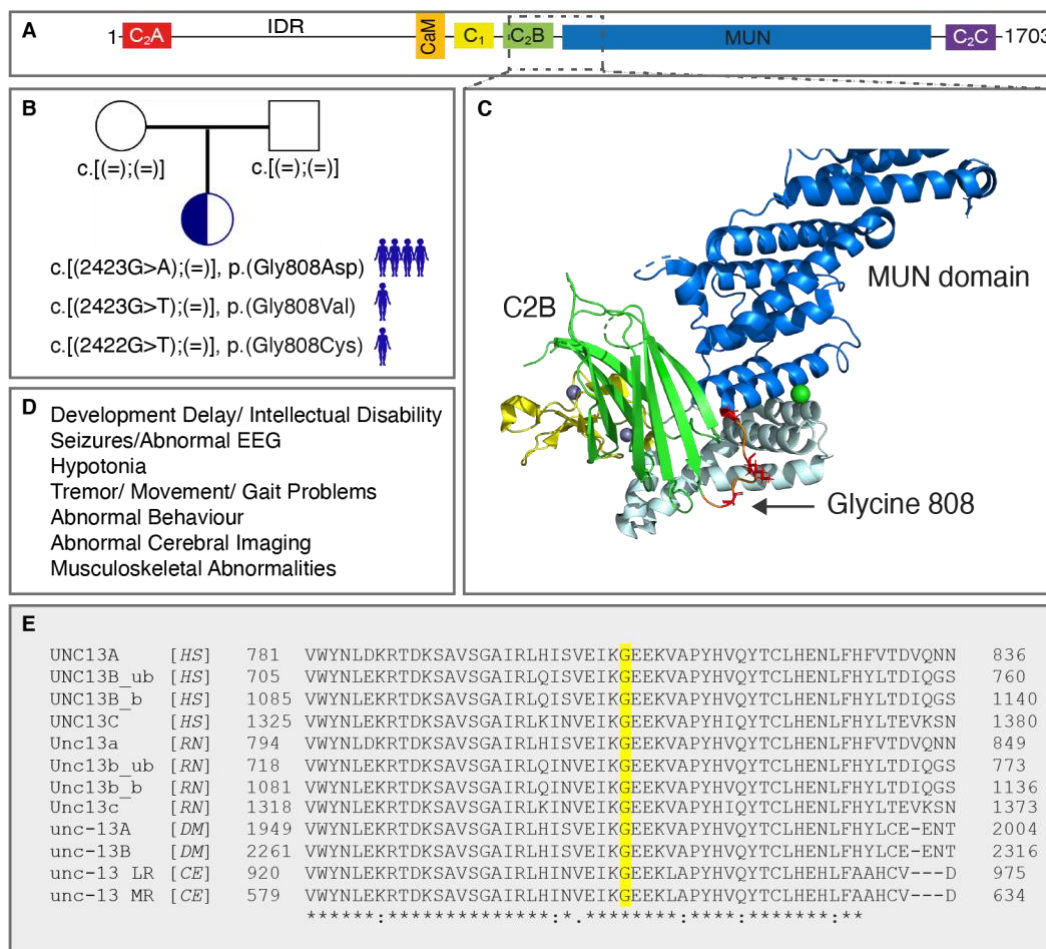


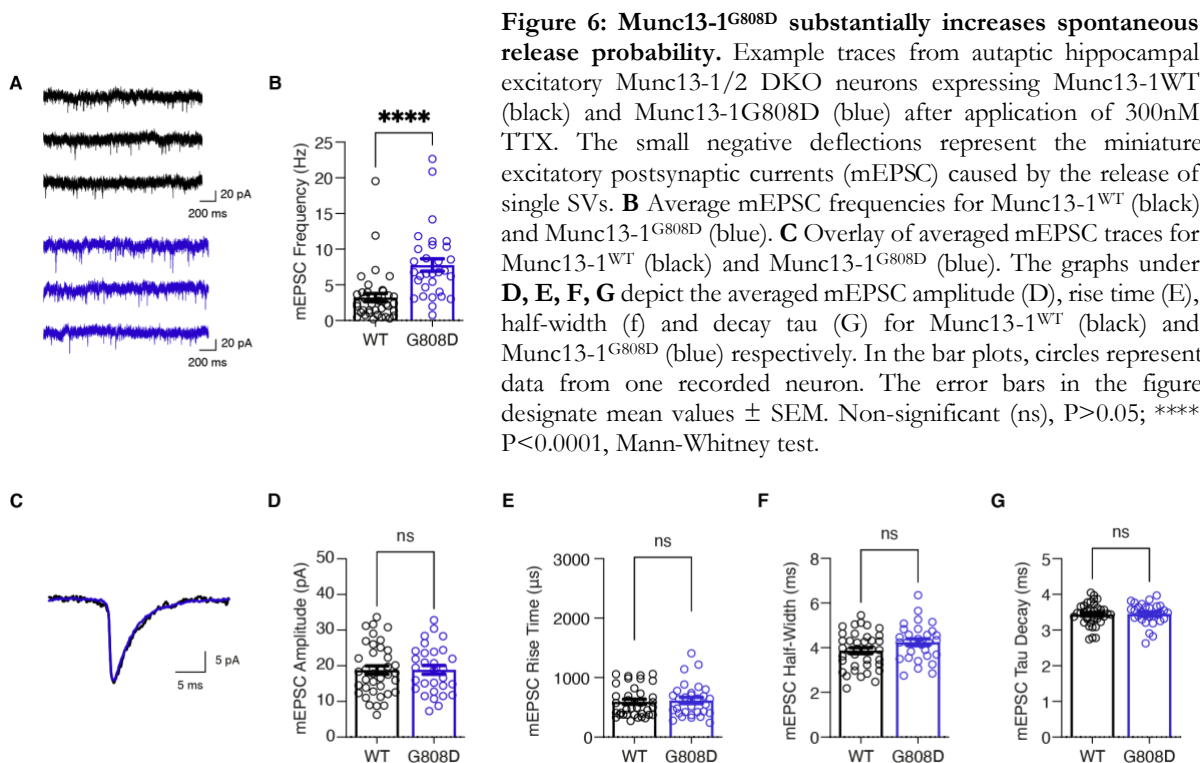
**Figure 5: The genetic and clinical spectrum of human *UNC13A* patient carrying a G808D variant. A** Schematic of the Munc13-1 domains structure. A dashed box labels the region encompassing the patient mutation G808D. **B** A pedigree chart showing the inheritance pattern of the variation: the parents have two unaffected alleles, whereas the child carries a *de novo* amino acid mutation at position 808. This inheritance pattern is shared in all six related patients. The mutated nucleotides with their respective positions are provided in square brackets. **C** Munc13-1 protein structure of the region indicated by the dashed box, adapted from PDB: 5UE8 (Xu et al., 2017). The arrow points to the affected AA, in the linker region between the MUN domain (blue) and the C2B domain (green). **D** Collection of common clinical symptoms of patients carrying the G808D variant. **E** Sequence alignment of the AA residues surrounding the glycine at position 808 is depicted for the four isoforms UNC13A, UNC13B\_ub, UNC13B\_b and UNC13C and across different species: human (HS), rat (RN), drosophila (DM) and *C. elegans* (CE). The relevant glycine is highlighted in yellow. Asterisks (\*) indicate fully conserved residues, a colon (:) indicates conservation of residues with strongly similar properties and period (.) indicates conservation of residues with weakly similar properties.

#### 4.1.1.2 Munc13-1<sup>G808D</sup> Boosts Spontaneous Release

The role of the patient-specific variant G808D was investigated in primary mouse hippocampal excitatory neurons that served as a model for human physiology. To achieve an unbiased functional readout for the Munc13-1 variation, all experiments in this study were conducted on a null background, meaning the neurons were lacking both Munc13-1 and Munc13-2 isoforms and obtained from the Munc13-1/2 double knockout (DKO) mouse brain. Since these mice exhibit no spontaneous and action potential (AP) evoked release, they die immediately after birth. Hence, they were isolated from a pregnant mouse on embryonic day 18 and their hippocampi, containing largely glutamatergic/excitatory neurons, were used for autaptic cultures. The hippocampal cells were seeded at very low density on an astrocyte microisland culture to ensure that single cells form synapses onto themselves. These neurons were infected with lentivirus containing rat Munc13-1 cDNA to rescue the genetically silenced neurons with exogenous Munc13-1 expression. In the context of this study, the relevant patient-specific point mutation was introduced in the rat Munc13-1 cDNA exchanging its amino acid G821, which is the corresponding glycine to the G808 found in human patients. This practice is valid because the rat cDNA shares 95% resemblance to the human Munc13-1 cDNA and is therefore believed to be functionally well conserved. For the benefit of the reader and to avoid confusion, the AA are designated according to the human sequence throughout the study.

The effect of the Munc13-1<sup>G808D</sup> mutation on synaptic transmission was evaluated recording spontaneous and evoked activity from the infected cells under whole-cell voltage clamp conditions. To allow for comparative functional analysis, Munc13-1/2 DKO neurons were infected with Munc13-1<sup>WT</sup> and Munc13-1<sup>G808D</sup> and WT- and variant-expressing neurons were recorded alternately. Activity was first examined at rest, which in scientific terms is also referred to as spontaneous release. Under unstimulated conditions, neurons are known to exhibit release of single SVs, leading to miniature excitatory postsynaptic currents (mEPSC). This release is considered spontaneous, independent of AP, and whether Ca<sup>2+</sup> influx is required for this type of release is highly debated. In the culture, the administration of tetrodotoxin (TTX) prevents AP firing by obstructing voltage-gated Na<sup>+</sup> channels. Two main parameters are considered in these recordings. Firstly, mEPSC frequency reflects the probability of single SV release events at the presynapse as well as providing a proxy for the number of synapses. Secondly, the mEPSC amplitude represents the neurotransmitter amount filled in a single SV and serves as a measure for postsynaptic receptor density. Lastly, the average mEPSC kinetics provides knowledge on the type of postsynaptic receptors available.

Munc13-1/2 DKO neurons rescued with Munc13-1<sup>G808D</sup> exhibit markedly increased mEPSC frequencies ( $P < 0.0001$ ) on average compared to DKO neurons rescued with the Munc13-1<sup>WT</sup> protein (Figure 6 A, B). In contrast, average mEPSC amplitudes in DKO neurons rescued with either WT or mutant protein were comparable (Figure 6 D). Evaluation of the kinetic parameters, including the rise time (20 % - 80 %), half-width (50 %) and decay time of the averaged mEPSC indicated no change (Figure 6, E-G), as seen by the nearly identical overlay of exemplary mEPSC average traces (Figure 6 C).



#### 4.1.1.3 Munc13-1<sup>G808D</sup> Increases the Vesicular Release Probability

The observed increase in mEPSC frequency revealed boosted probability of spontaneous SV fusion events in quiescent neurons expressing the Munc13-1<sup>G808D</sup> variant. This result attracted attention and induced further interest in studying the properties of evoked synaptic transmission. Neuronal depolarization from -70 mV to 0 mV for 1 ms evoked a single AP that invaded the presynaptic compartment, led to the release of neurotransmitter, and induced an excitatory postsynaptic current (EPSC), reflecting the AP- and  $\text{Ca}^{2+}$ -induced release of multiple SVs fusing with the plasma membrane. Evoked EPSCs amplitudes provide compound estimates of synaptic strength, reflecting the number of released SVs, their probability of release, the number of synapses and the number of postsynaptic receptors. EPSC kinetics reflect the properties of SV fusion and



the postsynaptic receptor types. DKO neurons rescued by the Munc13-1<sup>G808D</sup> protein elicited by trend larger EPSC amplitudes when depolarized ( $P>0.05$ ) in comparison to neurons expressing the Munc13-1<sup>WT</sup> (Figure 7 A, B). EPSC rise time (20 % - 80 %) was not altered between WT and mutant protein expression in DKO neurons (Figure 7 C), however, the 50% half-width of evoked EPSCs was significantly broader in Munc13-1<sup>G808D</sup> expressing neurons ( $P<0.001$ , Figure 7 D).

Munc13s are priming proteins, and their activity is critical for the generation of the readily-releasable pool (RRP). The number of primed, or readily-releasable SVs, can be evaluated by integrating the current elicited by the application of hypertonic sucrose solution (500 mM, seven seconds), which released all RRP vesicles at once. It is important to note that the acquisition of this parameter is carried out under  $Ca^{2+}$ -independent conditions. As is shown in Figure 7 E & F, the average pool size of Munc13-1<sup>WT</sup> and Munc13-1<sup>G808D</sup> expressing neurons are similar.

After obtaining estimates of RRP size and initial EPSC amplitudes, it is possible to calculate the probability of vesicular release (pVR; Figure 7 G). pVR is calculated by dividing the average EPSC current by the sucrose-evoked current and reports the percentage of SVs that fuse during a single AP, a measure of synaptic strength. The average pVR was dramatically increased in neurons expressing the Munc13-1<sup>G808D</sup> variant ( $P<0.0001$ ) compared to neurons expressing Munc13-1<sup>WT</sup>.

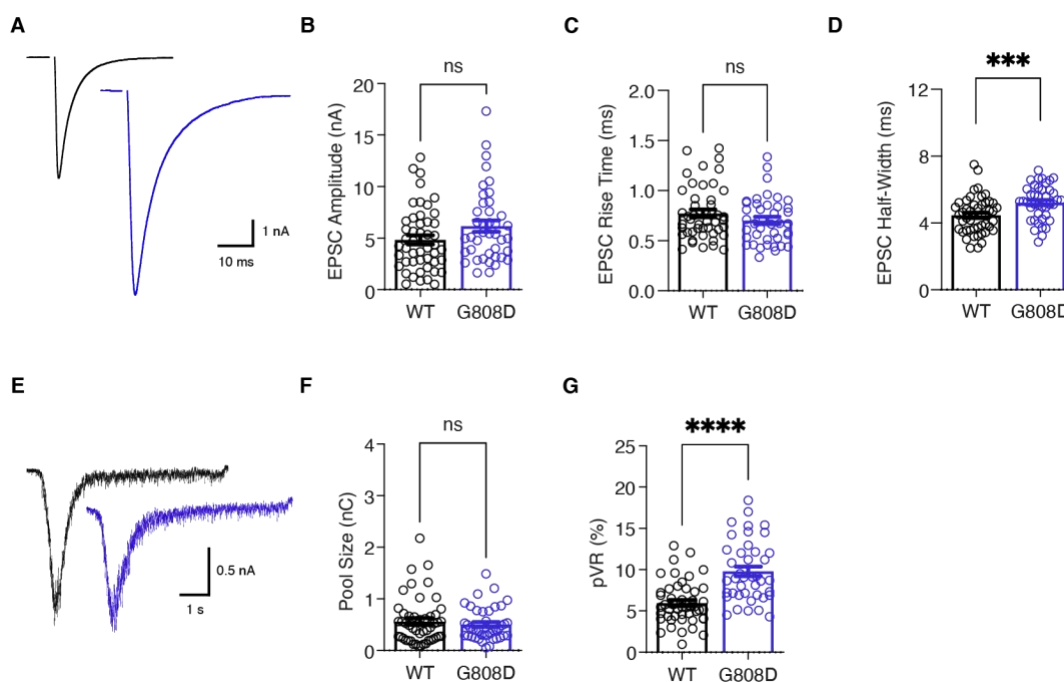


**Figure 7: Munc13-1<sup>G808D</sup> increases synaptic strength and vesicular release probability.** Recordings from autaptic hippocampal excitatory Munc13-1/2 DKO neurons expressing Munc13-1<sup>WT</sup> (black) and Munc13-1<sup>G808D</sup> (blue). (A) representative initial EPSC traces. B A bar graph illustrating average EPSC amplitudes plotted as mean  $\pm$  SEM. Initial EPSC amplitude of each neuron is illustrated by a circle. EPSC kinetic parameters: rise time (C) and half-width (D), are plotted as mean  $\pm$  SEM. E Sucrose-induced (500 mM) release of the RRP of SVs is exemplified with representative traces and (F) average RRP size is plotted as mean  $\pm$  SEM, while individual data is shown as circles. (G) The graph displays the average vesicular release probability (pVR) in neurons expressing Munc13-1<sup>WT</sup> (black) and Munc13-1<sup>G808D</sup> (blue). ns =  $P>0.05$ , \*\*\*  $P<0.001$ , \*\*\*\*  $P<0.0001$ , Mann-Whitney test.

#### 4.1.1.4 Munc13-1<sup>G808D</sup> Enhances Short-Term Synaptic Depression

High vesicular release probability in Munc13-1<sup>G808D</sup> was documented via two measures under resting conditions: by documentation of a significant increase in mEPSC event frequency, and the increased pVR. To test for activity-dependent modulation of neurotransmission during periods of sustained activity, and whether enhanced initial synaptic strength would affect activity-dependent synaptic activity, I measured the dynamics of neurotransmission under high-frequency stimulation conditions, by inducing AP trains at 10- and 40 Hz. Multiple processes in synaptic transmission are modulated during activity: the elevation in presynaptic Ca<sup>2+</sup> concentrations leads to the depletion of the RRP, an increase in their pVR, and increased rate of RRP replenishment (Zucker and Regehr, 2002).

Typically, WT neurons respond to high-frequency activity with a brief facilitation, followed by a reduction of the EPSC amplitudes during release, a phenomenon called short-term synaptic depression (STD). STD represents, in part, the balance between the depletion of readily-releasable SVs, and the rate of their replenishment, and Munc13s are known to counteract this depletion, as their activity is boosted by the increase in Ca<sup>2+</sup> to support the replenishment of new SVs (Lipstein et al., 2021; Lipstein et al., 2013). Showcased in Figure 8 A & C are example traces for 10 Hz and 40 Hz stimulus trains, recorded in neurons expressing Munc13-1<sup>WT</sup> and Munc13-1<sup>G808D</sup>. The normalized EPSC amplitudes in the graphs plotted in Figure 8 B & D show enhanced and faster short-term depression in DKO neurons expressing the variant Munc13-1<sup>G808D</sup>. This increased depression is in concert with increased synaptic strength under basal conditions, as a negative relationship has been shown to exist between these two parameters (i.e., increased pVR results in stronger synaptic depression, and vice versa). This increased depression can also be due to a reduced replenishment rate of newly-recruited SVs caused by the G808D mutation, and more experiments are necessary to corroborate such a mechanism.

Finally, I quantified the recovery after the train, by measuring the activity of the neuron starting two seconds after the end of the high-frequency train, through a 0.1 Hz stimulation (Figure 8 B, 4D, right part). WT neurons typically respond with augmentation following the train, but the mechanisms that lead to this augmentation are poorly studied *in vitro*. During the train, SVs are depleted, meaning that at the end of the train, the RRP is partially depleted. Residual Ca<sup>2+</sup> that accumulates during the train, increases pVR and also the rate of SV replenishment. After the train, residual Ca<sup>2+</sup> is still elevated, but quickly returns to baseline. The balance between the decay of pVR back to baseline and the replenishment of the SV pool will determine the degree of

augmentation. My data indicated that neurons expressing Munc13-1<sup>G808D</sup> exhibit a lower degree of augmentation after the train.

Finally, we challenged the neurons with PDBu, a diacylglycerol analog that activates Munc13s via binding to their C1 domain. Exposure to PDBu rapidly increases the evoked EPSC amplitude, by increasing pVR. In DKO neurons expressing the variant Munc13-1<sup>G808D</sup>, PDBu-induced potentiation was significantly smaller than in Munc13-1<sup>WT</sup> expressing neurons (Figure 8 E), which is in conjunction with the higher initial pVR – if the pVR is already increased under basal conditions, the effect of PDBu is expected to be smaller, due to a ceiling effect.

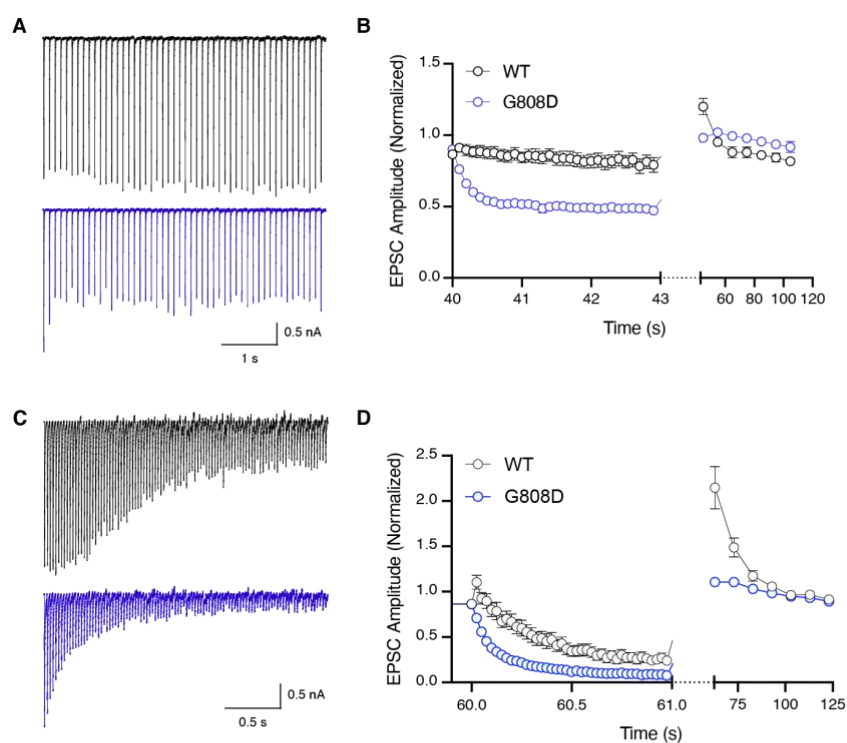


**Figure 8: Enhanced depression in Munc13-1<sup>G808D</sup> expressing neurons.**

Example traces of stimulated autaptic hippocampal excitatory Munc13-1/2 DKO neurons expressing Munc13-1<sup>WT</sup> (black) and Munc13-1<sup>G808D</sup> (blue) with AP trains of (A) 10 Hz frequency and (C) 40 Hz frequency. Normalized EPSC amplitudes are plotted for (B) 10 Hz and (D) 40 Hz frequency stimulation respectively, followed by continuous 0.1 Hz stimulation. E Potentiation after stimulation with PDBu (1 $\mu$ M) is plotted by normalizing amplitudes to average amplitudes before PDBu application as mean  $\pm$  SEM, while individual data is represented by circles. \*\*\*\* P < 0.0001, Mann-Whitney test.

## 4.1.2 Munc13-1<sup>Arg202</sup> Patient Variant

### 4.1.2.1 Genetics and Clinical Data

The arginine (R) variant at AA position 202 was particularly intriguing to investigate, since three patients carrying this mutation, which occurs in a region of unidentified significance, were examined with a severe disorder. The affected AA is located at the N-terminus of the Munc13-1 protein in an intrinsically disordered region (IDR) shortly after the C2A domain (AA 1-130). The IDR (AA 131-445) depicted in the representative protein schematic in Figure 9 A does not reveal any conformational folding due to its AA properties. Moreover, its function is not investigated. Generally, Munc13 protein isoforms display low homology at their N-termini, which has led to the notion that this region is critical for isoform-specific localization at the AZ, and that the IDR serves as a linker between the protein-localizing sequences and the functional, priming sequence. Surprisingly, despite this low sequence homology, high similarity is seen in sequence alignments of the region surrounding AA 202 in the Munc13-1 and ubMunc13-2 proteins from human and rat (Figure 9 D), indicating a possible function of this region.

A female patient born in 2004 was referred to us (top pedigree in Figure 9 B), that carries biallelic variations with one allele, inherited from the healthy mother, harbouring an insertion (338\_339insAAAGGACC) resulting in a frameshift, and likely rendering the truncated protein dysfunctional, as it will be missing the c-terminal, priming domains. Based on the clinical report indicating that the mother is healthy, we can conclude that UNC13A heterozygosity in humans does not have evident pathological consequences. On the second allele, a *de novo* R202H mutation was identified in the child that was missing in the parents' genetic screens. This patient was characterized by severe intellectual disability and a severe developmental delay with absent speech and no walking. The presence of seizures was associated with a severe epileptic encephalopathy. Clinical examination revealed a 3 standard deviations larger occipitofrontal head circumference than the mean, described as macrocephaly. Adding to this, hypotonia and musculoskeletal abnormality were diagnosed.

The severe clinical manifestation of this patient, which is accompanied by somewhat complex genetics, was rendered more significant by the identification of two additional patients. They are cousins with a homozygous R202 to cysteine (C) mutation inherited from their parents, who are healthy heterozygous carriers of the identical mutation, indicating that the mutation is of a recessive nature. The variation emerges from a different nucleotide exchange than that found in

the previous patient (see Figure 9 B lower panel). Similar to the patient described above, they exhibit severely compromised development, a severe developmental delay in terms of cognitive impairment and seizures. Further dysmorphic features include abnormal cerebral imaging and musculoskeletal abnormalities (Figure 9 C). Blind to the functional role of this protein region, we were prompted to gain insight into the role of this variant for Munc13-1 function, and to determine whether it is causal to the disorder. Of note, since we first became acquainted with a patient carrying the R202H mutation, cloning was designed to include this particular mutation resulting in the exchange of arginine to histidine in the Munc13-1 protein sequence.

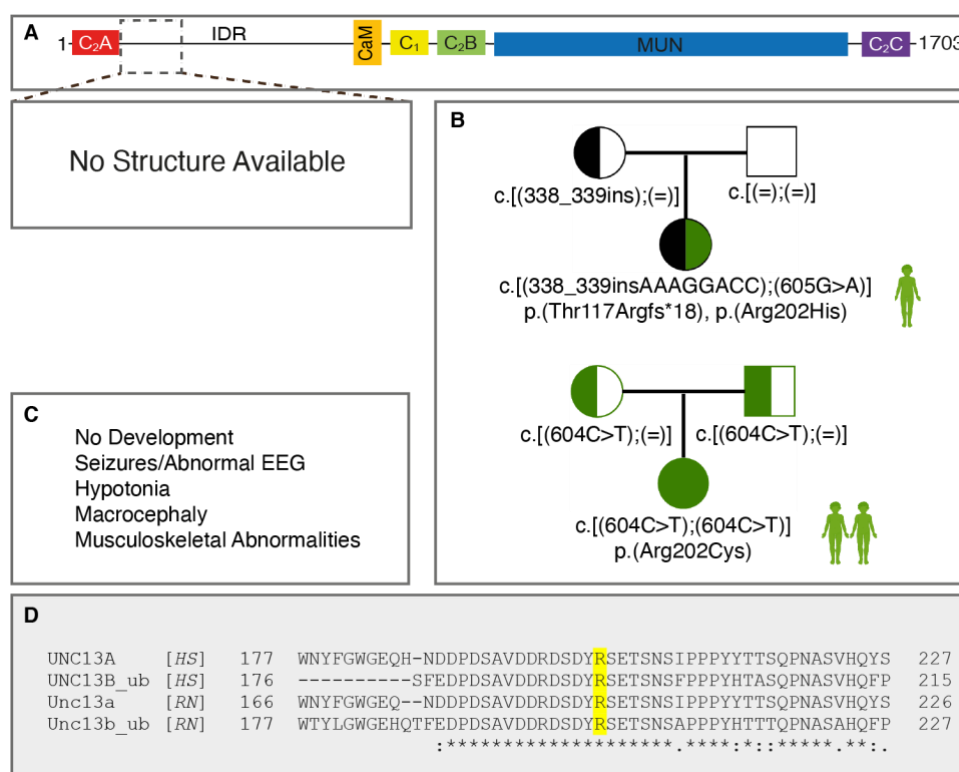


**Figure 9: Genetic and clinical phenotype of three human patients carrying a Munc13-1<sup>R202H</sup> variant.** **A** Munc13-1 domain structure displaying the various identified domains and a dashed box around the region encompassing the amino acid R202H. The three-dimensional structure of this region is unknown. **B** Pedigrees illustrating two types of genetic inheritance. The top pedigree shows a patient with a biallelic mutation in UNC13A, whereby one frameshift insertion inherited from the mother and resulting in early protein truncation. The second allele carries a de novo R202H mutation. The pedigree in the bottom reflects the genotype of two cousins carrying a homozygous R202H mutation inherited from both parents, indicating a recessive nature of the variation. The mutated nucleotides with their respective positions are provided in square brackets. **C** A collection of common clinical symptoms for the three patients carrying the R202H variant. **D** AA residues surrounding the arginine at position 202 of the human UNC13A protein sequence are depicted in a sequence alignment of the two Munc13 isoforms UNC13A and UNC13B\_ub in human (HS) and in rat (RN). The relevant arginine is highlighted in yellow. Asterisks (\*) indicate fully conserved residues, a colon (:) indicates conservation of residues with strongly similar properties and period (.) indicates conservation of residues with weakly similar properties.

#### 4.1.2.2 Spontaneous Release Characteristics in Low and High External $\text{Ca}^{2+}$ Concentrations

Similar to the experimental design in section 3.1.1.2, the patient-specific variant R202H was investigated in primary hippocampal excitatory/glutamatergic neurons obtained from a Munc13-1/2 double knockout (DKO) mouse. Since we cloned the patient-specific variant into rat Munc13-1 cDNA, the corresponding mutated AA was the arginine at position 201. Again, for the benefit of the reader and to avoid confusion in numbering, the patient-specific number (R202H) is retained throughout the study.

The effect of the Munc13-1<sup>R202H</sup> mutation on synaptic transmission was evaluated twice, using two different calcium and magnesium ( $\text{Ca}^{2+}$  &  $\text{Mg}^{2+}$ ) concentrations in the extracellular recording buffer. Typically, all recordings are conducted with 4 mM  $\text{Ca}^{2+}$  & 4 mM  $\text{Mg}^{2+}$  in the extracellular solutions. Under these conditions, SV release probability is high, and neurons tend to respond with STD to high frequency AP stimulation. While under these conditions phenotypes that are associated with SV recovery are easier to model, working under high  $\text{Ca}^{2+}$  and  $\text{Mg}^{2+}$  concentrations can also mask phenotypes that are associated with the dynamic increase of release probability during activity. Given that this N-terminal region of the protein has not been studied yet, we opted for a set of recordings at low  $\text{Ca}^{2+}/\text{Mg}^{2+}$  concentrations (2 mM  $\text{Ca}^{2+}$  & 2 mM  $\text{Mg}^{2+}$ ), to test for such potential phenotypes.

Munc13-1/2 DKO neurons were infected either with Munc13-1<sup>WT</sup> or with Munc13-1<sup>R202H</sup> and the WT- and mutant-expressing neurons were recorded alternately. Neuronal activity at resting condition was examined by blocking APs through TTX application and recording mEPSCs. Average mEPSC frequency, amplitudes, and kinetics are presented in Figure 10 A-G for recordings conducted in 2 mM  $\text{Ca}^{2+}$  &  $\text{Mg}^{2+}$ , and in Figure 10 H-N for recordings conducted at 4 mM  $\text{Ca}^{2+}$  &  $\text{Mg}^{2+}$ . Munc13-1/2 DKO neurons rescued with Munc13-1<sup>R202H</sup> exhibit no significant differences in any of these parameters compared with DKO neurons rescued with the Munc13-1<sup>WT</sup> protein (Figure 10;  $P > 0.05$  for all conditions). Of note, no change in mEPSC kinetics were found between recordings in 2 mM  $\text{Ca}^{2+}$  &  $\text{Mg}^{2+}$  and 4 mM  $\text{Ca}^{2+}$  &  $\text{Mg}^{2+}$ , as expected.

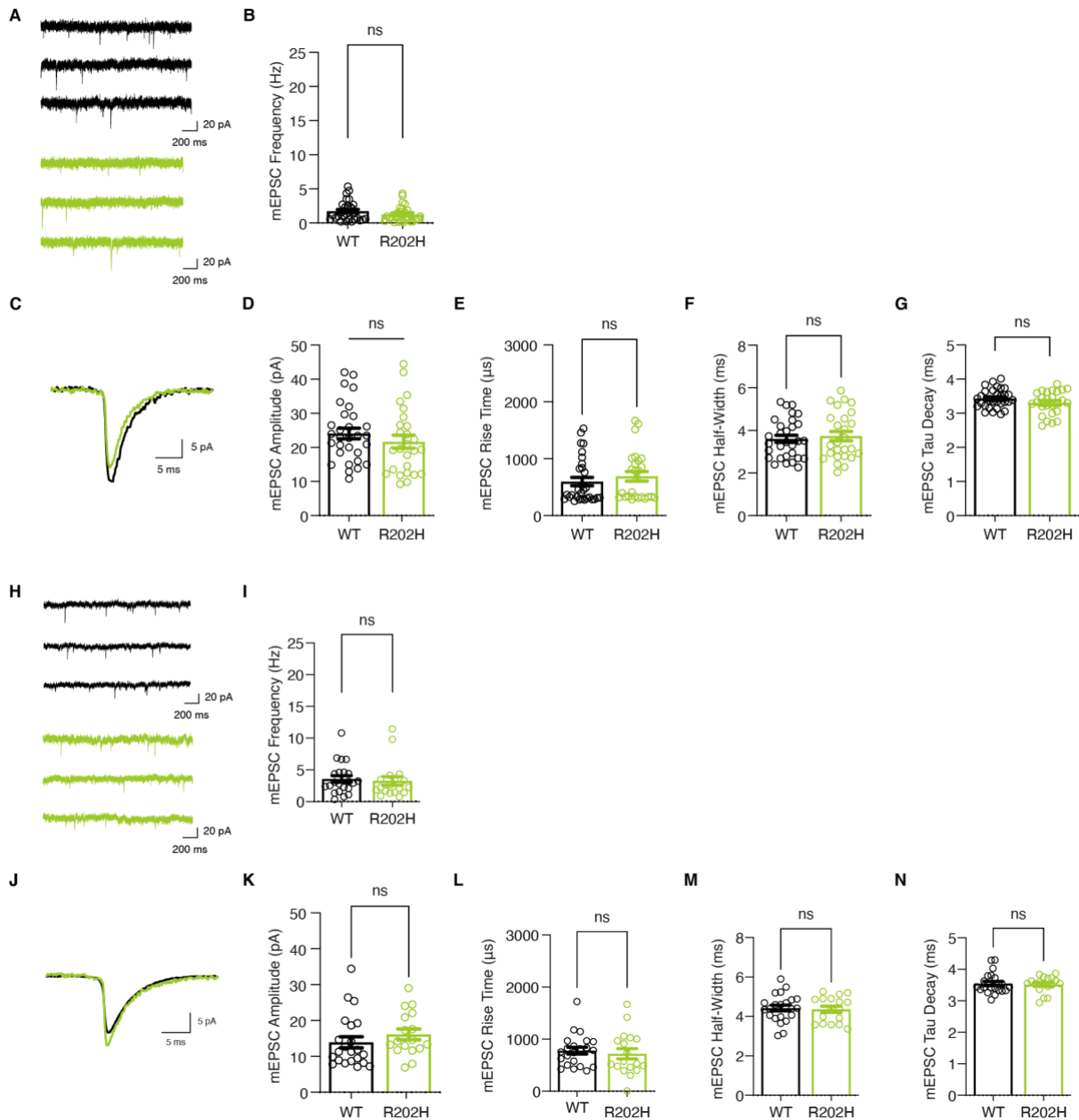


**Figure 10: Spontaneous release characteristics in Munc13-1<sup>R202H</sup> expressing neurons, recorded in low/physiological Ca<sup>2+</sup> condition.** **A** Miniature EPSC (mEPSC) example traces from autaptic hippocampal excitatory Munc13-1/2 DKO neurons expressing Munc13-1<sup>WT</sup> (black) and Munc13-1<sup>R202H</sup> (green) after application of 300nM TTX. **B** Average mEPSC frequencies for Munc13-1<sup>WT</sup> (black) and Munc13-1<sup>R202H</sup> (green). **C** A representative average mEPSC trace for Munc13-1<sup>WT</sup> (black) and Munc13-1<sup>R202H</sup> (green) is depicted in an overlay. The graphs in the lower panel under **D**, **E**, **F**, **G** depict the average mEPSC amplitude (**D**), average mEPSC rise time (**E**), average mEPSC half-width (**F**) and average mEPSC tau decay (**G**) for Munc13-1<sup>WT</sup> (black) and Munc13-1<sup>R202H</sup> (green) respectively. Each circle illustrates the data for one recorded neuron. The error bars in the figure designate mean values  $\pm$  SEM. Non-significant (ns) stands for  $P > 0.05$ , Mann-Whitney test. **Spontaneous release characteristics in Munc13-1<sup>R202H</sup> expressing neurons, recorded in high (4 mM) Ca<sup>2+</sup> condition.** **H** Miniature EPSC (mEPSC) example traces from autaptic hippocampal excitatory Munc13-1/2 DKO neurons expressing Munc13-1<sup>WT</sup> (black) and Munc13-1<sup>R202H</sup> (green) after application of 300nM TTX. **I** Average mEPSC frequencies for Munc13-1<sup>WT</sup> (black) and Munc13-1<sup>R202H</sup> (green). **J** A representative average mEPSC trace for Munc13-1<sup>WT</sup> (black) and Munc13-1<sup>R202H</sup> (green) is depicted in an overlay. The graphs in the lower panel under **K**, **L**, **M**, **N** depict the average mEPSC amplitude (**K**), average mEPSC rise time (**L**), average mEPSC half-width (**M**) and average mEPSC tau decay (**N**) for Munc13-1<sup>WT</sup> (black) and Munc13-1<sup>R202H</sup> (green) respectively. Each circle illustrates the data for one recorded neuron. The error bars in the figure designate mean values  $\pm$  SEM. Non-significant (ns) indicates  $P > 0.05$ , Mann-Whitney test.

### 4.1.2.3 Munc13-1<sup>R202H</sup> Abates Synaptic Strength

Electrophysiological measurements of Munc13-1<sup>R202H</sup>-expressing neurons at resting state revealed no change in spontaneous release characteristics compared to neurons expressing the Munc13-1<sup>WT</sup> protein. Next, we tested AP-dependent synaptic transmission and sucrose-induced evoked release.

A significant reduction in average evoked EPSC amplitudes was evident in Munc13-1<sup>R202H</sup> expressing neurons under 2 mM or 4 mM Ca<sup>2+</sup>/Mg<sup>2+</sup> condition (\*\* P<0.01 in Figure 11 B, \* P<0.05 in Figure 12 B), although this reduction was slightly milder in 4 mM Ca<sup>2+</sup> in comparison to the 2 mM Ca<sup>2+</sup> condition (Figure 11 A, 12 A). When evaluating EPSC kinetics, a significant reduction in the average EPSC rise time (20 % - 80 %) and the average EPSC half-width parameters was detected in the 2 mM Ca<sup>2+</sup> condition (\*\* P<0.01 in Figure 11 C, D). Controversially, both these parameters were not altered in the measurements performed in the 4 mM Ca<sup>2+</sup> condition (ns P>0.05 in Figure 12 C, D).

The RRP size was evaluated by hypertonic sucrose application to the extracellular solution. Figure 11 E, F show that the average pool size of Munc13-1<sup>R202H</sup>-expressing neurons is significantly reduced (\* P<0.05) at 2 mM Ca<sup>2+</sup> concentration in comparison to the average pool size depicted for Munc13-1<sup>WT</sup>-expressing neurons. Likewise, a noticeable reduction of the pool size is also visible in Munc13-1<sup>R202H</sup> expressing neurons in the 4 mM Ca<sup>2+</sup> concentration recordings (ns P>0.05 in Figure 12 E, F). Here it is noteworthy to mention that an ideal sample size for the recordings at 4 mM Ca<sup>2+</sup> concentration requires the acquisition of one additional culture. This would enable to assert whether this change is of significance or not. pVR (Figure 11 G), calculated as the proportion of RRP released by one AP, was largely reduced in neurons expressing the Munc13-1<sup>R202H</sup> variant at 2 mM Ca<sup>2+</sup> concentration (\* P<0.01) compared to Munc13-1<sup>WT</sup> protein expression. In contrast, there is no visible difference in the pVR in neurons recorded at 4 mM Ca<sup>2+</sup> conditions (ns P>0.05, Figure 12 G).



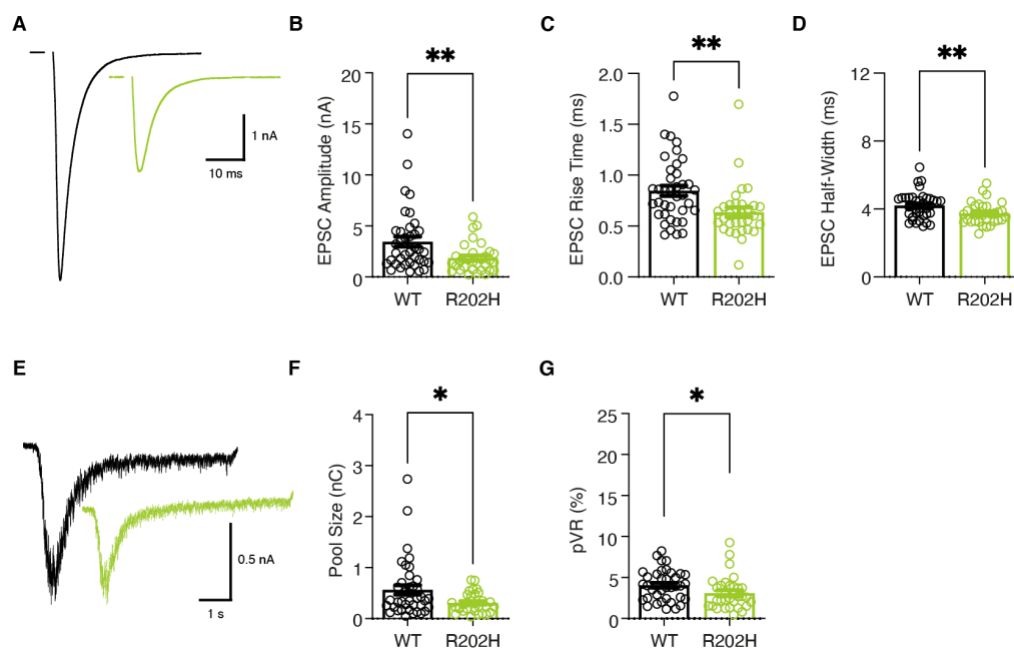


**Figure 11: Munc13-1<sup>R202H</sup> significantly reduces evoked release characteristics in low (2 mM) Ca<sup>2+</sup>.** Recordings from autaptic hippocampal excitatory Munc13-1/2 DKO neurons expressing Munc13-1<sup>WT</sup> (black) and Munc13-1<sup>R202H</sup> (green). **A** Representative initial EPSC traces are shown. **B** The initial EPSCs from each recorded neuron symbolized by a circle are plotted as mean  $\pm$  SEM. EPSC kinetic parameters, EPSC rise time (**C**) and EPSC half-width (**D**), are plotted as mean  $\pm$  SEM. **E** Sucrose-induced (500 nM) release of the RRP of SVs is exemplified with representative traces and average RRP size (**F**) is plotted as mean  $\pm$  SEM, while individual data is shown as circles. **G** The graph displays the average vesicular release probability (pVR) in neurons expressing Munc13-1<sup>WT</sup> (black) and Munc13-1<sup>R202H</sup> (green). \*P<0.05, \*\* P<0.01, Mann-Whitney test.

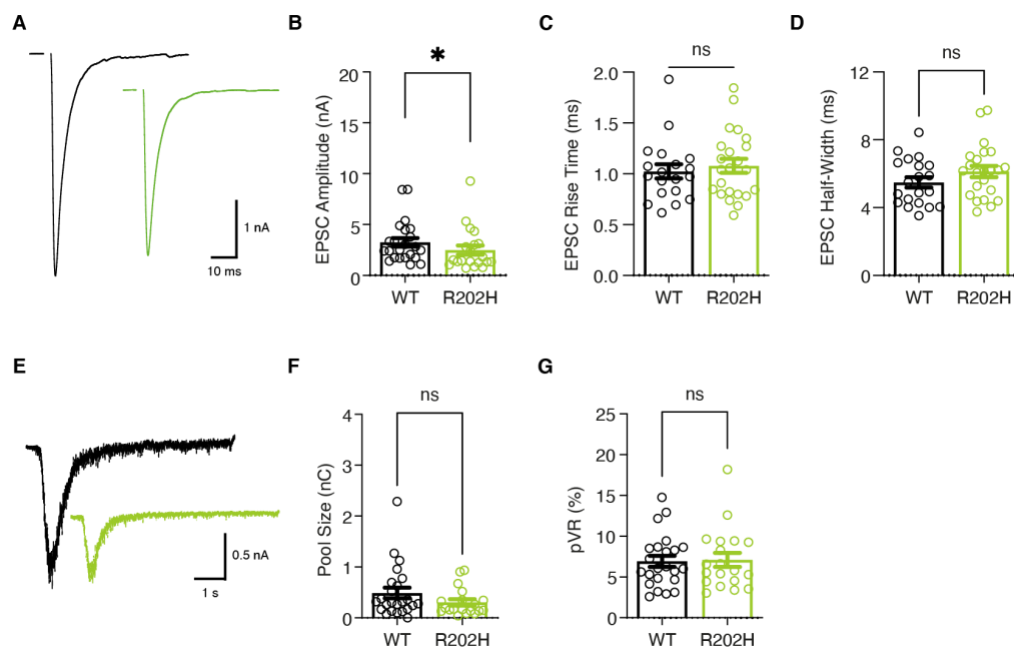


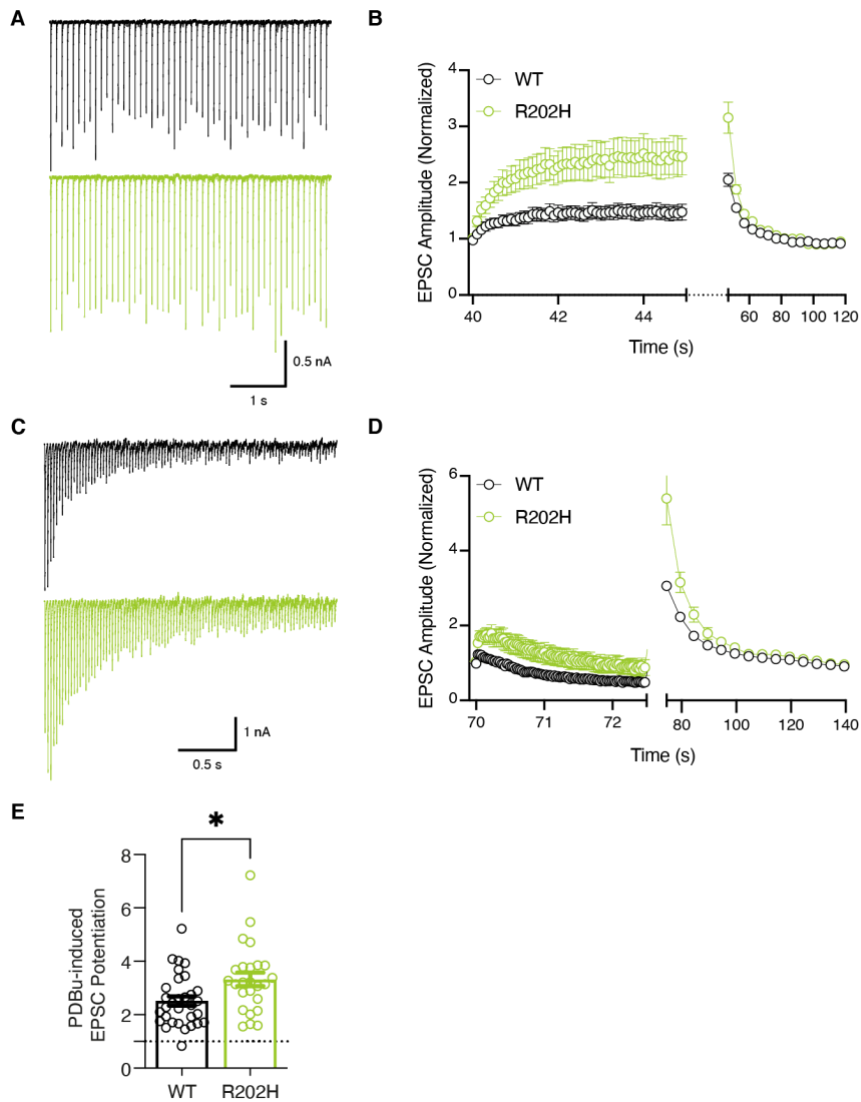
**Figure 12: Munc13-1<sup>R202H</sup> significantly reduces synaptic strength in high (4 mM) Ca<sup>2+</sup> recordings.** Autaptic hippocampal excitatory Munc13-1/2 DKO neurons expressing Munc13-1<sup>WT</sup> (black) and Munc13-1<sup>R202H</sup> (green). **A** Representative initial EPSC traces are shown. **B** The initial EPSCs from each recorded neuron symbolized by a circle are plotted as mean  $\pm$  SEM. EPSC kinetic parameters, EPSC rise time (**C**) and EPSC half-width (**D**), are plotted as mean  $\pm$  SEM. **E** Sucrose-induced (500 nM) release of the RRP of SVs is exemplified with representative traces and average RRP size (**F**) is plotted as mean  $\pm$  SEM, while individual data is shown as circles. **G** The graph displays the average vesicular release probability (pVR) in neurons expressing Munc13-1<sup>WT</sup> (black) and Munc13-1<sup>R202H</sup> (green). \*P<0.05, ns indicates P>0.05, Mann-Whitney test.

#### 4.1.2.4 Munc13-1<sup>R202H</sup> Facilitates at 10 Hz Frequency

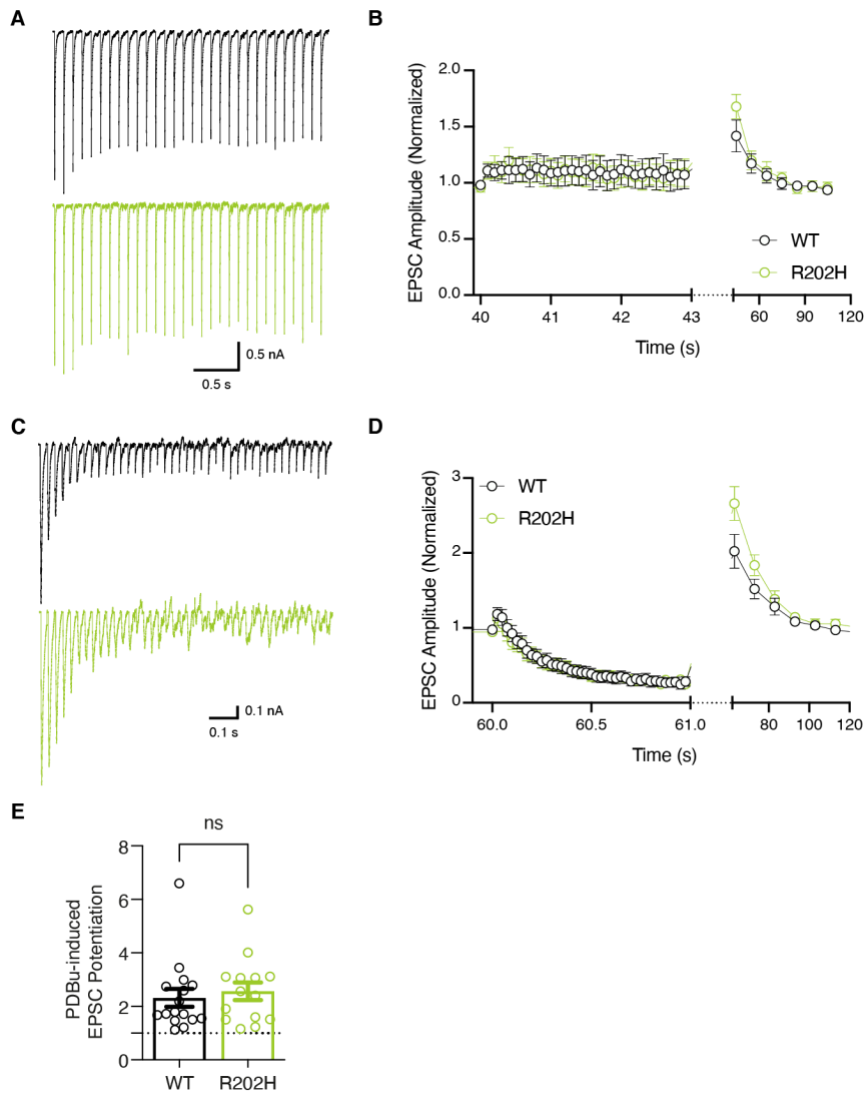
The abated evoked activity of Munc13-1<sup>R202H</sup>-expressing neurons under low Ca<sup>2+</sup> conditions, hinted that this mutation, which affects an unstudied Munc13-1 region, may exert a Ca<sup>2+</sup>-dependent effect, or an effect that is easier to reveal under lower Ca<sup>2+</sup> concentrations. Because the dynamics of short-term synaptic plasticity are critically dependent on Ca<sup>2+</sup>, I next assessed short-term synaptic plasticity characteristics during evoked trains of APs at 10 Hz and at 40 Hz frequency in Munc13-1/2 DKO neurons expressing the Munc13-1<sup>WT</sup> or the Munc13-1<sup>R202H</sup>.

Figure 13 A depicts a representative trace obtained during a 10 Hz frequency stimulus train. In low external Ca<sup>2+</sup>, the plot depicting the normalized EPSC amplitude average, EPSC facilitation is seen, in both Munc13-1<sup>WT</sup>-expressing neurons and in Munc13-1<sup>R202H</sup>-expressing neurons. Such facilitation is often observed under low Ca<sup>2+</sup>, which results in lower release probability. The magnitude of facilitation was much stronger in Munc13-1<sup>R202H</sup>-expressing neurons in comparison to WT (Figure 13 B), compatible with the reduced pVR measured under this condition (Figure 11 G). A similar change can be observed under 40 Hz train, but here, the higher frequency results in a net short-term depression (Figure 13 C, D). These findings were not reproduced under 4 mM external Ca<sup>2+</sup>, where the pattern of STP was similar for WT- and Munc13-1<sup>R202H</sup>-expressing neurons (Figure 14 A, B, C, D), again in agreement with no change in pvr under these recording conditions. In summary, the effect on synaptic STP, which was detected at 2 mM external Ca<sup>2+</sup>, could not be resolved at higher (4 mM) external Ca<sup>2+</sup>.

Exposure to PDBu activates Munc13-1 and recruits it to the plasma membrane, which rapidly increases the evoked EPSC amplitude over the period of tens of seconds until a plateau is reached, after which there is no increase anymore. This increase was attributed to an increase in release probability, rather than an increase in the RRP. In DKO neurons expressing the variant Munc13-1<sup>R202H</sup>, the PDBu induced potentiation was significantly higher than in Munc13-1<sup>WT</sup> expressing neurons (Figure 13 E), which is in conjunction with the lower initial vesicular release probability in Munc13-1<sup>R202H</sup> (Figure 11 G). At 4 mM Ca<sup>2+</sup> concentration no visible difference in PDBu-mediated EPSC potentiation are seen between Munc13-1<sup>WT</sup> and Munc13-1<sup>R202H</sup> (Figure 14 E), compatible with no change in initial release probability.



**Figure 13: Short-term synaptic facilitation in Munc13-1<sup>R202H</sup> expressing neurons in low (2 mM) Ca<sup>2+</sup> condition.** Stimulation of autaptic hippocampal excitatory Munc13-1/2 DKO neurons expressing Munc13-1<sup>WT</sup> (black) and Munc13-1<sup>R202H</sup> (green) with AP trains of (A) 10 Hz frequency and (C) 40 Hz frequency on average resulted in the presented example traces. Normalized EPSC amplitudes are plotted for (B) 10 Hz and (D) 40 Hz frequency stimulation respectively, followed by continuous 0.2 Hz stimulation. E Potentiation of EPSCs after stimulation with PDBu (1 $\mu$ M) is plotted by normalizing amplitudes to average amplitudes before PDBu application as mean  $\pm$  SEM, while individual data is represented by circles. \* P<0.05, Mann-Whitney test.



**Figure 14: Short-term synaptic plasticity in Munc13-1<sup>R202H</sup> expressing neurons resembles Munc13-1<sup>WT</sup> in high (4mM) Ca<sup>2+</sup> condition.** Stimulation of autaptic hippocampal excitatory Munc13-1/2 DKO neurons expressing Munc13-1<sup>WT</sup> (black) and Munc13-1<sup>R202H</sup> (green) with AP trains of (A) 10 Hz frequency and (C) 40 Hz frequency on average resulted in the presented example traces. Normalized EPSC amplitudes are plotted for (B) 10 Hz and (D) 40 Hz frequency stimulation respectively, followed by continuous 0.1 Hz stimulation. E Potentiation of EPSCs after stimulation with PDBu (1 $\mu$ M) is plotted by normalizing amplitudes to average amplitudes before PDBu application as mean  $\pm$  SEM, while individual data is represented by circles. ns indicates P > 0.05, Mann-Whitney test.

### 4.1.3 Munc13-1<sup>E52K</sup> Patient Variant

#### 4.1.3.1 Genetics and Clinical Data

The data obtained for the R202H variant suggested that N-terminal variations may act through a new mechanism, namely a loss of function of synaptic strength and RRP size. This is in strong contrast to the clear gain of function mechanism recorded for the P814L variation in (Lipstein et al., 2017), and the G808D variation studied here. I therefore chose to study an additional N-terminal variation in Munc13-1, E52K.

The patient described here harbours a mutation within the C2A domain at the very n-terminus of Munc13-1 (Figure 15 A). The C2A domain can only be identified in Munc13-1 and in the related ubMunc13-2, and is missing in other mammalian Munc13 isoforms and in non-mammalian UNC13A variants. It is known for its interaction with the n-terminal RIM zinc finger domain, which is crucial for the activation and localization of Munc13-1 at the presynaptic active zone. The affected AA residue at position 52 locates to the tip of a  $\beta$ -strand that is involved in heterodimerization with RIM (Figure 15 C)(Lu et al., 2006). In the patient, AA 52 is exchanged from glutamic acid (E) to lysine (K). This residue is conserved in the Munc13-1 and Munc13-2 paralogs in human and rat (Figure 15 E). The patient is homozygous to the variation, while each of his parents is heterozygous, making this variant likely recessive (Figure 15 B). At the age of 12 years the patient underwent a detailed clinical examination. The patient is presenting with a severe disorder: he is nonverbal, nonmobile, and is being tube fed. Furthermore, he displays a developmental age of 2-3 months characterized by severe intellectual disability. Other salient features are the prevalence of neonatal seizures and significant hypotonia. Additionally, dysmorphic features were reported, including microcephaly and abnormal cerebral imaging.

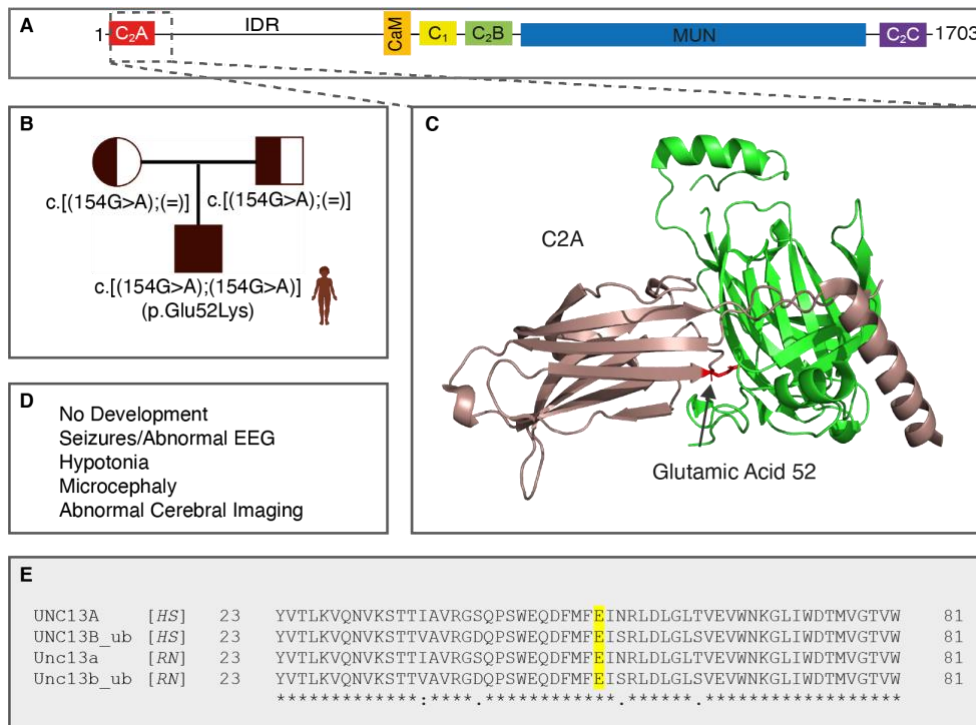


**Figure 15: Genetic and clinical phenotype of a human patient carrying a Munc13-1<sup>E52K</sup> variant.** **A** Munc13-1 domain structure displaying the various identified domains and a dashed box around the region encompassing the patient mutation E52K. **B** Pedigree illustrating the patient genotype. Both parents are carriers of the same variation, causing an exchange of a glutamic acid residue at amino acid 52 to a lysine. The affected individual is homozygous to the variation. The mutated nucleotides and their position in the human cDNA sequence are provided in square brackets. **C** The crystal structure of the region indicated roughly by the dashed box. The brown structure is the C2A domain, composed of a  $\beta$ -sheet structure followed by an  $\alpha$ -helix forming a heterodimer with the RIM1 zinc finger domain. The arrow points to the affected AA residue (in red). **D** A collection of clinical symptoms of the patient carrying the E52K variant. **E** Sequence Alignment shows that the AA residues surrounding the glutamic acid at position 52 in human are conserved in the Munc13 paralogs UNC13A and UNC13B\_ub in the human (HS) and rat (RN) sequence. The relevant glutamic acid is highlighted in yellow. Asterisks (\*) indicate fully conserved residues, a colon (:) indicates conservation of residues with strongly similar properties and period (.) indicates conservation of residues with weakly similar properties.

#### 4.1.3.2 Spontaneous and Evoked Release Characteristics of the Patient Variant Munc13-1<sup>E52K</sup>

Three rounds of experiments, including two independent viral productions, were performed for this mutation. The first experiment was aborted on the second day of recording because Munc13-1<sup>E52K</sup>-expressing neurons did not show any response to depolarization, and no rescue of the Munc13-1/2 DKO phenotype was observed. I speculated that the infection with the Munc13-1<sup>E52K</sup> virus was impaired. Of note, the lentivirus preparation and infection are done simultaneously for both WT and mutant viruses, and it is rare that only one of the viruses is non-functional, and I did not encounter such a situation during my studies. Two additional sets of electrophysiological recordings were attempted with a new batch of virus, where again Munc13-1<sup>WT</sup> was rescuing synaptic transmission, but Munc13-1<sup>E52K</sup> did not.

Subsequently, two cultures expressing Munc13-1<sup>WT</sup> and Munc13-1<sup>E52K</sup> were recorded, in which I focused on evoked and spontaneous release characteristics. I did not observe any evoked SV release in 15 cells that were documented for Munc13-1<sup>E52K</sup>. I only documented 15 neurons, however, many additional recordings where no response could be measured were made. They were aborted at the beginning of the experiment, and a new neuron was searched for, that may exhibit a response (Figure 16 A, B).

A loss of neurotransmitter release can be a consequence of a failure at many synaptic processes, including a dysfunction of the release machinery, loss of postsynaptic sensitivity, or a loss of the SV pool of readily-releasable vesicles. The latter mechanism is associated with the loss of Munc13 isoforms from the synapse (Imig et al., 2014; Siksou et al., 2009). To examine the latter, I measured the RRP size by applying a hypertonic sucrose solution. I could not measure sucrose-evoked currents in Munc13-1<sup>E52K</sup> expressing neurons (Figure 16 C, D), indicating that the loss of the RRP in Munc13-1/2 DKO neurons was not rescued by the Munc13-1<sup>E52K</sup> variant. In spite of a low number of recorded neurons, the data set is plotted and presented for clarity - to visualize the effect, which has been witnessed in three independent experiments.

Surprisingly, spontaneous activity recorded in Munc13-1<sup>E52K</sup> expressing neurons in the presence of TTX was partially rescued. Data analysis revealed miniature events in several neurons, albeit of reduced frequency (Figure 16 E, F). Miniature EPSC amplitude was also slightly lower, but not significantly (Figure 16 G, H). mEPSC kinetic parameters, such as mEPSC rise time (20 % - 80 %), mEPSC half-width (50 %) and the tau decay time were not altered in both conditions (Figure 16 I, J, K). While it is clear that these data are preliminary, the fact that spontaneous activity is

rescued, while evoked activity is not, is surprising. More data is necessary to substantiate these findings.

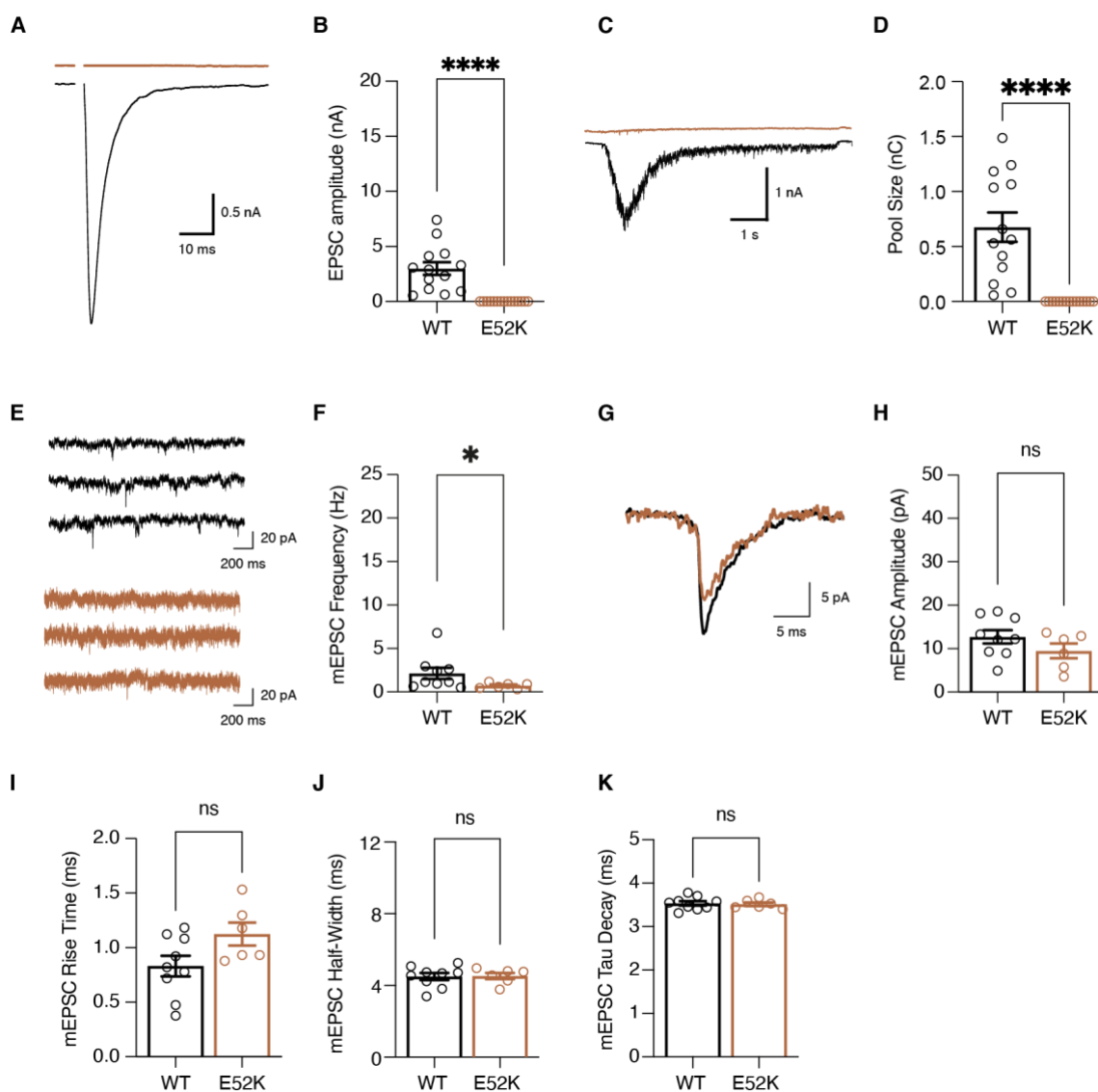


**Figure 16: Munc13-1<sup>E52K</sup> abolishes evoked release, but partially supports spontaneous release.** Recordings from autaptic hippocampal excitatory Munc13-1/2 DKO neurons expressing Munc13-1<sup>WT</sup> (black) and Munc13-1<sup>E52K</sup> (brown). **A** Representative initial EPSC traces are shown. **B** Initial EPSC amplitudes from each recorded neuron (open circles), and average amplitudes represented as mean  $\pm$  SEM. **C** Representative sucrose-induced currents, and average RRP size (**D**), plotted as mean  $\pm$  SEM. Individual data points are shown as circles. For the data in A-D, \*\*\*\* $P$ <0.0001, Mann-Whitney test,  $n=13$  for Munc13-1<sup>WT</sup>,  $n=15$  for Munc13-1<sup>E52K</sup>. **E** Miniature EPSC (mEPSC) traces from autaptic hippocampal excitatory Munc13-1/2 DKO neurons expressing Munc13-1<sup>WT</sup> (black) and Munc13-1<sup>E52K</sup> (brown) after application of 300 nM TTX. **F** Average mEPSC frequencies. **G** A representative averaged mEPSC trace for Munc13-1<sup>WT</sup> (black) and Munc13-1<sup>E52K</sup> (brown) is depicted in an overlay. The graphs in panel under **H**, **I**, **J**, **K** depict the average mEPSC amplitude (**H**), average mEPSC rise time (**I**), average mEPSC half-width (**J**) and average mEPSC tau of decay (**K**) for Munc13-1<sup>WT</sup> (black) and Munc13-1<sup>E52K</sup> (brown) respectively. Each circle illustrates averaged data for one recorded neuron. The error bars in the figure designate mean values  $\pm$  SEM. \*  $P$ <0.05, non-significant (ns) stands for  $P$ >0.05, Mann-Whitney test,  $n=9$  for Munc13-1<sup>WT</sup>,  $n=6$  for Munc13-1<sup>E52K</sup>.



#### 4.1.4 Munc13-1<sup>R799Q</sup> and Munc13-1<sup>N1013S</sup> Patient Variants

The so far analysed disease-related variants, Munc13-1<sup>G808D</sup>, Munc13-1<sup>R202H</sup>, and Munc13-1<sup>E52K</sup> were initially chosen since (1) they were conveyed to us at the beginning of this project, and (2) we were convinced of them being a good choice based on the accumulation of patients carrying these variations and based on their location in the protein sequence. Taking together, my data consolidates a gain of function mechanism for C2B-MUN linker domain mutations, where increased release probability is observed, and reveals a new disease-linked mechanism, whereby the N-terminal R202H and E52K variations acts via a loss of function mechanisms, reducing synaptic strength and release probability. The data also allows us to assign a potential function for the respective regions containing the mutations.

In the next section, I present data where I analysed two additional patient mutations. We experienced an overwhelming flow of patients in the course of time of my PhD and decided to pick patients on the basis of their genetic and clinical validation, the severity of the cases, and the location of the variants in the protein. Two patients with a severe clinical phenotypes carrying mutations situated in two functionally characterized domains of the Munc13-1 protein (the C2B domain and the C-terminal priming domain), were chosen for the next set of experiments.

##### 4.1.4.1 Genetics and Clinical Data for the Patient Variant Munc13-1<sup>R799Q</sup>

Here we report a patient with an arginine (R) mutation at AA position 799. This patient attracted our attention due to several reasons. First, it carries a mutation that is placed in the C2B domain (Figure 17 A, C), which is of functional importance for the Ca<sup>2+</sup>-dependent phospholipid binding of Munc13-1 to the active zone plasma membrane, and for activity-induced acceleration of SV priming (Lipstein et al., 2021; Lipstein et al., 2013). Secondly, it is in close vicinity to the G808D mutation and the earlier-characterized P814L variant that are both located in the linker sequence that connects the C2B domain to the MUN domain and which had been both characterized causing a gain of function. Third, the genetic data indicates that the patient is a homozygous carrier of the R799 to glutamine (Q) variant, which he inherited from his heterozygous parents, suggesting a potential loss of function phenotype. Forth, the clinical severity of the patients' syndrome led to a premature death at the age of three days (Figure 17 B). He was diagnosed with macrocephaly, abnormal cerebral imaging and musculoskeletal abnormalities (Figure 17 D). As can be appreciated in Figure 17 E, the arginine 799 in the human sequence is fully conserved in all known Munc13 isoforms of human, rat, fruit fly and the nematode *C. elegans*. The absolute sequence identity of this region indicates that it may be significant for the C2B domain stability or function. I used site-



#### 4.1.4.2 Synaptic Transmission is Largely Normal in Munc13-1<sup>R799Q</sup>-Expressing Neurons

The disease-related variant R799Q was investigated in primary mouse hippocampal excitatory neurons on a Munc13-1/2 DKO background. Neurons were infected with lentivirus containing either the WT or the mutated Munc13 variant. The role of the Munc13-1<sup>R799Q</sup> mutation on synaptic transmission was evaluated by recording spontaneous, AP-evoked activity, and plasticity-related parameters from infected cells.

Munc13-1/2 DKO neurons rescued with Munc13-1<sup>R799Q</sup> exhibit no noteworthy difference in mEPSC frequencies ( $P > 0.05$ ) on average compared to DKO neurons rescued with the Munc13-1<sup>WT</sup> protein (Figure 18 A, B). Similarly, average mEPSC amplitudes were comparable (Figure 18 D). No change was observed in kinetic parameters, such as rise time (20 % - 80 %) and half-width (50 %) and the decay time of mEPSCs (Figure 18, E-G), as is evidenced by the uniform shape of representative mEPSC average traces (Figure 18 C). Similarly, the size and kinetics of evoked release were also similar: EPSC amplitudes (Figure 19 A, B), rise time (20 % - 80 %) and EPSC half-width (50 %) were not altered between Munc13-1<sup>WT</sup>- and Munc13-1<sup>R799Q</sup>-expressing DKO neurons (Figure 19 C, D).

The size of the readily-releasable pool (RRP) of SVs was not changed in Munc13-1<sup>WT</sup> and Munc13-1<sup>R799Q</sup> expressing neurons (Figure 19 E & F). Accordingly, the average pV<sub>R</sub> was comparable for neurons expressing the Munc13-1<sup>R799Q</sup> variant and Munc13-1<sup>WT</sup> protein ( $P > 0.05$ ).

Synaptic short-term plasticity was measured by the induction of a series of depolarizations at frequencies of 10- and 40 Hz, mimicking periods of sustained activity. Example traces for 10 Hz and 40 Hz stimulus trains are presented in Figure 20 A & C, respectively. The normalized EPSC amplitudes in the plotted graphs in Figure 20 B & D show no significant difference between DKO neurons expressing the Munc13-1<sup>WT</sup> or the variant Munc13-1<sup>R799Q</sup>. Finally, the average EPSC potentiation in response to the application of PDBu was unaltered (Figure 20 E).

In summary, I could not resolve a phenotype for the R799Q disease-related variation in neurotransmission. Multiple reasons that could account for that are outlined in the discussion section. The likely one, however, is that this variant is not the cause for the disease in the affected individual.

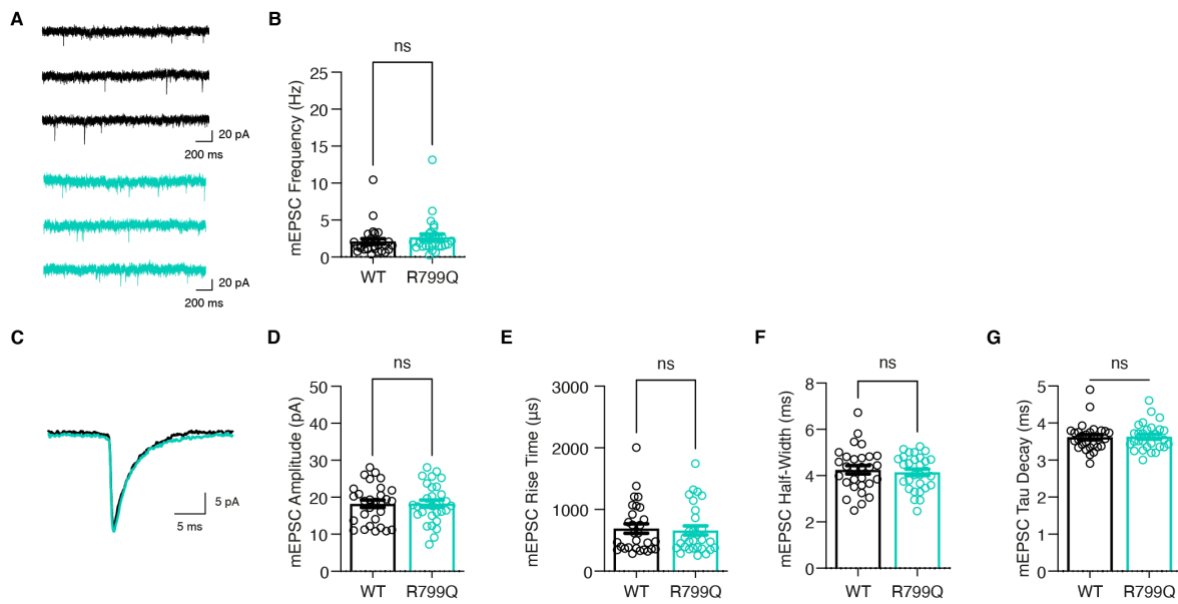


**Figure 18: Spontaneous release characteristics in Munc13-1<sup>R799Q</sup> expressing neurons.** **A** mEPSC example traces from autaptic hippocampal excitatory Munc13-1/2 DKO neurons expressing Munc13-1<sup>WT</sup> (black) and Munc13-1<sup>R799Q</sup> (turquoise) after application of 300 nM TTX, and **B** Average mEPSC frequencies. **C** A representative average mEPSC trace for Munc13-1<sup>WT</sup> (black) and Munc13-1<sup>R799Q</sup> (turquoise) is depicted in an overlay. The graphs in the lower panel under **D**, **E**, **F**, **G** depict the average mEPSC amplitude (**D**), average mEPSC rise time (**E**), average mEPSC half-width (**F**) and average mEPSC tau decay (**G**) for Munc13-1<sup>WT</sup> (black) and Munc13-1<sup>R799Q</sup> (turquoise) respectively. Each circle illustrates the data for one recorded neuron. The error bars in the figure designate mean values  $\pm$  SEM. Non-significant (ns) indicates  $P > 0.05$ , Mann-Whitney test.

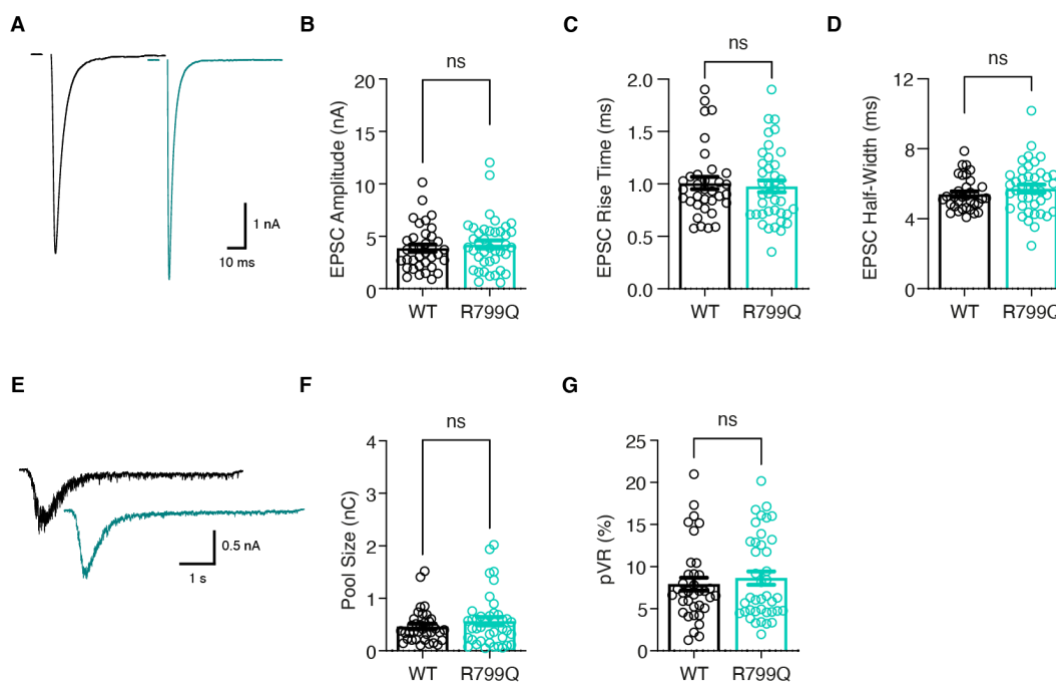


**Figure 19: Evoked release characteristics in Munc13-1<sup>R799Q</sup>-expressing neurons.** Autaptic hippocampal excitatory Munc13-1/2 DKO neurons expressing Munc13-1<sup>WT</sup> (black) and Munc13-1<sup>R799Q</sup> (turquoise). **A** Representative initial EPSC traces are shown. Average initial EPSC amplitudes (**B**), EPSC rise time (**C**), and EPSC half-width (**D**), are plotted as mean  $\pm$  SEM. **E** Sucrose-induced release of the RRP of SVs is exemplified with representative traces. Average RRP size (**F**) and vesicular release probability (pVR; **G**) in neurons expressing Munc13-1<sup>WT</sup> (black) and Munc13-1<sup>R799Q</sup> (turquoise). ns indicates  $P > 0.05$ , Mann-Whitney test. All data is plotted as mean  $\pm$  SEM, individual data points are shown as open circles.

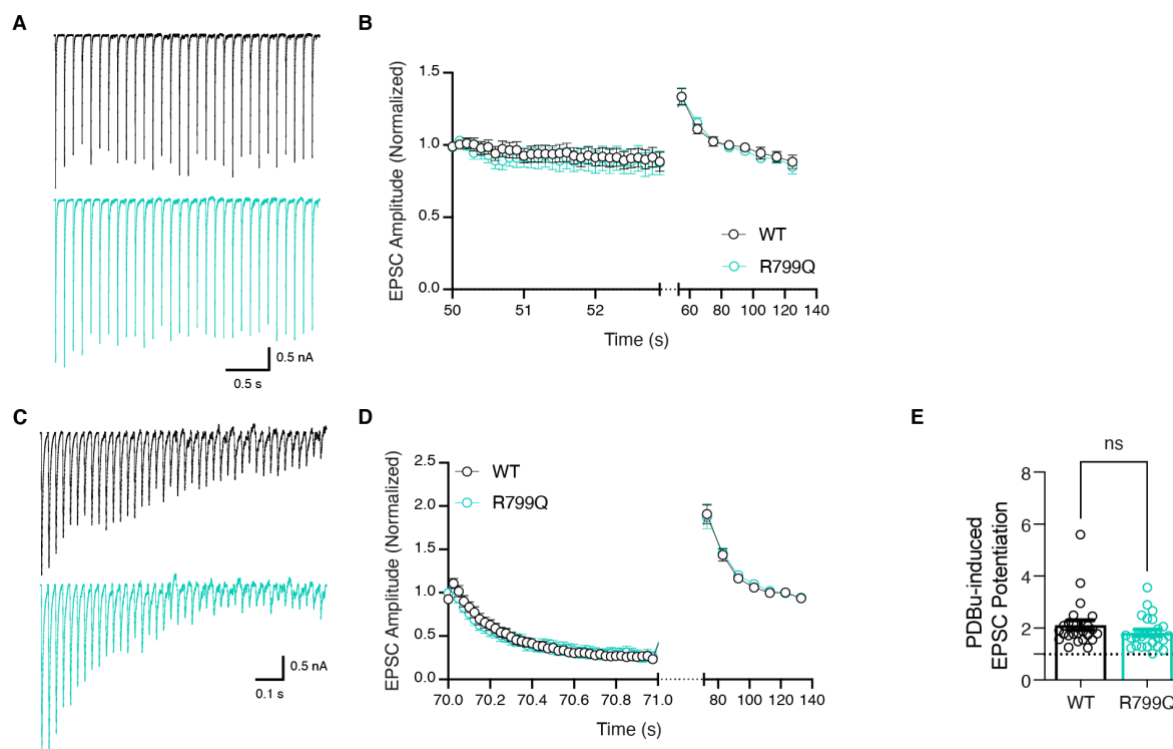


**Figure 20: Short-term synaptic plasticity in *Munc13-1<sup>R799Q</sup>*-expressing neurons resembles *Munc13-1<sup>WT</sup>*.** Example traces obtained from autaptic hippocampal excitatory *Munc13-1/2* DKO neurons expressing *Munc13-1<sup>WT</sup>* (black) and *Munc13-1<sup>R799Q</sup>* (turquoise), stimulated with AP trains at frequency of **(A)** 10 Hz and **(C)** 40 Hz. Normalized EPSC amplitudes are plotted for averaged traces obtained by stimulation at **(B)** 10 Hz and **(D)** 40 Hz respectively, followed by continuous 0.1 Hz stimulation. **E** Potentiation of EPSCs after stimulation with PDBu ( $1\mu\text{M}$ ) is plotted by normalizing amplitudes to average amplitudes before PDBu application as mean  $\pm$  SEM, while individual data is represented by circles. ns indicates  $P > 0.05$ , Mann-Whitney test.

#### 4.1.4.3 Genetics and Clinical Data of the Patient Variant Munc13-1<sup>N1013S</sup>

Our collaborators from Zurich referred to us a patient with a *de novo* asparagine (N) to serine (S) mutation at AA position 1013, which is well conserved in the Munc13-1 and the two Munc13-2 isoforms in human and rat (Figure 21 E). The patient's medical examination revealed a severe clinical picture, including developmental delay, intellectual disability and concomitant abnormal behaviour. Furthermore, a movement disorder besides hypotonia was diagnosed and additional dysmorphic features such as microcephaly and an abnormal cerebral imaging were assessed (Figure 21 D). This variation resides in the MUN domain (Figure 21 A, C), which mediates syntaxin binding and thereby SV priming, and is absolutely essential for transmitter release. I therefore hypothesized that the severe phenotype could be a result of this variation in this crucial domain. Supporting this is the position of this AA at the crystal structure, residing in an exposed region of the protein and close to a kink in the alpha helix structure (Figure 21 C). However, the *de novo* N1013S variation is also annotated in the genome aggregation database (gnomAD), which contains genome and exome sequences from mostly healthy individuals, and thus can also be a benign single nucleotide polymorphism (SNP) rather than a disease-causing variation. I aimed to utilize our experimental approach to test whether this variation is causal for the disease.

Of note, while the experiments for this mutation were conducted, we were informed by our collaborator that the genetic screen of the patient revealed another intronic splice site mutation inherited from the father (c.767+14A>G; 'c.', cDNA; 767, the respective position on the cDNA sequence; '+' extension to the intron on the 3' side; '14', following position 767, the 14<sup>th</sup> bp in the 3' intron on the gene sequence; A>G, the bp exchange) next to the *de novo* mutation within the same allele (Figure 21 B). Because this mutation is deep in the intron sequence, and because it is paternally inherited, it is unlikely to affect splicing or to cause harm.

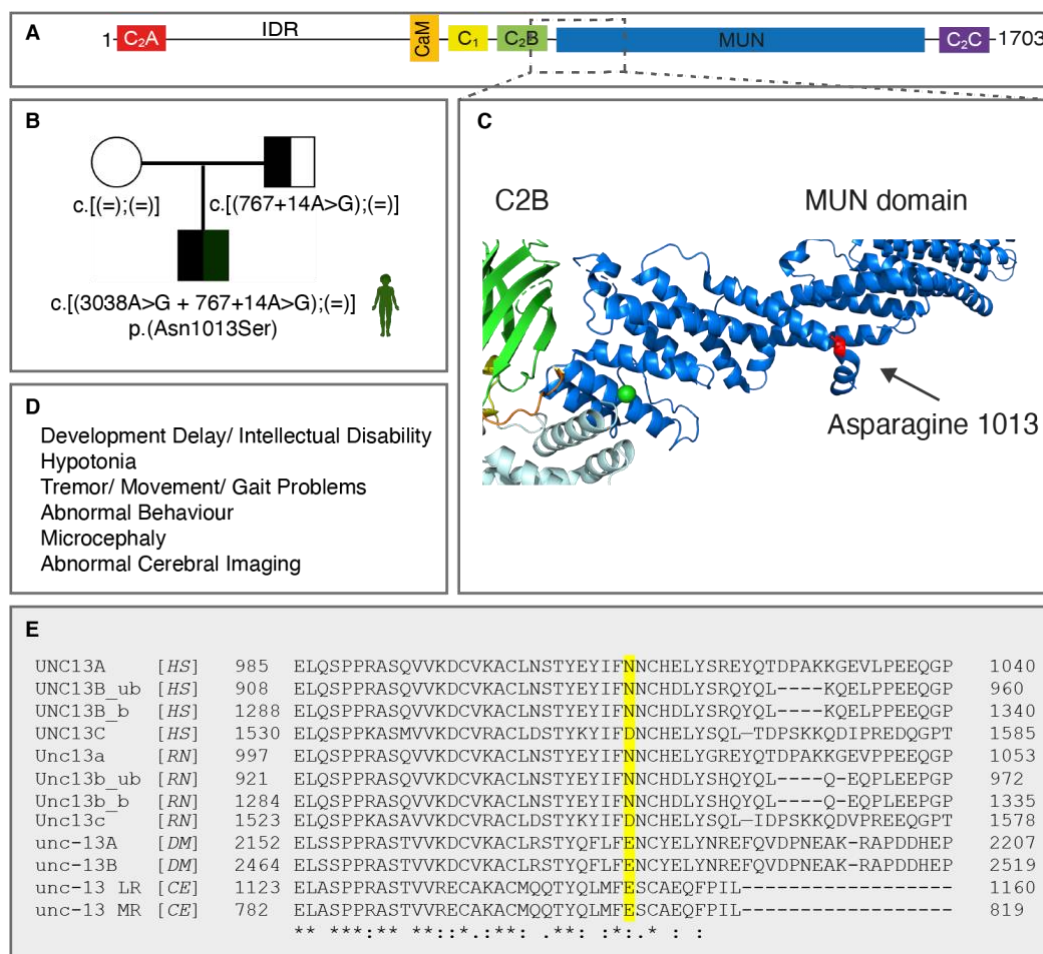


**Figure 21: Genetic and clinical phenotype of a human patient carrying a Munc13-1<sup>N1013S</sup> variant.** **A** Munc13-1 domain structure. A dashed box surrounds the region encompassing the patient mutation N1013S. **B** Pedigree illustrating the patient genotype. The father is unaffected but carries a single nucleotide exchange in an intron of the UNC13A gene. The patient inherited this allele from his father, and in addition carries a *de novo* N1013S mutation on the same allele. The mutated nucleotides with their respective positions are provided in square brackets. **C** Munc13-1 crystal structure of the region indicated roughly by the dashed box. The arrow points to the affected AA residue. The blue structure represents the MUN domain and the green structure the C2B domain. **D** Clinical symptoms of the patient carrying the *de novo* N1013S variant. **E** Sequence Alignment of the AA residues surrounding the asparagine at position 1013 in human is depicted for the four isoforms UNC13A, UNC13B\_ub, UNC13B\_b and UNC13C and across different species (human (HS), rat (RN), drosophila (DM) and *C. elegans* (CE)) in the existent isoforms. The relevant asparagine is highlighted in yellow. Asterisks (\*) indicate fully conserved residues, a colon (:) indicates conservation of residues with strongly similar properties and period (.) indicates conservation of residues with weakly similar properties.

#### 4.1.4.4 Synaptic Transmission is Largely Normal in Munc13-1<sup>N1013S</sup>-Expressing Neurons

I generated a Munc13-1 cDNA construct containing the N1013S exchange (N1026 in the rat cDNA).

I first monitored spontaneous miniature events in neurons under resting conditions. Munc13-1/2 DKO neurons rescued with the Munc13-1<sup>WT</sup> or the mutant Munc13-1<sup>N1013S</sup> protein did not exhibit any significant effect in terms of average mEPSC frequencies ( $P > 0.05$ , Figure 22 A, B). Similarly, average mEPSC amplitude (Figure 22 D) as well as kinetics (rise time, half-width, and decay time; Figure 22, E-G), which are all derived from the average mEPSC traces depicted in Figure 22 C, were comparable in DKO neurons rescued with WT or mutant protein.

EPSC release characteristics were measured by AP induction in Munc13-1<sup>WT</sup> or Munc13-1<sup>N1013S</sup>-expressing neurons. Similar EPSC amplitudes were recorded on average (Figure 23 A, B;  $P > 0.05$ ), and EPSC kinetics was similar (Figure 23 C, D). The readily-releasable pool (RRP) of SVs as depicted in Figure 23 E, F was not changed in Munc13-1<sup>WT</sup> and Munc13-1<sup>N1013S</sup> expressing neurons, and accordingly, the probability of vesicular release (pV<sub>R</sub>) as illustrated in Figure 23 G was comparable between conditions.

Depolarizations with AP trains at 10- and 40 Hz frequency, used to probe the neurons' behaviour during activity, were expectedly similar between conditions. Example traces for 10 Hz and 40 Hz stimulus trains are illustrated in Figure 24 A & C, respectively. Normalized EPSC amplitudes in the graphs in Figure 24 B & D show no change in short-term plasticity properties in DKO neurons expressing the Munc13-1<sup>WT</sup> or the Munc13-1<sup>N1013S</sup> variant. PDBu application resulted in similar pattern of potentiation (Figure 24 E).

In summary, the functional data does not support a deleterious role for the N1013S mutation.



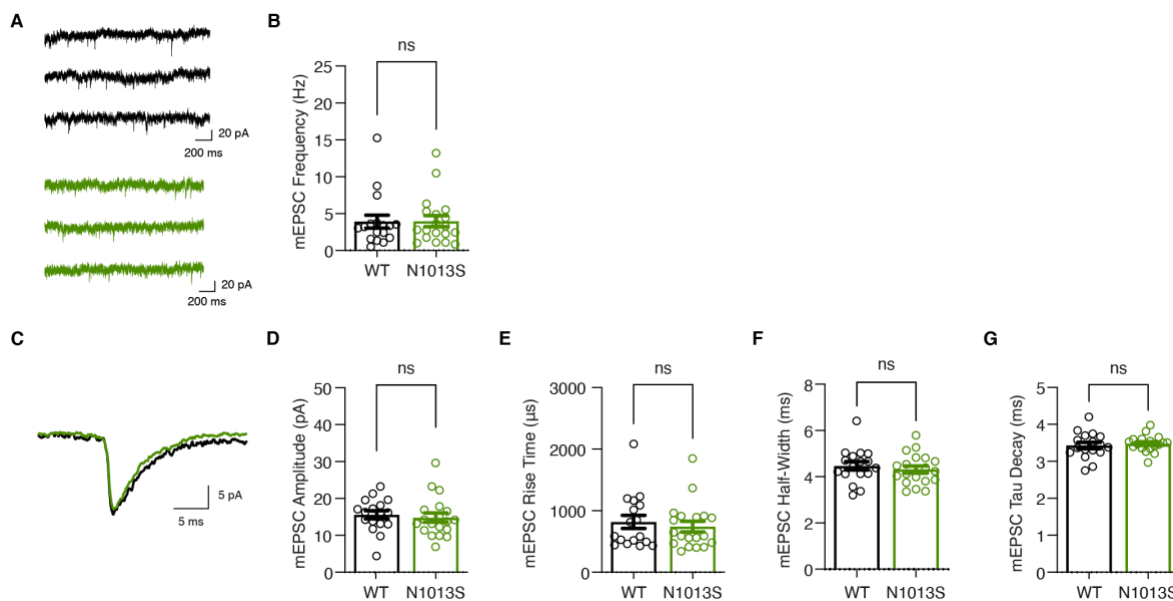


**Figure 22: Spontaneous release characteristics in Munc13-1<sup>N1013S</sup> expressing neurons.** **A** mEPSC example traces from autaptic hippocampal excitatory Munc13-1/2 DKO neurons expressing Munc13-1<sup>WT</sup> (black) and Munc13-1<sup>N1013S</sup> (dark green) after application of 300 nM TTX. **B** Average mEPSC frequencies. **C** A representative average mEPSC trace for Munc13-1<sup>WT</sup> (black) and Munc13-1<sup>N1013S</sup> (dark green) is depicted in an overlay. The graphs in the lower panel under **D**, **E**, **F**, **G** depict the average mEPSC amplitude (**D**), average mEPSC rise time (**E**), average mEPSC half-width (**F**) and average mEPSC tau decay (**G**) for Munc13-1<sup>WT</sup> (black) and Munc13-1<sup>N1013S</sup> (dark green) respectively. Each circle illustrates the data for one recorded neuron. The error bars in the figure designate mean values  $\pm$  SEM. Non-significant (ns) indicates  $P > 0.05$ , Mann-Whitney test.

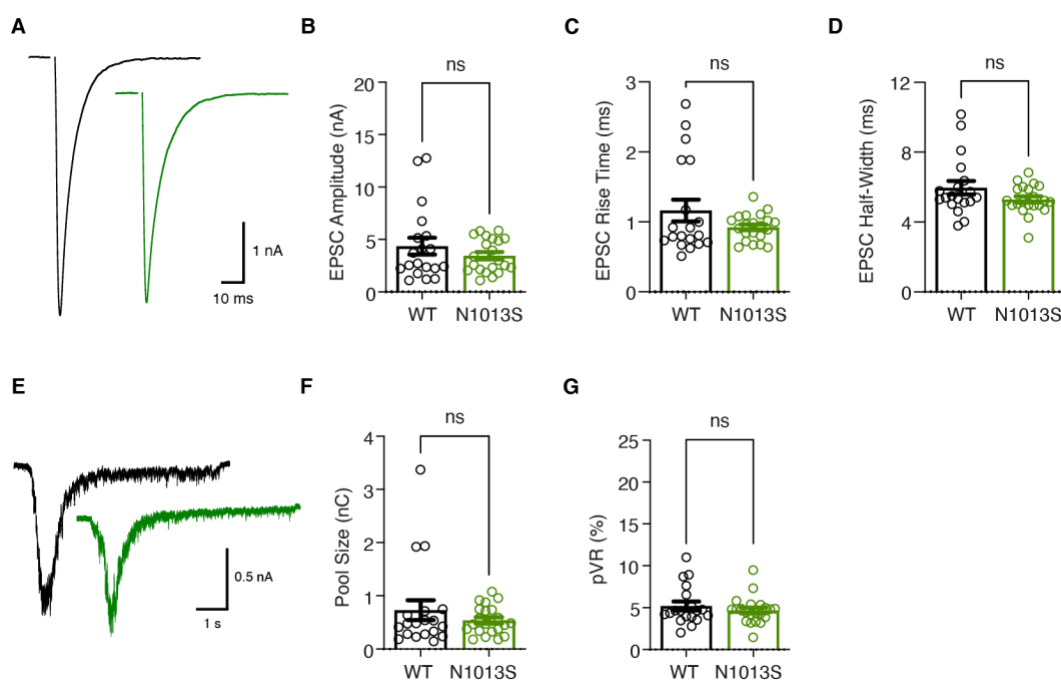


**Figure 23: Evoked release characteristics in Munc13-1<sup>N1013S</sup> expressing neurons.** Autaptic hippocampal excitatory Munc13-1/2 DKO neurons expressing Munc13-1<sup>WT</sup> (black) and Munc13-1<sup>N1013S</sup> (dark green). **A** Representative initial EPSC traces are shown. **B** The initial EPSCs from each recorded neuron symbolized by a circle are plotted as mean  $\pm$  SEM. EPSC kinetic parameters, EPSC rise time (**C**) and EPSC half-width (**D**), are plotted as mean  $\pm$  SEM. **E** Sucrose-induced release of the RRP of SVs is exemplified with representative traces, and average RRP size (**F**) is plotted as mean  $\pm$  SEM, while individual data points are shown as open circles. **G** The graph displays the average vesicular release probability (pVR) in neurons expressing Munc13-1<sup>WT</sup> (black) and Munc13-1<sup>N1013S</sup> (dark green). ns indicates  $P > 0.05$ , Mann-Whitney test.

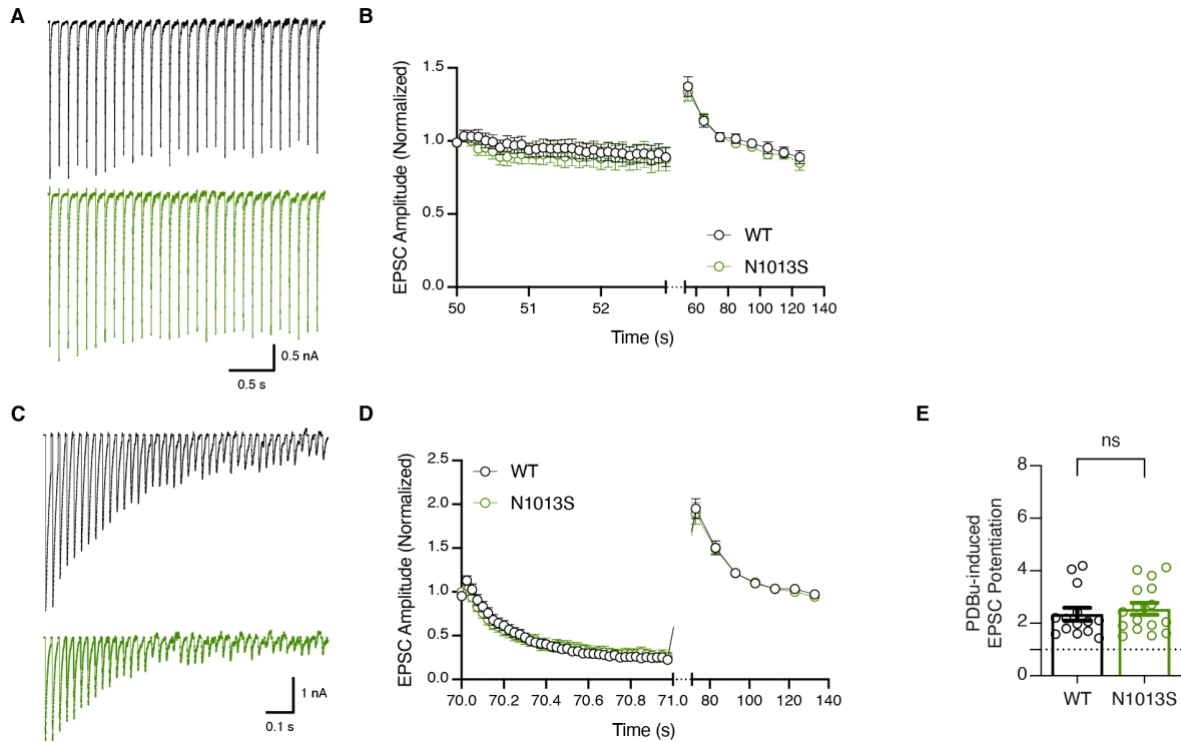


**Figure 24: No change in short-term synaptic plasticity characteristics in Munc13-1<sup>N1013S</sup>-expressing neurons.** Example traces of autaptic hippocampal excitatory Munc13-1/2 DKO neurons expressing Munc13-1<sup>WT</sup> (black) and Munc13-1<sup>N1013S</sup> (dark green) stimulated with AP trains at (A) 10 Hz frequency and (C) 40 Hz frequency. Normalized EPSC amplitudes are plotted for 10 Hz stimulation (B) and 40 Hz stimulation (D) respectively, followed by continuous 0.1 Hz stimulation. E Potentiation of EPSCs after stimulation with PDBu is plotted by normalizing amplitudes to average amplitudes before PDBu application. Data is presented as mean  $\pm$  SEM, while individual data is represented by open circles. ns indicates  $P > 0.05$ , Mann-Whitney test.

### 4.1.5 Expression Levels of Munc13-1 Patient-Specific Variants

Comparative electrophysiological recordings of Munc13-1<sup>WT</sup> and Munc13-1 disease-variants were the main experimental paradigm in this project so far. Using these recordings, I could classify variations as leading to gain-of-function of neurotransmission (i.e G808D), loss-of-function of neurotransmission (E52K, R202H), and to such that result in no functional consequences for neurotransmission (R799Q, N1013S). To consolidate these functional mechanisms, I implemented immunocytochemical and quantitative imaging approaches that enable to detect morphological parameters of the neuron. Assessing morphological parameters in parallel to functional parameters is not only necessary to provide a complete phenotypic characterization of the neuronal state, but also holds the potential to unravel phenotypes that cannot be detected in electrophysiological recordings.

To be able to bridge the functional and morphological data, I preformed the immunocytochemical analysis under similar conditions to those used during electrophysiological recordings. Importantly, all neurons were infected, fixed, stained and imaged in the same experiment, to facilitate cross comparison between conditions. Primary mouse hippocampal Munc13-1/2 DKO neurons were cultured in autapses and infected with the WT and disease-related variant containing Munc13-1 protein. On day 13 of the culture, autapses were fixed and stained with four different antibodies targeting the presynaptic compartment (vGlut1), the postsynaptic compartment (Shank2), the soma and dendrites (MAP2), and the exogenously expressed Munc13-1 protein, based on the c-terminal GFP tag. I used the GFP tag for detecting Munc13-1, and not the Munc13-1 antibody, as the latter introduces a slight background in immunocytochemistry. Finally, confocal microscopy was performed to acquire images. I used Imaris for image analysis, focusing on four major parameters:

1. The number of synapses in each neuron.
2. The degree of Munc13-1 colocalization in these synapses.
3. The intensity of the presynaptic signal, and,
4. The intensity of Munc13-1 signal at synapses.

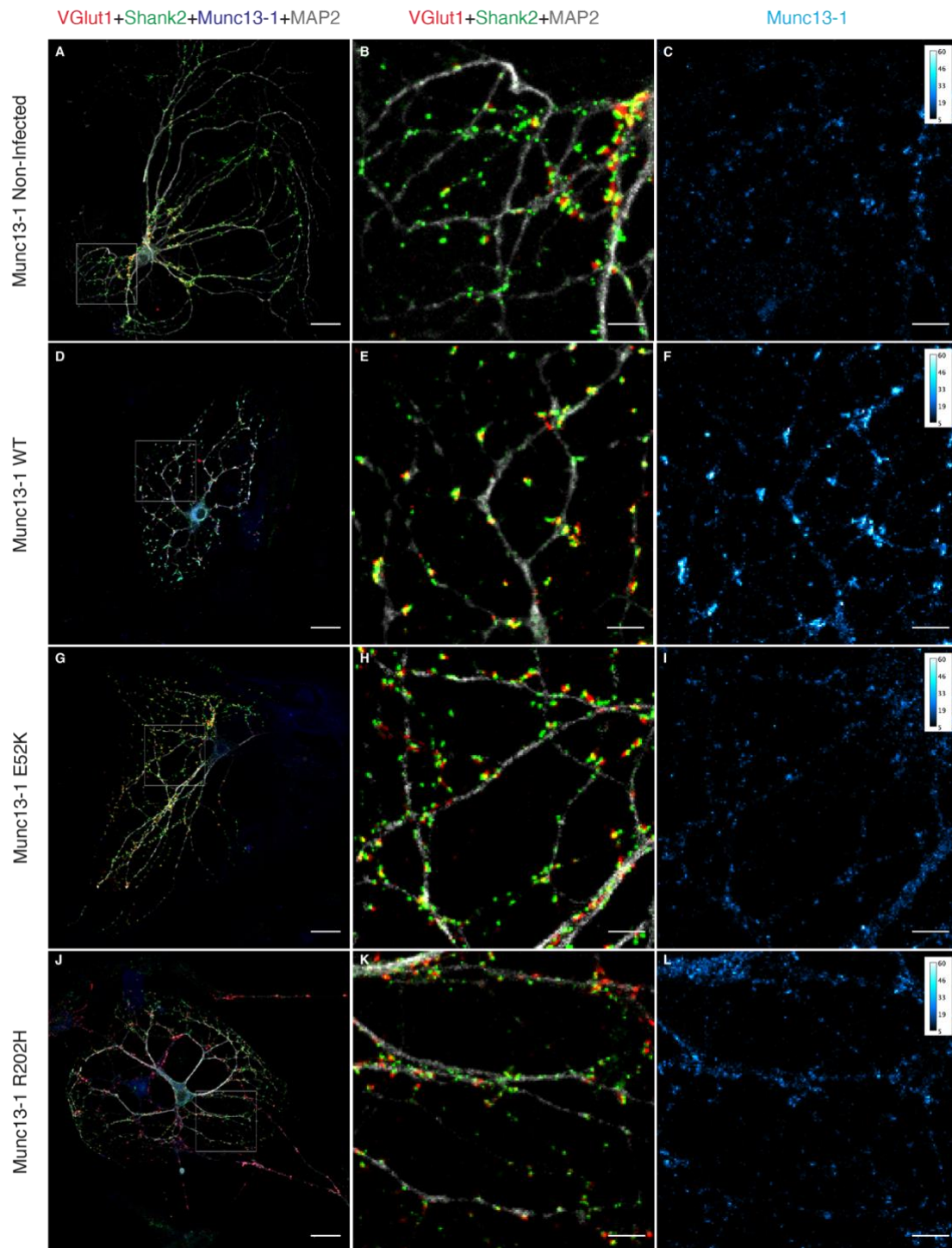


**Figure 25: Confocal Microscopy of Munc13-1<sup>WT</sup>, Munc13-1<sup>E52K</sup>, Munc13-1<sup>R202H</sup> expressing and non-infected Munc13-1/2 DKO (negative control) autaptic hippocampal glutamatergic neurons.** Autaptic hippocampal excitatory Munc13-1/2 DKO neurons either non-infected or infected with Munc13-1<sup>WT</sup>, Munc13-1<sup>E52K</sup> or Munc13-1<sup>R202H</sup> were subjected to immunofluorescent labelling using anti VGlut1 (presynaptic marker in red), Shank2 (postsynaptic marker in green), MAP2 (neuronal dendrites and soma in grey) and EGFP (C-terminally tagged to Munc13-1 in blue) antibodies. **A, D, G, J** Maximum intensity projection of a whole autaptic neuron, acquired in a z-stack from top to bottom, showing all four stainings merged. A square box indicates the region that is magnified in the neighbouring panels. Scale bars: 20  $\mu\text{m}$ . **B, E, H, K** Magnification (5x) of the square box outlined in the whole neuron image and visualization of synapses, where VGlut1 and Shank2 are colocalized. MAP2 indicates dendritic processes. Scale bars: 5  $\mu\text{m}$ . **C, F, I, L** Magnified (5x) images of the outlined box in the whole neuron image depicting only Munc13-1 expression in cyan hot. A calibration bar is set to demonstrate Munc13-1 expression levels, ranging from value 5 (dark) to 60 (light), where 60 indicates the highest intensity of Munc13-1 expression. Scale bars: 5  $\mu\text{m}$

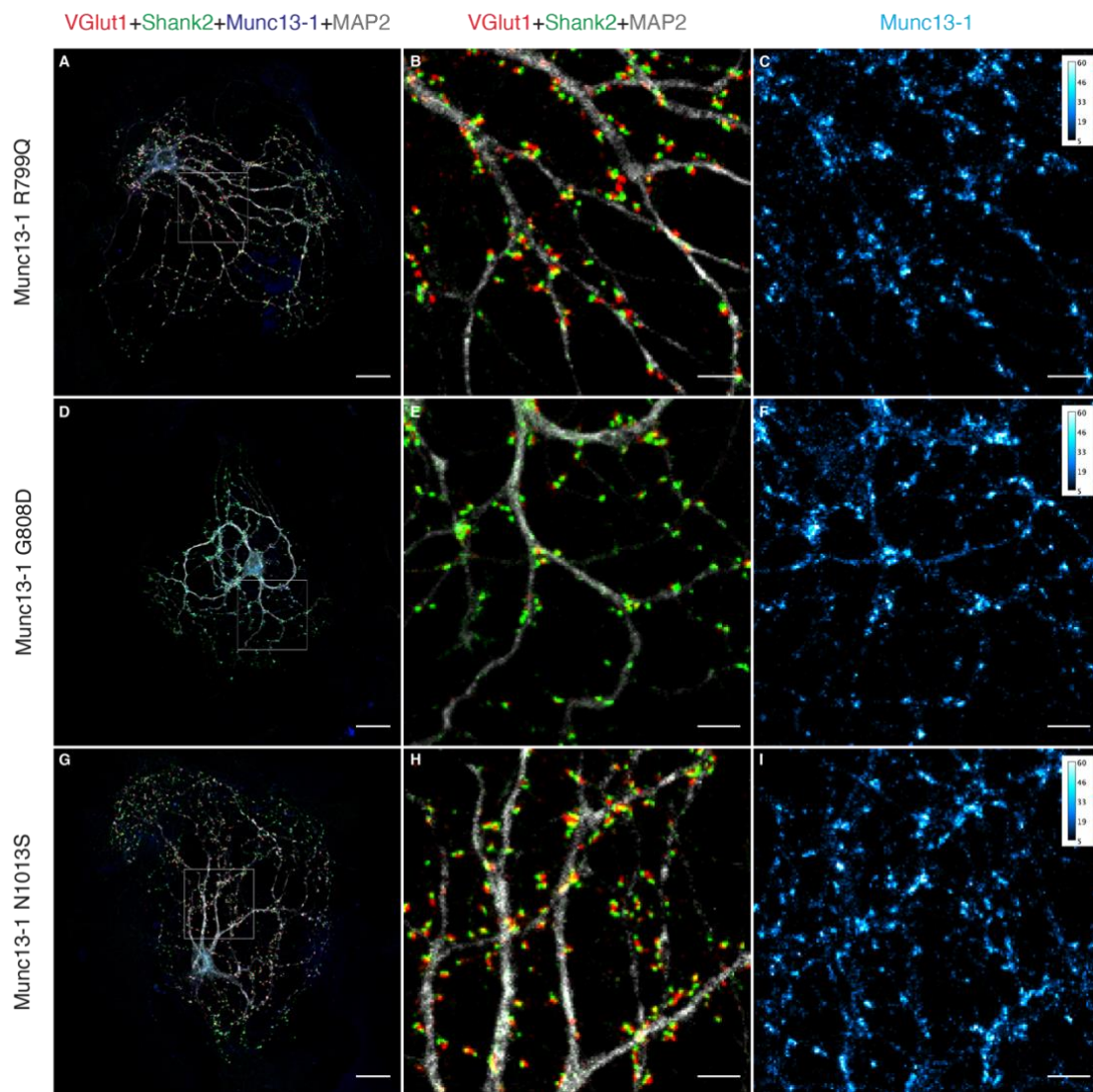


**Figure 26: Confocal Microscopy of Munc13-1<sup>R799Q</sup>, Munc13-1<sup>G808D</sup>, Munc13-1<sup>N1013S</sup> expressing Munc13-1/2 DKO autaptic hippocampal glutamatergic neurons.** Autaptic hippocampal excitatory Munc13-1/2 DKO neurons infected with Munc13-1<sup>R799Q</sup>, Munc13-1<sup>G808D</sup> or Munc13-1<sup>N1013S</sup> were subjected to immunofluorescent labelling against VGlut1 (presynaptic marker in red), Shank2 (postsynaptic marker in green), MAP2 (neuronal dendrites and soma in grey) and EGFP (C-terminally tagged to Munc13-1 in blue). **A, D, G, J** Maximum intensity projection of a whole autaptic neuron, acquired in a z-stack from top to bottom, showing all four staining's merged. A square box indicates the region that is magnified in the neighbouring panels. Scale bars: 20  $\mu\text{m}$ . **B, E, H, K** Magnification (5x) of the square box outlined in the whole neuron image and visualization of synapses, where VGlut1 and Shank2 are colocalized. MAP2 indicates dendritic processes. Scale bars: 5  $\mu\text{m}$ . **C, F, I, L** Magnified (5x) images of the outlined box in the whole neuron image depicting only Munc13-1 expression in cyan hot. Attached is a calibration bar ranging from value 5 (dark) to 60 (light), where 60 indicates the highest intensity of Munc13-1 expression. Scale bars: 5  $\mu\text{m}$



#### 4.1.5.1 The Number of Synapses is Similar under all Recorded Conditions

In non-infected neurons, as well as in Munc13-1<sup>WT</sup>, Munc13-1<sup>E52K</sup>, Munc13-1<sup>R202H</sup>, Munc13-1<sup>R799Q</sup>, Munc13-1<sup>G808D</sup> and Munc13-1<sup>N1013S</sup>- expressing neurons (middle lanes in Figure 25, 26) the presynaptic and postsynaptic compartments colocalize nicely as indicated by the yellow colour arising from vGlut1 (presynaptic marker, red) and Shank2 (postsynaptic marker, green) overlapping signal. The high degree of colocalization also proves the specificity of staining and validates the antibodies used. The objective for this experiment was to test whether the expression of any Munc13-1 disease-related variant has an effect on synapse development.

I defined synapses as puncta, in which the vGlut1 and Shank2 colocalized. The procedure was performed in the image analysis software Imaris, as described in the methods section. The number of synapses was similar throughout conditions (Figure 25 middle panel, Figure 26), although a slightly higher number was found for the non-transfected sample. However, images were only acquired for a small number of non-transfected neurons (n=12), and more data is required to substantiate this finding. It is important to mention that non-transfected neurons were not used as controls in any of the functional experiments described above.

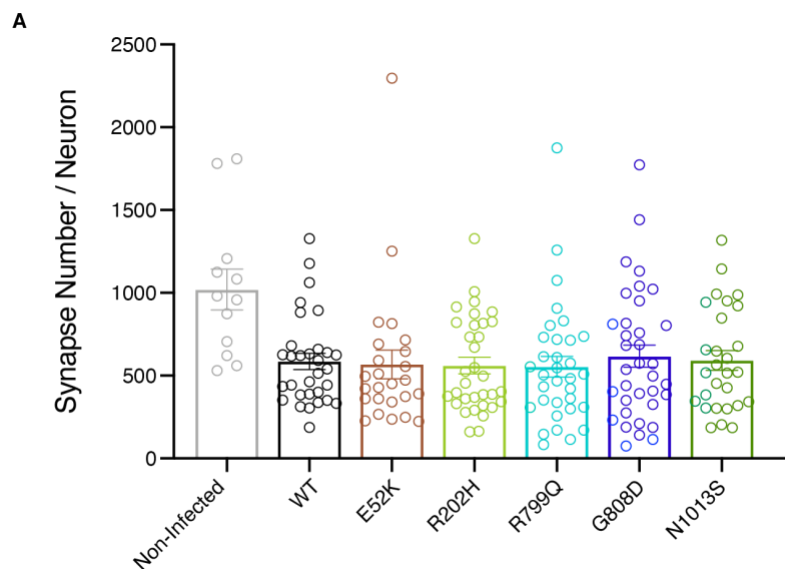


**Figure 27: Synapse number of Munc13-1 disease-related variants expressing neurons.** Autaptic hippocampal excitatory non-infected Munc13-1/2 DKO neurons (n=12), and neurons infected with Munc13-1<sup>WT</sup> (n=31), Munc13-1<sup>E52K</sup> (n=25), Munc13-1<sup>R202H</sup> (n=33), Munc13-1<sup>R799Q</sup> (n=33), Munc13-1<sup>G808D</sup> (n=35) and Munc13-1<sup>N1013S</sup> (n=28) were immunostained with vGlut1, Shank2, MAP2, and Munc13-1 antibodies, imaged, and the resulting signals were subjected to quantification analysis using the Imaris software. Data were obtained from two independent experiments representing two animals, except for the non-infected neurons that were obtained in a single experiment. **A** Overlapping surfaces of vGlut1 (presynaptic marker) and Shank2 (postsynaptic marker) within the surface of MAP2 (dendritic marker) were counted to estimate synapse number. P<0.01, one way-ANOVA.

#### 4.1.5.2 N-terminal Disease-Related Variations Impair Munc13-1 Localization in Synapses

I used the same images to determine whether the disease-related variations lead to changes in the degree of colocalization of Munc13-1 in synapses. I quantified the Munc13-1 signal that colocalized with the vGlut1-Shank2 signal. Example images from all recorded conditions are shown in Figure 25, 26. In the right panel, the Munc13-1 signal is shown, with the signal intensity indicated by the calibration bar. In non-infected, Munc13-1/2 DKO neurons, background signal resulting from the anti-GFP antibody and/or from the secondary antibody used is shown. (Figure 25 C), Munc13-1<sup>E52K</sup> (Figure 25 I) and Munc13-1<sup>R202H</sup> (Figure 25 L) infected cells as compared to the Munc13-1<sup>WT</sup> expression in Figure 25 F. On the other hand, expression of Munc13-1<sup>R799Q</sup>, Munc13-1<sup>G808D</sup> and Munc13-1<sup>N1013S</sup>, as can be seen in Figure 26 C, F, I, is comparable to Munc13-1<sup>WT</sup> (Figure 25 F).

When looking at the percentage of synapses that express Munc13-1 the results are very striking. Importantly, there is no Munc13-1 signal in non-infected Munc13-1/2 DKO neurons. Interestingly, the averages of Munc13-1<sup>E52K</sup> and Munc13-1<sup>R202H</sup> expression in synapses are much reduced, consistent with the observations in the electrophysiological readout, where they exhibit loss of function in some form. Munc13-1 expression levels in neurons infected with Munc13-1<sup>R799Q</sup>, Munc13-1<sup>G808D</sup> and Munc13-1<sup>N1013S</sup> are in terms of averages comparable to the Munc13-1<sup>WT</sup> expression levels (Figure 25).

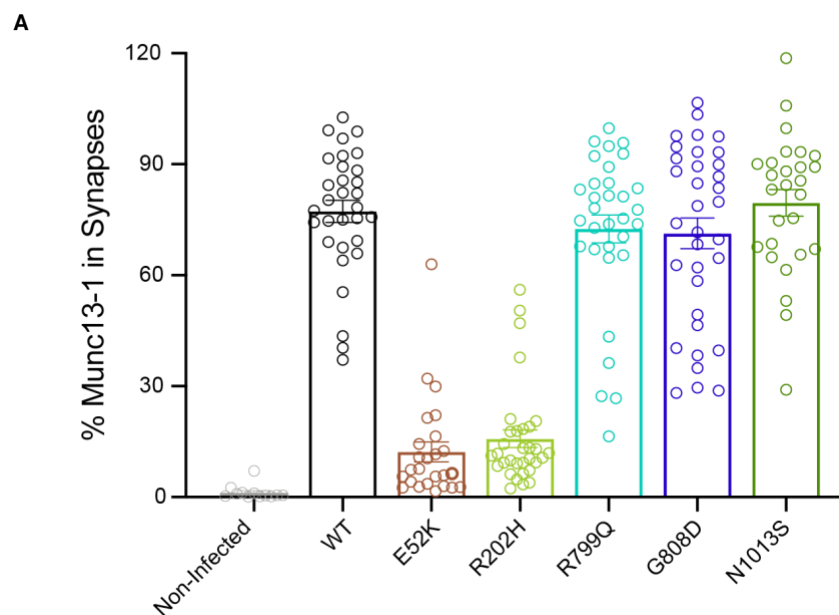


**Figure 28: Number of Munc13-1 colocalizing synapses in Munc13-1 disease-related variants expressing neurons.** Autaptic hippocampal excitatory non-infected Munc13-1/2 DKO neurons (n=12), and neurons infected with Munc13-1<sup>WT</sup> (n=31), Munc13-1<sup>E52K</sup> (n=25), Munc13-1<sup>R202H</sup> (n=33), Munc13-1<sup>R799Q</sup> (n=33), Munc13-1<sup>G808D</sup> (n=35) and Munc13-1<sup>N1013S</sup> (n=28) were immunostained with vGlut1, Shank2, MAP2, and Munc13-1 antibodies, imaged, and the resulting signals were subjected to quantification analysis using the Imaris software. Data were obtained from two independent experiments representing two animals, except for the non-infected neurons that were obtained in a single experiment. **A** The percentage of Munc13-1 positive puncta that colocalize with VGlut1-Shank2 puncta, defining Munc13-1 positive synapses within the surface of MAP2 (dendritic marker). P<0.0001, one way-ANOVA.

The reduced level of colocalization of Munc13-1 with vGlut1-Shank2 synapses in the E52K and R202H could be explained in two ways:

1. Munc13-1 is colocalized properly, but only in a subset of synapses.
2. Munc13-1 expression is reduced across all synapses.

If the former is correct, Munc13-1 intensity in the synapses where it is detected would be comparable to Munc13-1 expression levels in WT synapses. If the latter is correct, the expression levels of Munc13-1 puncta at synapses will be on average reduced. Quantification of the Munc13-1 signal intensity that colocalizes with vGlut1-Shank shows reduced intensity values, that are comparable to the background levels quantified in the non-infected neurons. In summary, this analysis supports the notion that Munc13-1 cannot be stabilized across all synapses of the neuron.

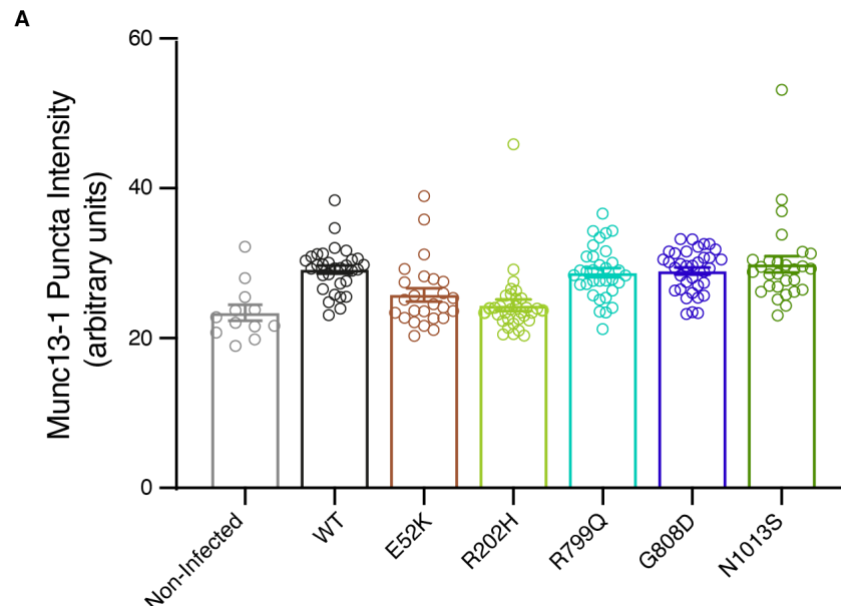


**Figure 29: Quantification of the Munc13-1 signal intensity in synapses expressing Munc13-1 disease-related variants.** Autaptic hippocampal excitatory non-infected Munc13-1/2 DKO neurons (n=12), and neurons infected with Munc13-1<sup>WT</sup> (n=31), Munc13-1<sup>E52K</sup> (n=25), Munc13-1<sup>R202H</sup> (n=33), Munc13-1<sup>R799Q</sup> (n=33), Munc13-1<sup>G808D</sup> (n=35) and Munc13-1<sup>N1013S</sup> (n=28) were immunostained with vGlut1, Shank2, MAP2, and Munc13-1 antibodies, imaged, and the resulting signals were subjected to quantification analysis using the Imaris software. Data were obtained from two independent experiments representing two animals, except for the non-infected neurons that were obtained in a single experiment. **A** The signal intensity of Munc13-1 positive puncta (represented in arbitrary values), that colocalize with VGlut1-Shank2 puncta, within the surface of MAP2 (dendritic marker). P<0.0001, one way-ANOVA.



### 4.1.5.3 Neurons Expressing the C-terminal N1013S Disease-Related Variation Show Stronger Presynaptic Signal Density

To assess whether Munc13-1-disease related variations cause changes to the presynaptic compartment, I evaluated the intensity of the vGlut1 signal within vGlut1-Shank2 puncta in non-infected neurons, as well as in neurons expressing the Munc13-1 disease-related variation. I unexpectedly observed that in neurons expressing the Munc13-1<sup>N1013S</sup> variation, vGlut1 puncta exhibit higher intensity. This was true also when analysing the data from each individual experiment separately. While the significance of this finding is unclear, it could indicate that this variant may affect synaptic processes at the level of the reserve SV pool, via a yet unidentified mechanism, that could not be unravelled in the functional assessment I performed here.

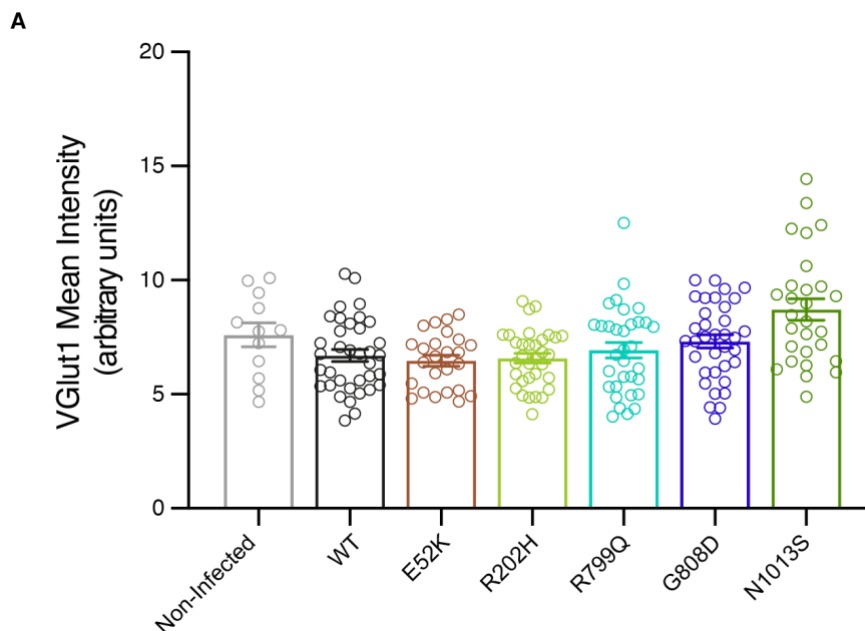


**Figure 30: Quantification of the vGlut1 signal intensity in synapses expressing Munc13-1 disease-related variants.** Autaptic hippocampal excitatory non-infected Munc13-1/2 DKO neurons (n=12), and neurons infected with Munc13-1<sup>WT</sup> (n=31), Munc13-1<sup>E52K</sup> (n=25), Munc13-1<sup>R202H</sup> (n=33), Munc13-1<sup>R799Q</sup> (n=33), Munc13-1<sup>G808D</sup> (n=35) and Munc13-1<sup>N1013S</sup> (n=28) were immunostained with vGlut1, Shank2, MAP2, and Munc13-1 antibodies, imaged, and the resulting signals were subjected to quantification analysis using the Imaris software. Data were obtained from two independent experiments representing two animals, except for the non-infected neurons that were obtained in a single experiment. **A** The signal intensity of vGlut1 positive puncta (represented in arbitrary values), colocalized with Shank2 and within the surface of MAP2 (dendritic marker). P<0.0001, one way-ANOVA.

## 5 Discussion

### 5.1 Munc13-1 Associated Neurodevelopmental Disorder

The goal of our project was to characterize synaptic transmission abnormalities in patients exhibiting a neurological disease associated with genetic defects in the *UNC13A* gene. In this context it is requisite to study the basic principles of SV priming, upstream of neurotransmitter release, and define the outstanding role of Munc13-1 in this highly synchronized process that is indispensable for neuron-to-neuron communication. A critical step for SV fusion comprises the assembly of the SNARE complex, consisting of vesicular membrane-associated synaptobrevin and plasma membrane-associated syntaxin-1 and SNAP-25, into a four-helix bundle (Söllner, 1993; Sutton et al., 1998). SNARE complex assembly and the concomitant SV fusion can solely be achieved with the function of the key regulator Munc13-1 protein, which chaperones SNARE complex assembly by opening syntaxin-1 with its MUN domain (Basu et al., 2005; Ma et al., 2011) and forms a tether between the SV and the plasma membranes through interaction of its C1-C2B region with the plasma membrane and the C2C domain with the SV membrane (Liu et al., 2016).

Crucial evidence for the significance of Munc13-1 activity in normal nervous system function were obtained via studying its knockout in mice and in other organisms, demonstrating that Munc13-1 predominantly governs SV priming in glutamatergic synapses (Augustin et al., 1999b) and thereby critically modulates synaptic neurotransmission. Varoqueaux *et al.* have shown that in mice, the double knockout of Munc13-1 and its paralog Munc13-2 is incompatible with life, since both glutamatergic and GABAergic neurotransmission are fully arrested, resulting in the absence of evoked and spontaneous neurotransmitter release (Varoqueaux et al., 2002). The c-terminal sequence of Munc13-1 is highly similar in all Munc13 paralogs, and displays high degree of sequence and functional conservation in the nervous system of species such as *Drosophila* and *C. elegans* (Aravamudan et al., 1999; Koch et al., 2000; Richmond et al., 1999).

Two independent reports presented two patients carrying single nucleotide exchanges in the *UNC13A* gene, suffering from a complex neurodevelopmental disorder manifested from birth (Engel et al., 2016; Lipstein et al., 2017). In the Department of Molecular Neurobiology at the Max Planck Institute of Experimental Medicine, Göttingen, one of these variations was functionally characterized (Lipstein et al., 2017). In the aftermath, an array of patients carrying *UNC13A* variations was reported to us, and a collaboration was initiated between the Institute of Medical Genetics in Zurich and our department, to combine clinical and genetic diagnosis with functional

studies of the relevant variations. An overwhelming number of patients, which by now reached 40, with variable inheritance patterns and clinical presentation, were reported from all around the world. The work presented here is the beginning of a long-term study of this novel disorder pertaining to the Munc13-1 protein, necessitating an in-depth investigation of Munc13-1 physiology. Given the significance of Munc13-1 in sustaining central nervous system function concomitant to the discovery of a large cohort of patients carrying UNC13A variants, this project focused on the functional characterization of selected patient-specific variants with respect to synaptic transmission abnormalities. In total, I present a cohort of 12 patients, altogether expressing variants in five different regions of the Munc13-1 protein, with variable genetic inheritances, such as haploinsufficiency, dominant negative and recessive inheritance, all characterized by a vast spectrum of clinical symptoms manifesting in a neurodevelopmental disorder. This study was conducted in succession to the previously published case study by Lipstein *et al.* that described a patient displaying a neurological disorder suggested to originate from a *de novo* variant in the Munc13-1 gene. In consistency with that and endorsing the therein established genotype-phenotype correlation as the root cause for the illness, I conducted functional characterization of additional patient-specific variants, including a patient expressing a variant that resides in close proximity to the previously reported proline 814 to leucine (P814L) mutation and displays strikingly similar function (G808D; Figure 6, 7), corroborating the previous findings. Furthermore, in this study I collected functional data assessing the effects of additional, newly-identified variants on synaptic transmission, to define whether they represent a cause for the clinical phenotypes manifested in the patients.

In aggregate, functional and morphological data obtained using electrophysiology and imaging suggest that variations in Munc13-1 act through at least two mechanisms, a loss of function and a gain of function of neurotransmission. Therefore, we expressed rat Munc13-1 mutations, equivalent to the patient-specific variants, in primary autaptic hippocampal neurons and tested the effect on glutamatergic neurotransmission in particular. Additionally, we used a microscopy approach to ascertain the localization and abundance of the Munc13-1 variants in autaptic hippocampal neurons.

## 5.2 Functional Assessment of Human Patient-Specific Variants using the Autaptic Culture System – Pros and Cons of the Experimental System

All experiments presented in this work were conducted in neurons that were obtained from Munc13-1/2 DKO mice and rescued with the rat Munc13-1<sup>WT</sup> protein or Munc13-1 protein carrying a disease-related variant. The rat, mouse, and human Munc13-1 isoforms exhibit very high similarity in the AA sequence:

**Table 2:** Amino acid identity amongst Munc13-1 isoforms from rat, human and mouse.

	Q9UPW8 UNC13A_HUMAN	Q62768 UNC13A_RAT	Q4KUS2 UNC13A_MOUSE
Q9UPW8 UNC13A_HUMAN	100 %	96.00 %	96.17 %
Q62768 UNC13A_RAT	96.00 %	100 %	98.83 %
Q4KUS2 UNC13A_MOUSE	96.17 %	98.83 %	100 %

This high sequence conservation is indicative of a highly conserved function of the protein in mammals, as well as a strong evolutionary pressure to conserve the protein sequence. It validates our selection to work with the rat cDNA, rather than that of mouse or human Munc13-1 cDNA.

Both functional and morphological analyses in this project were made in mouse neurons. Mouse tissue is conventionally used to study mammalian physiology, primarily because of the availability of tissue, the ability to create genetically-modified cells, and the ability to transduce them with exogenous cDNA. We do not know to what extent mouse neurons are similar to the respective human neurons from the same brain structure, but it is safe to assume that the principles of synaptic transmission are fully conserved. As an alternative to experiments in mouse neurons, experiments in human-derived iPSCs are now possible (Fenske et al., 2019; Rhee et al., 2019). Using such neurons is technically challenging, especially because they exhibit large diversity in their functional properties, possibly because they are differentiated to different developmental stages. Large variability is evident between clones of cells, even from the same patient, indicating that their extraction process is highly sensitive. While working with patient-derived iPSCs in projects like this is probably the future of biomedical sciences, such investment was not possible in the early stage of this project. Confirming the pathogenicity of several variations, the lab will now invest in isolation of patient-derived iPSCs from these patients for further investigation.

All experiments here made use of the autaptic culture system. The strength of this system is the simple monosynaptic circuitry, the possibility to expose the neurons to different drug treatments, a high degree of reproducibility, the possibility to screen for multiple phenotypes and

for many variations in relatively little time, and the possibility to culture neurons from mice with a lethal phenotype, like the Munc13-1/2 DKO mouse line. This experimental system has proven its robustness in a wide array of structure-function studies, including the investigation of gene products, in investigating different neuronal cell types, such as excitatory or inhibitory cells, and in studies of presynaptic mechanisms, and disease mechanisms using patient-specific variants (Camacho et al., 2017; Lipstein et al., 2017; Liu et al., 2016; Repetto et al., 2018; Xu et al., 2017). Pioneers of this technique have established stimulation protocols for the standardized readout of a wide range of synaptic properties, which can deduce both presynaptic and postsynaptic features of neurotransmission (Bekkers and Stevens, 1991; Burgalossi et al., 2012; Pyott and Rosenmund, 2002).

In the experiments presented here, I used lentiviral-mediated transduction of neurons from Munc13-1/2 DKO mice. A huge advantage of this experimental paradigm is that autaptic neurons from Munc13-1/2 deficient mice are silent – in these neurons no neurotransmission can be measured. This provides a clean and uncontaminated baseline for a non-ambiguous readout of the rescue-mediated properties of neurotransmission, eliminating the need for any assumptions during analysis. Munc13-1 WT and disease-related variants were cloned under the neuron-specific synapsin promoter, which is a relatively weak promoter, resulting in only mild levels of overexpression. While this experimental design is optimal for studying the properties of synaptic transmission induced by Munc13-1 disease variants, it is, of course, far from the situation in the patients' neurons – which express Munc13-2 and where Munc13-1 expression levels are normal. Further experiments with patient-derived iPSCs hold the potential to resolve these experimental limitations. Alternatively, the generation of dedicated knock-in mice carrying key variations will allow to study their effect under normal expression levels, in the presence of other Munc13-2 isoforms, and in the intact tissue. Generating such models is, however, highly time consuming, and with >40 patients documented, it is impossible to generate a model for each variation.

In sum, the experimental setup used here allowed me to interrogate how pre- and postsynaptic properties may change when Munc13-1 carries disease-related variations. Using this system, I was able to screen through a moderate number of variations and determine whether they are pathogenic or benign. Acknowledging the importance of investigating this in the context of human cells or *in vivo* in intact neuronal networks, I propose potential follow up approaches: knock-in mice for studying the effect of the variations on complex circuits with more than one neuron, and iPSCs for studying the effect of the variation in its genetic context. Only then can we achieve a full picture of the pathomechanisms.

### 5.2.1 Gain of Function in the Munc13-1<sup>G808D</sup>

The glycine (G) at AA 808 that resides in the seven AA long C2B-MUN-Linker (CML) region and is highly conserved across species (Figure 5 E), was found mutated to aspartic acid (D) in four patients and mutated to valine and cysteine in two additional patients. All six patients carrying an AA exchange at position 808 presented with strikingly similar clinical symptoms, including developmental delay, tremors or dyskinetic movement disorder, seizures, abnormal cerebral imaging and abnormal behaviour (Figure 5 D). The clinical similarity speaks in favour of these mutations exerting a comparable effect at the molecular level that translates to the pathophysiology observed in these patients.

To study the effect of this mutation on synaptic release properties, I focused on the G808D variation. I observed a significantly increased frequency of mEPSC events in neurons expressing the Munc13-1<sup>G808D</sup> mutant (Figure 6 B), with no effect on mEPSC amplitude. In accordance with this, I observed by trend larger EPSCs (Figure 7 A), accompanied by a significantly longer average EPSC half-width (Figure 7 D). Michelassi *et al.* describe a *C. elegans* C2B domain deficient mutant that exhibits increased neurotransmission, and at the same time displays slower average EPSC decay kinetics. Since the average mEPSCs kinetics were not changed in the C2B domain deficient mutant compared to WT, they concluded that an increased dispersion of single release events was the cause for the slower EPSC decay kinetics. Such an effect on evoked release rates in our system will require further substantiation, for example by deconvolution analysis.

Due to the somewhat larger EPSCs and unchanged RRP sizes, the average pV<sub>R</sub> dramatically increased (Figure 7 G). In agreement with increased release probability during single APs, short-term plasticity characteristics during trains of APs were changed: faster and stronger STD was apparent during 10 Hz and 40 Hz stimulus trains (Figure 8 B, D), likely reflecting a strong depletion of the RRP, faster than it can be refilled: enhanced depression could result due to reduced rates of RRP replenishment caused by the G808D mutation. Demonstrating this will require further investigation. Alongside increased depression we observed that EPSC amplitude immediately after the repetitive stimulation was not augmented as seen in Munc13-1<sup>WT</sup>-expressing neurons. The behaviour of a neuron after a train reflects a combination of processes including SV replenishment after depletion, and the return of the pV<sub>R</sub> from a potentiated level back to baseline. The precise mechanism underlying this observed augmentation after a train is not resolved yet at the level of the WT protein.

Lastly, PDBu mediated enhancement of pV<sub>R</sub> was significantly lower than in Munc13-1<sup>WT</sup> neurons, which is congruent to the fact that Munc13-1<sup>G808D</sup>-expressing neurons already exhibit a

significantly higher basal release probability. This finding is intriguing, as it indicates a crosstalk between the CML domain and the activity of the C1 domain. Alternatively, it can also result from a ‘ceiling effect’: PDBu acts through the potentiation of pVR. Because in Munc13-1<sup>G808D</sup>-expressing neurons the pVR is already potentiated, the effect of PDBu is blocked. Interestingly, a very similar set of observations - including increased pVR, increased mEPSC frequency, and lack of responsiveness to PDBu - was made in the past for a point mutation (H567K) in the C1 domain of Munc13-1. This suggests a shared function of C1 mutation and the CML region mutations in the Munc13-1 protein (Figure 8, (Rhee et al., 2002)).

The phenotype documented here for the G808D mutation phenocopies the phenotype observed for the P814L mutation – suggesting with a high probability that mutations in the CML region exert a similar effect. Lipstein *et al.* have described the *de novo* P814L variant with a gain of function due to a higher basal release probability with significantly increased mEPSC frequency and vesicular release probability as we observed in our recordings. With respect to STP characteristics, similar depression patterns were seen for Munc13-1<sup>P814L</sup>-expressing neurons and Munc13-1<sup>G808D</sup>-expressing neurons during stimulation at 10- and 40 Hz, and the lack of augmentation during recovery from stimulation was similar. The overall similarity in phenotype is striking and together with the high number of patients found to carry variations in this region, allows to draw the conclusion that variations in the CML are causal for the disorder, and likely result in similar consequences to the protein function.

Following the publication by Lipstein *et al.*, Michelassi *et al.* studied the disease-related P814L in *C. elegans*, in conjunction with the C2B domain. Mechanistically, they proposed a model, where the CML maintains an autoinhibitory state of the C2B domain, that keeps release probability low until Ca<sup>2+</sup> and PIP/PIP<sub>2</sub> mediated activation of the Munc13-1 paralog Unc-13A releases this autoinhibition and increases release probability (Michelassi et al., 2017). Given the comparable electrophysiological readout, the G808D mutation is also expected to perturb the autoinhibitory state of the Ca<sup>2+</sup>-unbound C2B domain, setting in motion a hyperexcited state manifesting in enhanced basal release probability. While the P814L was only studied in the context of the C2B domain, the C1 domain is also thought to be maintained in an autoinhibitory state. Our data support a model where mutations in the CML domain also release the autoinhibition of the C1 domain, making it constitutively active. Such a model can account for the similarity between the phenotypes of the G808D mutation, the P814L mutation, and the C1 domain mutation H567K.

The CML region contains 7 AAs: **GEEKVAP**. For reference, the Munc13-1 protein contains 1703 AA. So far, we identified 10 patients with variations in this region: G808, variations are carried by six patients, more than any other variation in our patient cohort; three patients carry

variations in AA P814, and one patient carries a variation in AA K811. In sum, we have ten patients with *de novo* variations that locate to the CML region, the patients largely overlap in their symptoms, and my data demonstrate that the functional consequences of the P814L and G808D variations to synaptic transmission is essentially identical. Taken together, I conclude that the CML region is a hot-spot region in the Munc13-1 protein, where variations cause brain disease.

### 5.2.2 Loss of Function in the Munc13-1<sup>R202H</sup>

The R202H mutation is located in a region that is described as intrinsically disordered (IDR, see Figure 9 A). Based on its AA properties it is likely to be unstructured, and studies on its functional importance are scarce. However, AAs in close vicinity to R202 are conserved in Munc13-1 and ubMunc13-2 between human and rat, pointing to its significance (Figure 9 D). We know of three patients, one with an R202H mutation and two expressing an R202C mutation, all of which exhibit a severe neurodevelopmental disorder, including severely perturbed development, going hand in hand with intellectual disability, seizures, hypotonia, musculoskeletal abnormalities and abnormal cerebral imaging (Figure 9). Of note, we did not pay attention to the presence of a biallelic frameshift mutation in the second *UNC13A* allele (Figure 9 B upper panel) in the patient carrying the R202H mutation, since we know that the mother carries the same frameshift and is healthy. This allows us to conclude that heterozygosity for Munc13-1 is tolerated in humans.

One set of recordings was performed at low  $\text{Ca}^{2+}$  &  $\text{Mg}^{2+}$  concentration to unmask phenotypes related to the modulation of release probability that otherwise may be hard to detect at higher  $\text{Ca}^{2+}$  &  $\text{Mg}^{2+}$  concentration. From our electrophysiological measurements at low and high  $\text{Ca}^{2+}$  &  $\text{Mg}^{2+}$  concentration we deduced no change in spontaneous release characteristics (Figure 10;  $P > 0.05$  for all conditions). In both conditions we observed significantly reduced synaptic strength, with a significant reduction in average evoked EPSC amplitudes, while this reduction was milder in the high  $\text{Ca}^{2+}$  &  $\text{Mg}^{2+}$  concentration (\*\*  $P < 0.01$  in Figure 11 B, \*  $P < 0.05$  in Figure 12 B). A significant change in EPSC kinetics only becomes apparent at low  $\text{Ca}^{2+}$  &  $\text{Mg}^{2+}$  condition where we observed marked reduction of EPSC rise time and half-width (\*\*  $P < 0.01$  in Figure 11 C, D) for the R202H mutant, which was not evident in the high  $\text{Ca}^{2+}$  &  $\text{Mg}^{2+}$  concentration. Typically, kinetic parameters are a measure for SV fusion and postsynaptic receptor properties. However, knowing that clamping artifacts can induce changes in kinetic parameters, and that those are often occurring in autaptic recordings, this finding will have to be carefully examined. However, changes in EPSC release kinetics have been observed in the context of Munc13s, in a series of experiments with the UNC13-L isoform in *C. elegans*, where similar to our findings, a faster rise



time and decay kinetics were observed compared to WT controls. This was interpreted to propose that UNC13-L affects ACh release kinetics, but the mechanism for this finding is unclear (Figure 3, (Hu et al., 2013)).

A significantly reduced pool size for the R202H mutation was recorded at low  $\text{Ca}^{2+}$  &  $\text{Mg}^{2+}$  concentration, which amounted to a significantly reduced vesicular release probability (\* $P < 0.05$ , Figure 11 F, G). This effect was not mirrored in the recording performed at high  $\text{Ca}^{2+}$  &  $\text{Mg}^{2+}$  concentration, where the pool size for Munc13-1<sup>R202H</sup>-expressing neurons was only reduced by tendency. Note that the sample size of the recordings at high  $\text{Ca}^{2+}$  &  $\text{Mg}^{2+}$  concentration is small and therefore I propose that the number of recorded neurons should be increased to the normal standard (~40 neurons per condition) to resolve the difference. An optimal experimental design would be to conduct measurements in the same neurons and change the external  $\text{Ca}^{2+}$  &  $\text{Mg}^{2+}$  concentration during the recording, so that a comparison between the two conditions for the same neuron can be made.

Plasticity was observed in the form of short-term facilitation at low  $\text{Ca}^{2+}$  &  $\text{Mg}^{2+}$  concentration, in which the Munc13-1<sup>R202H</sup>-expressing neurons exhibited much stronger facilitation compared to WT at 10 Hz stimuli (Figure 13 B), reflecting the previously observed reduction in pVR. At 40 Hz this depression was evident, with R202H exhibiting milder depression (Figure 13 D), again reflecting the reduced pVR. No change was observed for the STP characteristics recorded at high  $\text{Ca}^{2+}$  &  $\text{Mg}^{2+}$  concentration.

In summary, my functional data, albeit preliminary, suggests that mutations in the R202 position result in a loss of function phenotype – reduction in the size of the SV pool and in evoked release. This functional finding is supported by the immunostaining data, where in Munc13-1<sup>R202H</sup>-expressing neurons, less Munc13-1 was found in synapses. Together, I can propose that the R202 mutation disrupts the localization and stabilization of Munc13-1 in synapses. The massively reduced Munc13-1 levels at the synapse lead to a reduced degree of SV priming, and to loss of synaptic strength.

Several studies suggest an inhibitory role for the IDR between C2A and C1 domain. By means of several N-terminal truncation mutants, Camacho *et al.* investigated how the Munc13-1 N-terminus regulates vesicle fusion efficiency. From their structure-function studies, they concluded that the region sandwiched between C2A and C1 domain (comprising residues 150-519) negatively regulates vesicular release probability, so that in its absence release probability is higher (Figure 2, (Camacho et al., 2017)). Since we are only looking at a single AA exchange, it is difficult to align our findings with that assigned by Camacho *et al.*

In summary, the R202H mutation is exerting a dampening/loss of function effect on vesicular release probability, thereby exhibiting reduced synaptic strength and vesicular release, which was highlighted in the low  $\text{Ca}^{2+}$  &  $\text{Mg}^{2+}$  recordings and partially replicated at high  $\text{Ca}^{2+}$  &  $\text{Mg}^{2+}$  concentration. Congruently, we see a profoundly reduced amount of Munc13-1<sup>R202H</sup> colocalizing to synapses in contrast to Munc13-1<sup>WT</sup> employing exactly the same experimental procedure as for the electrophysiology recordings (Figure 25 L & 28 B). These findings support the idea that synapses expressing Munc13-1<sup>R202H</sup> are weaker and may be less capable of supporting synaptic transmission. More studies are needed to decipher the mechanism by which this variation interferes with Munc13-1 function. However, with three patients documented carrying this mutation, and with the preliminary functional and immunohistochemical data, it is highly likely that this variation is causal for brain disease.

### 5.2.3 The Munc13-1<sup>E52K</sup> Variation Leads to a Loss of Function Phenotype

Another patient variant at the N-terminal region of Munc13-1 that is fully conserved in Munc13-1 and ubMunc13-2 from human and rat, is E52K (Figure 24 E). It is located in the C2A domain that forms a heterodimer with RIM to activate and localize Munc13-1 to the active zone (Figure 24 A)(Camacho et al., 2017). The patient is homozygous for this mutation (Figure 24 B) and suffers from a very critical illness displaying in a developmental age of 2-3 months at a biological age of 12 years. The extent of his illness can be estimated by the fact that the patient is being tube fed and is affected severely by seizures and hypotonia (Figure 24 D).

To my utmost surprise, neither AP-evoked, nor sucrose-induced release was rescued in Munc13-1<sup>E52K</sup>-expressing neurons (Figure 25 A, C). The complete absence of sucrose-induced release points to a loss of the SV pool. A handful of cells were tested for spontaneous release characteristics. Importantly, mEPSC events were observed in the E52K recordings (Figure 25 E, G), and within the low number of tested cells revealed a lower number of mEPSC events in comparison to Munc13-1<sup>WT</sup>-expressing cells. The complete lack of rescue prompted me to test whether the viral vector and the virus produced actually results in protein expression. The immunohistochemical analysis and quantification in Figure 29 show that in Munc13-1<sup>E52K</sup>-expressing neurons, a stronger Munc13-1 signal can be detected in comparison to non-infected neurons, indicating that some expression does occur, but the final amount of Munc13-1 in synapses is very low.

The Munc13-1 C2A domain can form two types of interactions, C2A-C2A homodimerization, or heterodimerization with the RIM zinc finger domain. The glutamic acid (E) at position 52 is one of the evolutionarily conserved residues involved in heterodimer formation with RIM and localizes at the interface with the RIM zinc finger (Lu et al., 2006). The Munc13/RIM heterodimer is important for the recruitment of Munc13 to the active zone (Andrews-Zwilling et al., 2006). This finding was supported by the observation that selective disruption of the Munc13/RIM heterodimer in hippocampal and calyx of Held synapses leads to a decrease in synaptic vesicle priming (Betz et al., 2001; Dulubova et al., 2005). Insinuating a conserved function across species, the UNC-13L C2A domain, the *C. elegans* ortholog of Munc13-1, has been described to play a role in anchoring UNC-13L to the active zone (Hu et al., 2013).

In the absence of Munc13s, the complete absence of spontaneous and evoked release has been well-characterized. The most parsimonious explanation to the finding that the E52K mutation does not support evoked release, is that it cannot localize to the proper position at the active zone. This is supported by the immunocytochemistry data, showing that Munc13-1<sup>E52K</sup> poorly colocalizes at synapses. Under this scenario, the fact that spontaneous release can be measured could indicate that low Munc13-1 levels may still be present at the active zone, but that these are insufficient to support evoked release. In this context, more biochemical experiments to look at the effect of the R202H mutation on Munc13-1 interaction with RIM may shed light on the mechanism by which this variation disrupts Munc13-1 localization.

Other scenarios to explain the pathogenicity of this variant are also possible, but less likely: a related observation was described in a study on synaptogenesis, where a similar phenotype as we observe in our recordings, namely the absence of AP-evoked release and the presence of spontaneous activity, was observed in premature neurons that initially lack N-type Ca<sup>2+</sup> channels in the vicinity to release sites, which is necessary for Ca<sup>2+</sup>-dependent synaptic transmission (Basarsky et al., 1994). This observation gives rise to the notion that our E52K mutation might interfere with some developmental function that is a prerequisite for evoked transmission. An interaction of voltage-gated calcium channels (VGCCs) to Munc13 C2B domain has been demonstrated *in vitro* (Calloway et al., 2015), and a decrease in AP-evoked presynaptic Ca<sup>2+</sup> influx was shown upon knockdown of Munc13-1. To solve, whether the observed failure in evoked synaptic transmission was mediated by interruption of a possible interaction with VGCC, I propose co-labelling of Munc13-1<sup>E52K</sup> with a VGCC marker, such as Cav2.1. Differences in the expression pattern of VGCCs would further substantiate the hypothesis. Since evoked transmission is absolutely dependent on Ca<sup>2+</sup> influx and it has been shown that several presynaptic proteins, of particular interest RIM, interact with VGCCs (Han et al., 2011; Kaeser et al., 2011; Liu

et al., 2011), I also suggest that a possible interference with the function of a VGCC interactor could lead to the perturbation in evoked release.

Regardless of the mechanism by which the E52K variation affects synaptic transmission, experiments in continental patient-derived iPSC neuronal cultures coupled with imaging to assess Munc13-1 levels could be beneficial in identifying pharmacological reagents that may stabilize and increase the Munc13-1 levels at the synapse.

#### **5.2.4 Wildtype-Like Rescue in Neurons Expressing Munc13-1<sup>R799Q</sup> and Munc13-1<sup>N1013S</sup> Variations**

A clinically severely affected and already deceased patient carrying a homozygous R799Q mutation that is situated in the highly conserved C2B domain was studied in our experimental system. The C2B domain is highly conserved in all four mammalian Munc13 isoforms as well as in *Drosophila* and *C. elegans* orthologs of Munc13 pointing to its conserved function. It acts as a Ca<sup>2+</sup>-dependent phospholipid binding domain, which binds to PIP and PIP<sub>2</sub> at the active zone plasma membrane upon binding of two Ca<sup>2+</sup> ions. Thereby, it potentiates Munc13 priming rate during activity, serving as key modulator for short-term synaptic plasticity.

The premature death of the patient at 3 days age and diagnosis of macrocephaly, abnormal cerebral imaging and musculoskeletal abnormalities were additional factors that prompted us to investigate this variant. To my surprise, the clinical phenotype of the R799Q patient variant was not reflected by a phenotype in our experimental system - I saw no change in spontaneous or evoked release and no change in STP characteristics. An extreme discrepancy exists between the severity of the patient's clinical presentation, and the WT-like rescue of synaptic transmission properties. The most parsimonious explanation for this discrepancy is that the R799Q variation is not the cause of the disease, but rather an unidentified and harmful genetic modification at the non-coding region of the genome. For alternative explanations highlighting potential shortcomings of the experimental system used here, see below. In summary, at this point, since I don't see any changes compared to the WT readout in electrophysiological properties, I would exclude a pathogenic effect of the R799Q variation.

A second mutation where I could not detect a phenotype on synaptic transmission measured at our setup, is the N1013S mutation located in the MUN domain. However, regarding this mutation, we were always in doubt. The clinical presentation of the patient is very severe, displaying developmental delay, hypotonia, tremors, abnormal behaviour including several other salient symptoms. Hence, it was worth the effort to try and decipher a functional phenotype.

However, the genetic diagnosis is complicated, with an intronic variation of unknown significance, and a *de novo* variation, that is also identified in a large dataset of healthy individuals. I was not able to observe any difference in the synaptic transmission characteristics in neurons expressing this variant. This could be an indication that such complex genetical inheritance patterns are less suitable for investigation in our experimental system (see more below).

These mutations resemble a *de novo* heterozygous methionine to isoleucine mutation (M1269I) in the highly conserved MUN domain that was characterized in the supplementary data in (Lipstein et al., 2017). It was identified in a schizophrenia patient, however, did not alter any of the functional parameters tested in synaptic transmission.

There are multiple reasons that can explain why our experimental approach cannot detect a phenotype:

1. Overexpression. The lentiviral constructs are equipped with the synapsin promoter to confine the expression of the protein in question into neurons. It is estimated that the total expression levels of Munc13s under these conditions may exceed the WT levels by a factor of 2-4 fold. It is possible that under physiological expression levels, a variation like the R799Q is harmful, but that the mild overexpression by the lentivirus is already sufficient to overcome this harm.
2. It is possible, but unlikely, that some variations are only relevant in a subset of neurons, for example, in inhibitory neurons only.
3. A phenotype could only be detected in patient-derived neurons, as it is affected by other cellular factors that are specific in the cell.
4. It is also possible that effects of this variation can be detected only in the *in vivo* context, or only in the context of the human brain.
5. Finally, it is possible that other assays or other experimental conditions must be used for testing the effect of Munc13 variation. Here, for example, an unbiased examination of vGlut1 expression levels in the context of the N1013S may have unravelled an effect of this variation at synapses, that could not be detected in electrophysiological recordings.

While it is important to remember all of these factors, to date the autaptic system remains the best and most descriptive system to characterize presynaptic phenotypes. Using patient-derived iPSCs, or generating knock-in mouse models may resolve some of these issues, but these approaches are typically slower, and require more means. An optimal scenario is to combine multiple approaches, cell types and organisms (e.g., in Lipstein *et al.* recordings in excitatory and inhibitory neurons, and

assessment of phenotypes in *C. elegans*) to validate a benign or pathogenic phenotype for each variation.

### 5.3 Munc13-1 Subcellular Localization and Quantification in Autaptic Hippocampal Glutamatergic Neurons

Thus far, we have described five patient variants with respect to their electrophysiological properties. In parallel, we used the unique advantage of autaptic cultures that grant better visibility in immunostainings and can capture the amount of Munc13-1 protein per neuron in both WT and variant-expressing neurons at the synaptic compartment upon exogenous lentiviral infection. For synaptic localization we used established markers that label the presynapse (VGlut1) and postsynapse (Shank2), constituting a synapse at sites of colocalization within the MAP2 labelled region (Rhee et al., 2019). We show a set of non-infected cells as negative control that served to estimate any background signal in our image analysis approach. In all other conditions tested, (WT, E52K, R202H, R799Q, G808D, N1013S) we observed on average 500 synapses per neuron at DIV 13 (Figure 27 A). In comparison, Ripamonti *et al.* counted approximately 200 pre- and postsynaptic puncta, amounting to approximately 200 synapses in WT autaptic hippocampal glutamatergic neurons at DIV 14 (Ripamonti et al., 2017). Considering that the spread in the synapse number per neuron ranges chiefly from 200 to 1000, inherent to the fact that the imaged autaptic neurons vary in size, and considering the massive improvement in image acquisition and analysis techniques, my data well-agrees with that of Ripamonti *et al.*, and further corroborates that no defect in synaptogenesis is present in rescued Munc13-1/2 DKO neurons (Varoqueaux et al., 2002). The comparable number of synapses, and the similar degree of vGlut1 signal intensity in all conditions except in neurons expressing Munc13-1<sup>N10103S</sup> (Figure 30), indicates that at large, the infected neurons are of comparable nature.

A triple colocalization analysis was used to quantify Munc13-1 signal in synapses and unfolded a strong protein localization deficit for mutations that exhibited a loss of function in the electrophysiological measurements. Under noninfected condition, the signal for Munc13-1, obtained using an anti-GFP antibody targeted against a c-terminal GFP tag in frame of the Munc13-1 protein, is close to zero. The minimal deviation from zero is a caveat of the automated analysis that applies the same thresholds for each channel and computes all images equally. Slight background detection cannot be avoided, and this route of analysis prevents a biased readout and enables standardized analysis across all conducted experiments.

A signal for Munc13-1<sup>E52K</sup> was only detected in around 12 % synapses, whereas only 16 % synapses had a signal for Munc13-1<sup>R202H</sup>. The remaining tested patient variants had comparable expression level as seen for Munc13-1<sup>WT</sup>. This means that the effects I observed in the electrophysiological recordings for the G808D, R799Q and N1013S mutation do not arise from differences in expression level compared to Munc13-1<sup>WT</sup>. Regarding the R799Q and N1013S, we can exclude that this WT-like rescue is caused by massive excess of Munc13-1 in synapses, as both the localization degree as well as the Munc13-1 signal intensity were comparable to WT. The G808D mutation is also expressed at similar levels to Munc13-1<sup>WT</sup>, thus we can rule out that the gain of function that is visible for the G808D mutant in the electrophysiological readout is originating from differential protein localization or expression levels at synapses.

An astounding discovery was the profoundly low number of synapses expressing Munc13-1<sup>E52K</sup> and Munc13-1<sup>R202H</sup>. These findings suggest that the observed loss of function for these mutants is due to a heavy loss of mutant Munc13-1 localization to the synapse and corroborate the finding that the N-terminal Munc13-1 region is critical for the localization of Munc13-1 proteins to the active zone (Deng et al., 2011; Dulubova et al., 2005; Schoch et al., 2002). When the function of the N-terminal region is compromised, Munc13-1 proteins might fail to localize to the active zone, and undergo degradation, which explains the overall reduction in expression. A novel aspect here is that this function was only described for the C2A domain and a short sequence thereafter, but is not known for residues in the IDR.

## 5.4 Conclusion

I characterized five patients, who carry a single nucleotide exchange in their *UNC13A* gene in a heterozygous or homozygous composition and display a severe neurodevelopmental syndrome with overlapping neurological symptoms. I propose that patient variant G808D exerts a dominant negative effect, in convergence with the previously described P814L mutation, by boosting SV release probability. The accumulation of patient variants in the C2B-MUN-Linker region indicates this region is a disease hotspot where recurrent *de novo* missense mutations exert a pathological effect. Secondly, based on our findings that reveal a loss of function and a loss of Munc13-1 synaptic localization in two patient variants, we propose that variations in the Munc13-1 N-terminus control its active zone localization and abundance. A recurring number of patients with variation in the R202 residue point to a second potential hotspot. Finally, the presence of Munc13-1 variants R799Q and N1013S at synapses did not induce any change in neurotransmitter release properties. Therefore, we cannot determine pathogenicity of these variants. More work, utilizing

additional protocols that assess synaptic function and morphology, will be required to determine whether these variants are indeed benign. The increased vGlut1 signal intensity at synapses may indicate that the N1013S indeed exerts pathogenicity at the synapse via other mechanisms, that were not tested here.

Collectively, the presented evidence proposes that presynaptic neurotransmission defects likely cause the pathophysiology in patients. This thesis was made with the intention to expand our knowledge of the cell biological mechanisms in this rare disease, and brain diseases in general, and to initiate a platform of shared knowledge of patient phenotypes, genetic modes of transmission, and molecular and cellular mechanisms of pathogenicity, with the hope that this knowledge will aid in the development of therapies for commonly experienced symptoms, such as seizures.

Based on the experience and knowledge gained here, I believe that the future steps in this project should include the development of faster *in vitro* approaches to diagnose patients, for example by performing multielectrode array recording in mass cultures of patient-derived iPSC neurons to detect gain- or loss of function phenotypes, that can then be studied in more detail using the autaptic system. Loss of function phenotypes can also be diagnosed via simple western-blot analysis or immunostaining against the Munc13-1 protein in patient-derived iPSCs, to determine its abundance. Such approaches would allow a fast initial screen for variant pathogenicity and will aid to focus the mechanistic studies on variations with high pathogenic potential. The in-depth characterization of additional variations is necessary to identify converging mechanisms between variations, the identification of which will assist in the development of therapeutic approaches. Finally, the next steps of this project should include means to identify clinical heterogeneity, and to find the factors that determine the course and severity of this syndrome.



## 6 Bibliography

Ahmed, S., Maruyama, I.N., Kozma, R., Lee, J., Brenner, S., and Lim, L. (1992). The *Caenorhabditis elegans* unc-13 gene product is a phospholipid-dependent high-affinity phorbol ester receptor. *Biochem J* 287 (Pt 3), 995-999.

Andrews-Zwilling, Y.S., Kawabe, H., Reim, K., Varoqueaux, F., and Brose, N. (2006). Binding to Rab3A-interacting molecule RIM regulates the presynaptic recruitment of Munc13-1 and ubMunc13-2. *J Biol Chem* 281, 19720-19731.

Anna-Leigh Brown, M.E.W., Pietro Fratta (2021). Common ALS/FTD risk variants in UNC13A exacerbate its cryptic splicing and loss upon TDP-43 mislocalization.

Aravamudan, B., Fergestad, T., Davis, W.S., Rodesch, C.K., and Broadie, K. (1999). *Drosophila* UNC-13 is essential for synaptic transmission. *Nat Neurosci* 2, 965-971.

Ashery, U., Koch, H., Scheuss, V., Brose, N., and Rettig, J. (1999). A presynaptic role for the ADP ribosylation factor (ARF)-specific GDP/GTP exchange factor msec7-1. *Proc Natl Acad Sci U S A* 96, 1094-1099.

Augustin, I., Betz, A., Herrmann, C., Jo, T., and Brose, N. (1999a). Differential expression of two novel Munc13 proteins in rat brain. *Biochem J* 337 (Pt 3), 363-371.

Augustin, I., Rosenmund, C., Sudhof, T.C., and Brose, N. (1999b). Munc13-1 is essential for fusion competence of glutamatergic synaptic vesicles. *Nature* 400, 457-461.

Baker, K., Gordon, S.L., Melland, H., Bumbak, F., Scott, D.J., Jiang, T.J., Owen, D., Turner, B.J., Boyd, S.G., Rossi, M., *et al.* (2018). SYT1-associated neurodevelopmental disorder: a case series. *Brain* 141, 2576-2591.

Basarsky, T.A., Parpura, V., and Haydon, P.G. (1994). Hippocampal synaptogenesis in cell culture: developmental time course of synapse formation, calcium influx, and synaptic protein distribution. *J Neurosci* 14, 6402-6411.

Basu, J., Betz, A., Brose, N., and Rosenmund, C. (2007). Munc13-1 C1 domain activation lowers the energy barrier for synaptic vesicle fusion. *J Neurosci* 27, 1200-1210.

Basu, J., Shen, N., Dulubova, I., Lu, J., Guan, R., Guryev, O., Grishin, N.V., Rosenmund, C., and Rizo, J. (2005). A minimal domain responsible for Munc13 activity. *Nat Struct Mol Biol* 12, 1017-1018.

Bekkers, J.M., and Stevens, C.F. (1991). Excitatory and Inhibitory Autaptic Currents in Isolated Hippocampal-Neurons Maintained in Cell-Culture. *Proceedings of the National Academy of Sciences of the United States of America* 88, 7834-7838.

Berryer, M.H., Hamdan, F.F., Klitten, L.L., Moller, R.S., Carmant, L., Schwartzenuber, J., Patry, L., Dobrzaniecka, S., Rochefort, D., Neugnot-Ceroli, M., *et al.* (2013). Mutations in SYNGAP1 cause intellectual disability, autism, and a specific form of epilepsy by inducing haploinsufficiency. *Hum Mutat* 34, 385-394.

- Betz, A., Ashery, U., Rickmann, M., Augustin, I., Neher, E., Sudhof, T.C., Rettig, J., and Brose, N. (1998). Munc13-1 is a presynaptic phorbol ester receptor that enhances neurotransmitter release. *Neuron* 21, 123-136.
- Betz, A., Okamoto, M., Benseler, F., and Brose, N. (1997). Direct interaction of the rat unc-13 homologue Munc13-1 with the N terminus of syntaxin. *J Biol Chem* 272, 2520-2526.
- Betz, A., Thakur, P., Junge, H.J., Ashery, U., Rhee, J.S., Scheuss, V., Rosenmund, C., Rettig, J., and Brose, N. (2001). Functional interaction of the active zone proteins Munc13-1 and RIM1 in synaptic vesicle priming. *Neuron* 30, 183-196.
- Bohme, M.A., Beis, C., Reddy-Alla, S., Reynolds, E., Mampell, M.M., Grasskamp, A.T., Lutzkendorf, J., Bergeron, D.D., Driller, J.H., Babikir, H., *et al.* (2016). Active zone scaffolds differentially accumulate Unc13 isoforms to tune Ca(2+) channel-vesicle coupling. *Nat Neurosci* 19, 1311-1320.
- Brenner, S. (1974). The genetics of *Caenorhabditis elegans*. *Genetics* 77, 71-94.
- Brose, N., Hofmann, K., Hata, Y., and Sudhof, T.C. (1995). Mammalian homologues of *Caenorhabditis elegans* unc-13 gene define novel family of C2-domain proteins. *J Biol Chem* 270, 25273-25280.
- Burgalossi, A., Jung, S., Man, K.N., Nair, R., Jockusch, W.J., Wojcik, S.M., Brose, N., and Rhee, J.S. (2012). Analysis of neurotransmitter release mechanisms by photolysis of caged Ca(2)(+) in an autaptic neuron culture system. *Nat Protoc* 7, 1351-1365.
- Calakos, N., Schoch, S., Sudhof, T.C., and Malenka, R.C. (2004). Multiple roles for the active zone protein RIM1alpha in late stages of neurotransmitter release. *Neuron* 42, 889-896.
- Calloway, N., Gouzer, G., Xue, M., and Ryan, T.A. (2015). The active-zone protein Munc13 controls the use-dependence of presynaptic voltage-gated calcium channels. *Elife* 4.
- Camacho, M., Basu, J., Trimbuch, T., Chang, S., Pulido-Lozano, C., Chang, S.S., Duluvova, I., Abo-Rady, M., Rizo, J., and Rosenmund, C. (2017). Heterodimerization of Munc13 C2A domain with RIM regulates synaptic vesicle docking and priming. *Nat Commun* 8, 15293.
- Chen, Z., Cooper, B., Kalla, S., Varoqueaux, F., and Young, S.M., Jr. (2013). The Munc13 proteins differentially regulate readily releasable pool dynamics and calcium-dependent recovery at a central synapse. *J Neurosci* 33, 8336-8351.
- Cooper, B., Hemmerlein, M., Ammermuller, J., Imig, C., Reim, K., Lipstein, N., Kalla, S., Kawabe, H., Brose, N., Brandstatter, J.H., *et al.* (2012). Munc13-independent vesicle priming at mouse photoreceptor ribbon synapses. *J Neurosci* 32, 8040-8052.
- Cross-Disorder Group of the Psychiatric Genomics, C. (2013). Identification of risk loci with shared effects on five major psychiatric disorders: a genome-wide analysis. *Lancet* 381, 1371-1379.
- Das, J., Xu, S., Pany, S., Guillory, A., Shah, V., and Roman, G.W. (2013). The pre-synaptic Munc13-1 binds alcohol and modulates alcohol self-administration in *Drosophila*. *J Neurochem* 126, 715-726.

- De Rubeis, S., He, X., Goldberg, A.P., Poultney, C.S., Samocha, K., Cicek, A.E., Kou, Y., Liu, L., Fromer, M., Walker, S., *et al.* (2014). Synaptic, transcriptional and chromatin genes disrupted in autism. *Nature* *515*, 209-215.
- Deng, L., Kaeser, P.S., Xu, W., and Sudhof, T.C. (2011). RIM proteins activate vesicle priming by reversing autoinhibitory homodimerization of Munc13. *Neuron* *69*, 317-331.
- Diekstra, F.P., Van Deerlin, V.M., van Swieten, J.C., Al-Chalabi, A., Ludolph, A.C., Weishaupt, J.H., Hardiman, O., Landers, J.E., Brown, R.H., Jr., van Es, M.A., *et al.* (2014). C9orf72 and UNC13A are shared risk loci for amyotrophic lateral sclerosis and frontotemporal dementia: a genome-wide meta-analysis. *Ann Neurol* *76*, 120-133.
- Diekstra, F.P., van Vught, P.W., van Rheenen, W., Koppers, M., Pasterkamp, R.J., van Es, M.A., Schelhaas, H.J., de Visser, M., Robberecht, W., Van Damme, P., *et al.* (2012). UNC13A is a modifier of survival in amyotrophic lateral sclerosis. *Neurobiol Aging* *33*, 630 e633-638.
- Dimova, K., Kalkhof, S., Pottratz, I., Ihling, C., Rodriguez-Castaneda, F., Liepold, T., Griesinger, C., Brose, N., Sinz, A., and Jahn, O. (2009). Structural insights into the calmodulin-Munc13 interaction obtained by cross-linking and mass spectrometry. *Biochemistry* *48*, 5908-5921.
- Dimova, K., Kawabe, H., Betz, A., Brose, N., and Jahn, O. (2006). Characterization of the Munc13-calmodulin interaction by photoaffinity labeling. *Biochim Biophys Acta* *1763*, 1256-1265.
- Dulubova, I., Lou, X., Lu, J., Huryeva, I., Alam, A., Schneggenburger, R., Sudhof, T.C., and Rizo, J. (2005). A Munc13/RIM/Rab3 tripartite complex: from priming to plasticity? *EMBO J* *24*, 2839-2850.
- Dulubova, I., Sugita, S., Hill, S., Hosaka, M., Fernandez, I., Sudhof, T.C., and Rizo, J. (1999). A conformational switch in syntaxin during exocytosis: role of munc18. *EMBO J* *18*, 4372-4382.
- Duncan, R.R., Betz, A., Shipston, M.J., Brose, N., and Chow, R.H. (1999). Transient, phorbol ester-induced DOC2-Munc13 interactions in vivo. *J Biol Chem* *274*, 27347-27350.
- Durand, C.M., Betancur, C., Boeckers, T.M., Bockmann, J., Chaste, P., Fauchereau, F., Nygren, G., Rastam, M., Gillberg, I.C., Anckarsater, H., *et al.* (2007). Mutations in the gene encoding the synaptic scaffolding protein SHANK3 are associated with autism spectrum disorders. *Nat Genet* *39*, 25-27.
- Engel, A.G., Selcen, D., Shen, X.M., Milone, M., and Harper, C.M. (2016). Loss of MUNC13-1 function causes microcephaly, cortical hyperexcitability, and fatal myasthenia. *Neurol Genet* *2*, e105.
- Fenske, P., Grauel, M.K., Brockmann, M.M., Dorn, A.L., Trimbuch, T., and Rosenmund, C. (2019). Autaptic cultures of human induced neurons as a versatile platform for studying synaptic function and neuronal morphology. *Sci Rep* *9*, 4890.
- Fornasiero, E.F., Mandad, S., Wildhagen, H., Alevra, M., Rammner, B., Keihani, S., Opazo, F., Urban, I., Ischebeck, T., Sakib, M.S., *et al.* (2018). Precisely measured protein lifetimes in the mouse brain reveal differences across tissues and subcellular fractions. *Nat Commun* *9*, 4230.
- Friedrich, R., Gottfried, I., and Ashery, U. (2013). Munc13-1 Translocates to the Plasma Membrane in a Doc2B- and Calcium-Dependent Manner. *Front Endocrinol (Lausanne)* *4*, 119.

- Fromer, M., Pocklington, A.J., Kavanagh, D.H., Williams, H.J., Dwyer, S., Gormley, P., Georgieva, L., Rees, E., Palta, P., Ruderfer, D.M., *et al.* (2014). De novo mutations in schizophrenia implicate synaptic networks. *Nature* *506*, 179-184.
- Gai, X., Xie, H.M., Perin, J.C., Takahashi, N., Murphy, K., Wenocur, A.S., D'Arcy, M., O'Hara, R.J., Goldmuntz, E., Grice, D.E., *et al.* (2012). Rare structural variation of synapse and neurotransmission genes in autism. *Mol Psychiatry* *17*, 402-411.
- Gauthier, J., Spiegelman, D., Piton, A., Lafreniere, R.G., Laurent, S., St-Onge, J., Lapointe, L., Hamdan, F.F., Cossette, P., Mottron, L., *et al.* (2009). Novel de novo SHANK3 mutation in autistic patients. *Am J Med Genet B Neuropsychiatr Genet* *150B*, 421-424.
- Gracheva, E.O., Hadwiger, G., Nonet, M.L., and Richmond, J.E. (2008). Direct interactions between *C. elegans* RAB-3 and Rim provide a mechanism to target vesicles to the presynaptic density. *Neurosci Lett* *444*, 137-142.
- Grant, S.G., O'Dell, T.J., Karl, K.A., Stein, P.L., Soriano, P., and Kandel, E.R. (1992). Impaired long-term potentiation, spatial learning, and hippocampal development in fyn mutant mice. *Science* *258*, 1903-1910.
- Hammarlund, M., Palfreyman, M.T., Watanabe, S., Olsen, S., and Jorgensen, E.M. (2007). Open syntaxin docks synaptic vesicles. *PLoS Biol* *5*, e198.
- Han, Y., Kaeser, P.S., Sudhof, T.C., and Schneggenburger, R. (2011). RIM determines Ca<sup>2+</sup> channel density and vesicle docking at the presynaptic active zone. *Neuron* *69*, 304-316.
- Hu, Z., Tong, X.J., and Kaplan, J.M. (2013). UNC-13L, UNC-13S, and Tomosyn form a protein code for fast and slow neurotransmitter release in *Caenorhabditis elegans*. *Elife* *2*, e00967.
- Imig, C., Min, S.W., Krinner, S., Arancillo, M., Rosenmund, C., Sudhof, T.C., Rhee, J., Brose, N., and Cooper, B.H. (2014). The morphological and molecular nature of synaptic vesicle priming at presynaptic active zones. *Neuron* *84*, 416-431.
- Jamain, S., Quach, H., Betancur, C., Rastam, M., Colineaux, C., Gillberg, I.C., Soderstrom, H., Giros, B., Leboyer, M., Gillberg, C., *et al.* (2003). Mutations of the X-linked genes encoding neuroligins NLGN3 and NLGN4 are associated with autism. *Nat Genet* *34*, 27-29.
- Junge, H.J., Rhee, J.S., Jahn, O., Varoqueaux, F., Spiess, J., Waxham, M.N., Rosenmund, C., and Brose, N. (2004). Calmodulin and Munc13 form a Ca<sup>2+</sup> sensor/effector complex that controls short-term synaptic plasticity. *Cell* *118*, 389-401.
- Kaeser, P.S., Deng, L., Wang, Y., Dulubova, I., Liu, X., Rizo, J., and Sudhof, T.C. (2011). RIM proteins tether Ca<sup>2+</sup> channels to presynaptic active zones via a direct PDZ-domain interaction. *Cell* *144*, 282-295.
- Kalla, S., Stern, M., Basu, J., Varoqueaux, F., Reim, K., Rosenmund, C., Ziv, N.E., and Brose, N. (2006). Molecular dynamics of a presynaptic active zone protein studied in Munc13-1-enhanced yellow fluorescent protein knock-in mutant mice. *J Neurosci* *26*, 13054-13066.
- Kazanietz, M.G., Lewin, N.E., Bruns, J.D., and Blumberg, P.M. (1995). Characterization of the cysteine-rich region of the *Caenorhabditis elegans* protein Unc-13 as a high affinity phorbol ester receptor. Analysis of ligand-binding interactions, lipid cofactor requirements, and inhibitor sensitivity. *J Biol Chem* *270*, 10777-10783.

- Koch, H., Hofmann, K., and Brose, N. (2000). Definition of Munc13-homology-domains and characterization of a novel ubiquitously expressed Munc13 isoform. *Biochem J* *349*, 247-253.
- Lai, Y., Choi, U.B., Leitz, J., Rhee, H.J., Lee, C., Altas, B., Zhao, M., Pfuetzner, R.A., Wang, A.L., Brose, N., *et al.* (2017). Molecular Mechanisms of Synaptic Vesicle Priming by Munc13 and Munc18. *Neuron* *95*, 591-607 e510.
- Lipstein, N., Chang, S., Lin, K.H., Lopez-Murcia, F.J., Neher, E., Taschenberger, H., and Brose, N. (2021). Munc13-1 is a Ca(2+)-phospholipid-dependent vesicle priming hub that shapes synaptic short-term plasticity and enables sustained neurotransmission. *Neuron* *109*, 1-21.
- Lipstein, N., Sakaba, T., Cooper, B.H., Lin, K.H., Strenzke, N., Ashery, U., Rhee, J.S., Taschenberger, H., Neher, E., and Brose, N. (2013). Dynamic control of synaptic vesicle replenishment and short-term plasticity by Ca(2+)-calmodulin-Munc13-1 signaling. *Neuron* *79*, 82-96.
- Lipstein, N., Schaks, S., Dimova, K., Kalkhof, S., Ihling, C., Kolbel, K., Ashery, U., Rhee, J., Brose, N., Sinz, A., *et al.* (2012). Nonconserved Ca(2+)/calmodulin binding sites in Munc13s differentially control synaptic short-term plasticity. *Mol Cell Biol* *32*, 4628-4641.
- Lipstein, N., Verhoeven-Duif, N.M., Michelassi, F.E., Calloway, N., van Hasselt, P.M., Pienkowska, K., van Haften, G., van Haelst, M.M., van Empelen, R., Cuppen, I., *et al.* (2017). Synaptic UNC13A protein variant causes increased neurotransmission and dyskinetic movement disorder. *J Clin Invest* *127*, 1005-1018.
- Liu, K.S., Siebert, M., Mertel, S., Knoche, E., Wegener, S., Wichmann, C., Matkovic, T., Muhammad, K., Depner, H., Mettke, C., *et al.* (2011). RIM-binding protein, a central part of the active zone, is essential for neurotransmitter release. *Science* *334*, 1565-1569.
- Liu, X., Seven, A.B., Camacho, M., Esser, V., Xu, J., Trimbuch, T., Quade, B., Su, L., Ma, C., Rosenmund, C., *et al.* (2016). Functional synergy between the Munc13 C-terminal C1 and C2 domains. *Elife* *5*.
- Lu, J., Machius, M., Dulubova, I., Dai, H., Sudhof, T.C., Tomchick, D.R., and Rizo, J. (2006). Structural basis for a Munc13-1 homodimer to Munc13-1/RIM heterodimer switch. *PLoS Biol* *4*, e192.
- Ma, C., Li, W., Xu, Y., and Rizo, J. (2011). Munc13 mediates the transition from the closed syntaxin-Munc18 complex to the SNARE complex. *Nat Struct Mol Biol* *18*, 542-549.
- Ma, C., Su, L., Seven, A.B., Xu, Y., and Rizo, J. (2013). Reconstitution of the vital functions of Munc18 and Munc13 in neurotransmitter release. *Science* *339*, 421-425.
- Maruyama, I.N., and Brenner, S. (1991). A phorbol ester/diacylglycerol-binding protein encoded by the unc-13 gene of *Caenorhabditis elegans*. *Proc Natl Acad Sci U S A* *88*, 5729-5733.
- Michelassi, F., Liu, H., Hu, Z., and Dittman, J.S. (2017). A C1-C2 Module in Munc13 Inhibits Calcium-Dependent Neurotransmitter Release. *Neuron* *95*, 577-590 e575.
- Mignot, C., von Stulpnagel, C., Nava, C., Ville, D., Sanlaville, D., Lesca, G., Rastetter, A., Gachet, B., Marie, Y., Korenke, G.C., *et al.* (2016). Genetic and neurodevelopmental spectrum of SYNGAP1-associated intellectual disability and epilepsy. *J Med Genet* *53*, 511-522.

- Missler, M., Zhang, W., Rohlmann, A., Kattenstroth, G., Hammer, R.E., Gottmann, K., and Sudhof, T.C. (2003). Alpha-neurexins couple Ca<sup>2+</sup> channels to synaptic vesicle exocytosis. *Nature* *423*, 939-948.
- Mochida, S., Orita, S., Sakaguchi, G., Sasaki, T., and Takai, Y. (1998). Role of the Doc2 alpha-Munc13-1 interaction in the neurotransmitter release process. *Proc Natl Acad Sci U S A* *95*, 11418-11422.
- Neeb, A., Koch, H., Schurmann, A., and Brose, N. (1999). Direct interaction between the ARF-specific guanine nucleotide exchange factor msec7-1 and presynaptic Munc13-1. *Eur J Cell Biol* *78*, 533-538.
- Nguyen, M., Alfonso, A., Johnson, C.D., and Rand, J.B. (1995). *Caenorhabditis elegans* mutants resistant to inhibitors of acetylcholinesterase. *Genetics* *140*, 527-535.
- Nguyen, T.A., Lehr, A.W., and Roche, K.W. (2020). Neuroligins and Neurodevelopmental Disorders: X-Linked Genetics. *Front Synaptic Neurosci* *12*, 33.
- Orita, S., Naito, A., Sakaguchi, G., Maeda, M., Igarashi, H., Sasaki, T., and Takai, Y. (1997). Physical and functional interactions of Doc2 and Munc13 in Ca<sup>2+</sup>-dependent exocytotic machinery. *J Biol Chem* *272*, 16081-16084.
- Peca, J., Feliciano, C., Ting, J.T., Wang, W., Wells, M.F., Venkatraman, T.N., Lascola, C.D., Fu, Z., and Feng, G. (2011). Shank3 mutant mice display autistic-like behaviours and striatal dysfunction. *Nature* *472*, 437-442.
- Purcell, S.M., Moran, J.L., Fromer, M., Ruderfer, D., Solovieff, N., Roussos, P., O'Dushlaine, C., Chambert, K., Bergen, S.E., Kahler, A., *et al.* (2014). A polygenic burden of rare disruptive mutations in schizophrenia. *Nature* *506*, 185-190.
- Pyott, S.J., and Rosenmund, C. (2002). The effects of temperature on vesicular supply and release in autaptic cultures of rat and mouse hippocampal neurons. *J Physiol* *539*, 523-535.
- Rajabli, F., Feliciano-Astacio, B.E., Cukier, H.N., Wang, L., Griswold, A.J., Hamilton-Nelson, K.L., Adams, L.D., Rodriguez, V.C., Mena, P.R., Tejada, S., *et al.* (2021). Linkage of Alzheimer disease families with Puerto Rican ancestry identifies a chromosome 9 locus. *Neurobiol Aging* *104*, 115 e111-115 e117.
- Reddy-Alla, S., Bohme, M.A., Reynolds, E., Beis, C., Grasskamp, A.T., Mampell, M.M., Maglione, M., Jusyte, M., Rey, U., Babikir, H., *et al.* (2017). Stable Positioning of Unc13 Restricts Synaptic Vesicle Fusion to Defined Release Sites to Promote Synchronous Neurotransmission. *Neuron* *95*, 1350-1364 e1312.
- Repetto, D., Brockhaus, J., Rhee, H.J., Lee, C., Kilimann, M.W., Rhee, J., Northoff, L.M., Guo, W., Reissner, C., and Missler, M. (2018). Molecular Dissection of Neurobeachin Function at Excitatory Synapses. *Front Synaptic Neurosci* *10*, 28.
- Rhee, H.J., Shaib, A.H., Rehbach, K., Lee, C., Seif, P., Thomas, C., Gideons, E., Guenther, A., Krutenko, T., Hebisch, M., *et al.* (2019). An Autaptic Culture System for Standardized Analyses of iPSC-Derived Human Neurons. *Cell Rep* *27*, 2212-2228 e2217.

- Rhee, J.S., Betz, A., Pyott, S., Reim, K., Varoqueaux, F., Augustin, I., Hesse, D., Sudhof, T.C., Takahashi, M., Rosenmund, C., *et al.* (2002). Beta phorbol ester- and diacylglycerol-induced augmentation of transmitter release is mediated by Munc13s and not by PKCs. *Cell* *108*, 121-133.
- Richmond, J.E., Davis, W.S., and Jorgensen, E.M. (1999). UNC-13 is required for synaptic vesicle fusion in *C. elegans*. *Nat Neurosci* *2*, 959-964.
- Richmond, J.E., Weimer, R.M., and Jorgensen, E.M. (2001). An open form of syntaxin bypasses the requirement for UNC-13 in vesicle priming. *Nature* *412*, 338-341.
- Ripamonti, S., Ambrozkiwicz, M.C., Guzzi, F., Gravati, M., Biella, G., Bormuth, I., Hammer, M., Tuffy, L.P., Sigler, A., Kawabe, H., *et al.* (2017). Transient oxytocin signaling primes the development and function of excitatory hippocampal neurons. *Elife* *6*.
- Rodriguez-Castaneda, F., Maestre-Martinez, M., Coudeville, N., Dimova, K., Junge, H., Lipstein, N., Lee, D., Becker, S., Brose, N., Jahn, O., *et al.* (2010). Modular architecture of Munc13/calmodulin complexes: dual regulation by Ca<sup>2+</sup> and possible function in short-term synaptic plasticity. *EMBO J* *29*, 680-691.
- Rosenmund, C., Sigler, A., Augustin, I., Reim, K., Brose, N., and Rhee, J.S. (2002). Differential control of vesicle priming and short-term plasticity by Munc13 isoforms. *Neuron* *33*, 411-424.
- Sakaba, T., and Neher, E. (2001). Calmodulin Mediates Rapid Recruitment of Fast-Releasing Synaptic Vesicles at a Calyx-Type Synapse. *Neuron* *32*, 1119-1131.
- Sakaguchi, G., Orita, S., Naito, A., Maeda, M., Igarashi, H., Sasaki, T., and Takai, Y. (1998). A novel brain-specific isoform of beta spectrin: isolation and its interaction with Munc13. *Biochem Biophys Res Commun* *248*, 846-851.
- Sakamoto, H., Ariyoshi, T., Kimpara, N., Sugao, K., Taiko, I., Takikawa, K., Asanuma, D., Namiki, S., and Hirose, K. (2018). Synaptic weight set by Munc13-1 supramolecular assemblies. *Nat Neurosci* *21*, 41-49.
- Scheiffele, P., Fan, J., Choih, J., Fetter, R., and Serafini, T. (2000). Neuroligin expressed in nonneuronal cells triggers presynaptic development in contacting axons. *Cell* *101*, 657-669.
- Schoch, S., Castillo, P.E., Jo, T., Mukherjee, K., Geppert, M., Wang, Y., Schmitz, F., Malenka, R.C., and Sudhof, T.C. (2002). RIM1alpha forms a protein scaffold for regulating neurotransmitter release at the active zone. *Nature* *415*, 321-326.
- Shen, N., Guryev, O., and Rizo, J. (2005). Intramolecular occlusion of the diacylglycerol-binding site in the C1 domain of munc13-1. *Biochemistry* *44*, 1089-1096.
- Shin, O.H., Lu, J., Rhee, J.S., Tomchick, D.R., Pang, Z.P., Wojcik, S.M., Camacho-Perez, M., Brose, N., Machius, M., Rizo, J., *et al.* (2010). Munc13 C2B domain is an activity-dependent Ca<sup>2+</sup> regulator of synaptic exocytosis. *Nat Struct Mol Biol* *17*, 280-288.
- Siddiqui, S.S. (1990). Mutations affecting axonal growth and guidance of motor neurons and mechanosensory neurons in the nematode *Caenorhabditis elegans*. *Neurosci Res Suppl* *13*, S171-190.

- Siksou, L., Varoqueaux, F., Pascual, O., Triller, A., Brose, N., and Marty, S. (2009). A common molecular basis for membrane docking and functional priming of synaptic vesicles. *Eur J Neurosci* *30*, 49-56.
- Silva, A.J., Paylor, R., Wehner, J.M., and Tonegawa, S. (1992). Impaired spatial learning in alpha-calmodulin kinase II mutant mice. *Science* *257*, 206-211.
- Söllner, T.B., M. K.; Whiteheart, S. W.; Scheller, R. H.; Rothman, J. E. (1993). A Protein Assembly-Disassembly Pathway In Vitro That May Correspond to Sequential Steps of Synaptic Vesicle Docking, Activation, and Fusion. *Cell* *75*, 409-418.
- Sørensen, M.V.a.J.B. (2021). SNAREopathies: Diversity in Mechanisms and Symptoms | Elsevier Enhanced Reader. *Neuron* *107*, 22-37.
- Stevens, D.R., Wu, Z.X., Matti, U., Junge, H.J., Schirra, C., Becherer, U., Wojcik, S.M., Brose, N., and Rettig, J. (2005). Identification of the minimal protein domain required for priming activity of Munc13-1. *Curr Biol* *15*, 2243-2248.
- Sudhof, T.C. (1995). The synaptic vesicle cycle: a cascade of protein-protein interactions. *Nature* *375*, 645-653.
- Sutton, R.B., Fasshauer, D., Jahn, R., and Brunger, A.T. (1998). Crystal structure of a SNARE complex involved in synaptic exocytosis at 2.4 Å resolution. *Nature* *395*, 347-353.
- Szatmari, P., Paterson, A.D., Zwaigenbaum, L., Roberts, W., Brian, J., Liu, X.Q., Vincent, J.B., Skaug, J.L., Thompson, A.P., Senman, L., *et al.* (2007). Mapping autism risk loci using genetic linkage and chromosomal rearrangements. *Nat Genet* *39*, 319-328.
- Telemenakis, I., Benseler, F., Stenius, K., Sudhof, T.C., and Brose, N. (1997). Rat homologues of yeast sec7p. *Eur J Cell Biol* *74*, 143-149.
- Van Der Loos, H.G., E.M. (1972). Autapses in neocortex cerebri: synapses between a pyramidal cell's axon and its own dendrites. *Brain Research* *48*, 355-360.
- van Eijk, R.P.A., Jones, A.R., Sproviero, W., Shatunov, A., Shaw, P.J., Leigh, P.N., Young, C.A., Shaw, C.E., Mora, G., Mandrioli, J., *et al.* (2017). Meta-analysis of pharmacogenetic interactions in amyotrophic lateral sclerosis clinical trials. *Neurology* *89*, 1915-1922.
- van Es, M.A., Veldink, J.H., Saris, C.G., Blauw, H.M., van Vught, P.W., Birve, A., Lemmens, R., Schelhaas, H.J., Groen, E.J., Huisman, M.H., *et al.* (2009). Genome-wide association study identifies 19p13.3 (UNC13A) and 9p21.2 as susceptibility loci for sporadic amyotrophic lateral sclerosis. *Nat Genet* *41*, 1083-1087.
- Varoqueaux, F., Aramuni, G., Rawson, R.L., Mohrmann, R., Missler, M., Gottmann, K., Zhang, W., Sudhof, T.C., and Brose, N. (2006). Neuroligins determine synapse maturation and function. *Neuron* *51*, 741-754.
- Varoqueaux, F., Sigler, A., Rhee, J.S., Brose, N., Enk, C., Reim, K., and Rosenmund, C. (2002). Total arrest of spontaneous and evoked synaptic transmission but normal synaptogenesis in the absence of Munc13-mediated vesicle priming. *Proc Natl Acad Sci U S A* *99*, 9037-9042.



- Varoqueaux, F., Sons, M.S., Plomp, J.J., and Brose, N. (2005). Aberrant morphology and residual transmitter release at the Munc13-deficient mouse neuromuscular synapse. *Mol Cell Biol* 25, 5973-5984.
- Wang, S., Choi, U.B., Gong, J., Yang, X., Li, Y., Wang, A.L., Yang, X., Brunger, A.T., and Ma, C. (2017). Conformational change of syntaxin linker region induced by Munc13s initiates SNARE complex formation in synaptic exocytosis. *EMBO J* 36, 816-829.
- Wang, Y., Okamoto, M., Schmitz, F., Hofmann, K., and Sudhof, T.C. (1997). Rim is a putative Rab3 effector in regulating synaptic-vesicle fusion. *Nature* 388, 593-598.
- Weimer, R.M., Gracheva, E.O., Meyrignac, O., Miller, K.G., Richmond, J.E., and Bessereau, J.L. (2006). UNC-13 and UNC-10/rim localize synaptic vesicles to specific membrane domains. *J Neurosci* 26, 8040-8047.
- Wu, M.N., Littleton, J.T., Bhat, M.A., Prokop, A., and Bellen, H.J. (1998). ROP, the *Drosophila* Sec1 homolog, interacts with syntaxin and regulates neurotransmitter release in a dosage-dependent manner. *EMBO J* 17, 127-139.
- Xu, J., Camacho, M., Xu, Y., Esser, V., Liu, X., Trimbuch, T., Pan, Y.Z., Ma, C., Tomchick, D.R., Rosenmund, C., *et al.* (2017). Mechanistic insights into neurotransmitter release and presynaptic plasticity from the crystal structure of Munc13-1 C1C2BMUN. *Elife* 6.
- Yang, X., Wang, S., Sheng, Y., Zhang, M., Zou, W., Wu, L., Kang, L., Rizo, J., Zhang, R., Xu, T., *et al.* (2015). Syntaxin opening by the MUN domain underlies the function of Munc13 in synaptic-vesicle priming. *Nat Struct Mol Biol* 22, 547-554.
- Zikich, D., Mezer, A., Varoqueaux, F., Sheinin, A., Junge, H.J., Nachliel, E., Melamed, R., Brose, N., Gutman, M., and Ashery, U. (2008). Vesicle priming and recruitment by ubMunc13-2 are differentially regulated by calcium and calmodulin. *J Neurosci* 28, 1949-1960.
- Zucker, R.S., and Regehr, W.G. (2002). Short-term synaptic plasticity. *Annu Rev Physiol* 64, 355-405.

# Acknowledgements

**Thank you, Noa!** – with you I have always felt a sense of security. I couldn't have enjoyed my PhD time, if it wasn't for your relaxed attitude towards my blunders. I feel so proud to have you as a supervisor, because I see you genuinely striving hard for the cause of science. You make concepts sound so easy all the time, which is only because you grasp them so well. I look up to you for being a super woman who manages family and work so superb! Thank you for everything!

**Thank you, Nils!** – I feel very privileged for the opportunity of doing a PhD in your lab. I greatly appreciate the way you encourage and support your lab members when they face any problem. Thank you for providing such an easy atmosphere to talk and for taking good care of your staff members!

**Thank you, Prof. Thomas Dresbach** and **Prof. Tiago Outeiro** for serving on my thesis advisory committee and always encouraging me!

Thank you to all non-scientific colleagues:

...**Ramona & Lydia** – for taking care of my dishes and always greeting me with this huge smile on your faces!

...**Birgit** – for your kind help and patience. I apologize for being so difficult when it comes to administrative stuff.

...**Bianca & Marion** from the animal husbandry – for your outstanding support!

...**HaJo & Martin** – for excellent IT support, particularly during the pandemic!

A big thank you to all scientific colleagues:

...**Miso** – you helped me a great deal in image analysis and figure preparation & **Heiko** – for teaching me three different microscopes and on short notice. I am sincerely grateful to you both!

...**Ali, HongJun & ChungKu** – for your company during night shifts, for always helping out, despite me being annoying at times; for the jokes when passing by me in the corridor and always being so kind to me! Many thanks to **Jeong Seop** who granted me access to his setup and ensured that I was provided regularly with astrocyte cultures for my experiments!

...AGCT Lab – **Fritz, Christiane, Yvonne, Diana**, you make a lot of things possible that would otherwise be laborious. Thank you for solving my requests so fast, despite your tight work routine!

...**Anja, Astrid, Sabine, Sally & Manu** – you are the backbone of the department. I always look up to you for being so well organized and always having a backup reagent at hand! Thank You!

...**Holger** – thank you for always listening to my requests and explaining me long hours how to perform analysis in Igor!

...**Caro, Fran** – for the hourslong conversations, sharing your experiences and always giving the best advice. I enjoyed laughing loads with you!

...**Cordelia, Marilyn, Kerstin, James, Sonja, Ben, Theo, Dilja, Erinn** – all of you were always very kind and supportive when I approached you with a concern. Thank you!

...**Valentina, Jutta, Heba, Sofia, Dragana, Sven, Mareike, Ines, Alien, Kirsten, Valentin, Frederike, Lucia, Ute, Frederike, Lydia, Natalia, Paula, Sun, Karla, Steffanie** – you provided an extraordinary working atmosphere, endless hours of conversations, massive encouragement and memorable encounters in the hallway. I can never thank you all enough for being such great fellows!

Whoever is attached to my life deserves an applaud for being good audience to my superfluous talks. To all friends, in and outside the lab, **Priyanka, Amara, Hilansi**, you have accompanied me during a very beautiful phase of my life. You were undoubtedly part and parcel of this flavoursome experience. I am still in awe of this great journey that is approaching an end. I came happy and I will leave with great joy taking piggyback this pleasant journey. Everyone has taught me something! With each person I associate a great quality that I wish to own myself. Sincerely grateful to have met you all!

My sincerest gratitude to the ones who are my biggest encouragement, **my parents!** I thank you wholeheartedly and with deep appreciation for envisioning me at this stage when I was lacking perspective. You have been a pillar of strength and ideals in all quests of life. I will never be able to express the gratitude that you deserve to be honoured with, because I sincerely feel that I owe everything to you after God's grace. This thesis is dedicated to you, you are the driving force behind it! In fact, all my family deserves to be acclaimed for having had patience with me and bearing with me. Thanks to **my Sami** for your affectionate companionship and always covering my back! Thanks to **my sister** for being only a phone call away! Thanks to **my brother** for being a source of comfort in my life and thanks to **my sister-in-law** for hour long conversations that help me sort myself. I have been blessed with so many nice people, so are **my in-laws**, who are worthy to be thanked for their love and support. Thank you everyone!